

Including reservoirs in ab initio  
transport calculations for single molecules

The model of absorbing boundaries: implementation and  
application to the variation of the conductance with gate and  
bias voltage

Zur Erlangung des akademischen Grades eines  
DOKTORS DER NATURWISSENSCHAFTEN

von der Fakultät für Physik der Universität (TH)  
Karlsruhe

genehmigte

DISSERTATION

von

Dipl. Phys. Andreas Arnold aus Rödermark

Tag der mündlichen Prüfung: 26.01.2007

Referent: Dr. F. Evers

Korreferent: Prof. Dr. P. Wölfle



# Contents

<b>1</b>	<b>Introduction</b>	<b>1</b>
<b>2</b>	<b>Experimental techniques contacting single molecules</b>	<b>9</b>
2.1	Mechanically controlled break junction . . . . .	10
2.2	STM experiments . . . . .	13
2.3	Electromigration . . . . .	15
<b>3</b>	<b>Electron Transport calculations with ab initio methods</b>	<b>17</b>
3.1	Calculations for large molecules: Density functional theory . .	18
3.2	Coupling molecules to leads: Quantum chemistry with open boundaries . . . . .	21
3.3	Applying bias voltages: non-equilibrium calculations . . . . .	23
3.4	Transport from density functional theory calculations . . . . .	26
<b>4</b>	<b>Coupling of molecules to leads: Self-energies</b>	<b>29</b>
4.1	Basic formalism . . . . .	30
4.2	Role of the self-energy . . . . .	31
4.3	Understanding self-energies as absorbing boundaries . . . . .	33
4.3.1	Model self-energy . . . . .	34
4.3.2	How to check the convergence of the results . . . . .	35
4.4	Test calculation: a tight binding chain . . . . .	40
4.4.1	Absorbing boundaries . . . . .	42
<b>5</b>	<b>Test of algorithm for reservoirs in equilibrium</b>	<b>47</b>
5.1	Screening of the electric field on metal electrodes . . . . .	47
5.2	Open vs. closed boundaries: charge density . . . . .	49
5.3	Transmission function . . . . .	52

<b>6</b>	<b>Coulomb blockade with DFT</b>	<b>57</b>
6.1	Coulomb blockade and density functional theory . . . . .	57
6.2	Charging the molecule with a gate: flow of orbital energies . .	59
<b>7</b>	<b>Applying a finite bias voltage: non-equilibrium Stark effect</b>	<b>63</b>
7.1	The Stark effect . . . . .	63
7.2	Stark effect induced by finite bias . . . . .	64
7.3	Transport including the bias voltage . . . . .	69
7.4	Addendum: Artificial symmetries and their effect on transport	71
<b>8</b>	<b>Application: Bipyridine – candidate for a molecular switch?</b>	<b>75</b>
8.1	Tilting of free molecule . . . . .	76
8.2	Bipyridine between Gold leads: tilting with a gate . . . . .	81
8.3	Effect of a gate: Orbital flow and Coulomb blockade . . . . .	85
8.4	Modeling screening of leads with image charges . . . . .	91
8.5	Orbital shift under applied bias voltage . . . . .	92
8.6	Structure relaxation under applied voltage . . . . .	103
<b>9</b>	<b>Metal organic complexes: molecular magnetism</b>	<b>107</b>
9.1	Ruthenium as central atom: a stable spin zero molecule as test	110
9.2	Iron as central atom: Spin filter? . . . . .	118
9.3	Cobalt as central atom: Kondo physics . . . . .	120
<b>10</b>	<b>Summary</b>	<b>123</b>
<b>A</b>	<b>Program package TURBOMOLE</b>	<b>127</b>
A.0.1	Relaxation of atomic structures . . . . .	129
A.0.2	Including gates into TURBOMOLE . . . . .	129
A.0.3	Transport calculations with TURBOMOLE . . . . .	130
<b>B</b>	<b>Explicit calculation of the coupled density matrix</b>	<b>133</b>
<b>C</b>	<b>Analytical calculation of the transmission of a tight-binding chain with a triple barrier</b>	<b>135</b>

# List of Figures

1.1	Schematic structure of a diode molecule . . . . .	1
1.2	$I(V)$ -curve of diode molecule . . . . .	2
1.3	Kondo effect in organic molecules . . . . .	4
1.4	Molecule showing hysteresis . . . . .	5
2.1	MCBJ: schematic setup . . . . .	10
2.2	A stable Gold-molecule-Gold contact . . . . .	11
2.3	Experimental data from MCBJ . . . . .	12
2.4	Schematic view on STM experiments . . . . .	13
2.5	STM experiments in a poly-electrolyte solution . . . . .	14
4.1	Coupling of molecules to leads . . . . .	29
4.2	The coupled molecule split into parts . . . . .	30
4.3	Scheme of the DoS for coupled molecules . . . . .	32
4.4	Reflecting and absorbing boundaries . . . . .	34
4.5	Flow of Benzene di-thiol orbitals . . . . .	37
4.6	Orbitals of Benzene di-thiol . . . . .	38
4.7	Transmission of Benzene for different number of coupled gold atoms. . . . .	39
4.8	Dependence of the transmission on the parameter $\eta$ . . . . .	41
4.9	Dependence of the transmission on the parameter $\eta$ for larger system . . . . .	41
4.10	Tight binding chain . . . . .	42
4.11	Transmission of the tight binding chain (numerical and analytical) . . . . .	44
4.12	Error in the transmission for different $L$ . . . . .	44
4.13	Error in the transmission for different $\beta$ . . . . .	45
4.14	Error in the transmission for different $\eta$ . . . . .	45

5.1	Geometry of a point charge between two gold tips . . . . .	47
5.2	Screening of metal electrodes . . . . .	48
5.3	Screening of gold pyramids, small distance . . . . .	50
5.4	Screening of gold pyramids, large distance . . . . .	50
5.5	Screening of back-on-back gold pyramids . . . . .	50
5.6	Excess electron density on the gold cluster for different geometries . . . . .	51
5.7	Geometry of Benzene between 14 atom leads and the gate. . .	52
5.8	Ground state density of Benzene di-thiol . . . . .	53
5.9	Difference of the density between open and closed boundaries .	53
5.10	Transmission of BDT, comparison of bulk and model $\Sigma$ . . . .	54
5.11	Transmission of BDT for fixed $\mu$ and $N$ . . . . .	55
6.1	Schematic picture for the shifting of orbital energies . . . . .	58
6.2	Screening of the 14 atom pyramid for Benzene di-thiol . . . .	60
6.3	Charge on BDT over gate charge . . . . .	60
6.4	Orbital flow of BDT for different gate charge. . . . .	61
6.5	Transmission of BDT for different gate charge. . . . .	62
7.1	Flow of BDT orbitals in a constant electric field . . . . .	64
7.2	Orbitals of Benzene di-thiol in vacuum and an electric field. .	65
7.3	Electron number of BDT and leads for different applied voltage	66
7.4	Electron number of Benzene for different applied voltage . . .	67
7.5	Flow of Benzene orbitals under applied voltage . . . . .	67
7.6	Orbitals of Benzene di-thiol under applied bias voltage. . . . .	68
7.7	Transmission function for Benzene molecule for different bias voltages . . . . .	69
7.8	$I(V)$ -curve for Benzene . . . . .	70
7.9	Structure for the relaxation of the BDT molecule between leads	72
7.10	Transmission through BDT for different coupling angle . . . .	73
8.1	4,4'-Bipyridine . . . . .	75
8.2	Energy dependence for Bipyridine in vacuum . . . . .	78
8.3	Energy dependence for Bipyridine between 2 Gold atoms . . .	78
8.4	Energy dependence for protonized Bipyridine . . . . .	79
8.5	Orbitals of Bipyridine in vacuum . . . . .	80
8.6	Energy dependence for Bipyridine in vacuum, different methods	81
8.7	Bipyridine between 71 Gold atom pyramids . . . . .	82

8.8	Bipyridine between 14 gold atom pyramids . . . . .	83
8.9	Transmission function of Bipyridine under variation of $\Phi$ . . . . .	84
8.10	Different lead geometries . . . . .	86
8.11	Screening of a Au-(100) surface . . . . .	87
8.12	Screening of a Au-(111) surface . . . . .	87
8.13	Orbital flow for Bipyridine . . . . .	88
8.14	Bipyridine: orbital energies for different gate charge . . . . .	89
8.15	Transmission of Bipyridine for two different gate charges . . . . .	90
8.16	Orbitals of Bipyridine in vacuum and an electric field. . . . .	93
8.17	Orbital energies for Bipyridine in vacuum and an electric field. . . . .	94
8.18	Orbital energies for negative charged Bipyridine in vacuum and an electric field. . . . .	94
8.19	LUMO+4 of Bipyridine . . . . .	96
8.20	Level crossing at high voltages . . . . .	96
8.21	Excess electron number on the Bipyridine under applied bias voltage . . . . .	97
8.22	Orbital energies of Bipyridine under applied voltage . . . . .	97
8.23	Orbitals of Bipyridine under applied voltage . . . . .	98
8.24	Difference in electron line density for applied bias voltage . . . . .	100
8.25	Transmission of Bipyridine under applied voltage . . . . .	101
8.26	Transmission of Bipyridine for different functionals . . . . .	102
8.27	Position of the LUMO for different charge on the Bipyridine . . . . .	103
8.28	Schematic picture of the artificial level shift under $V_{\text{bias}}$ . . . . .	104
8.29	$I(V)$ -curve for Bipyridine in non-equilibrium . . . . .	104
8.30	Transmission of Bipyridine (optimized structure) . . . . .	106
9.1	$\text{Ru}^{2+}$ bis-terpyridyl complex . . . . .	107
9.2	Schematic structure of the d-orbitals of transition metals cou- pled to 6 N-atoms. Left is the low spin structure, where all 6 spins are paired. Right is the high spin, where only two spins are paired. . . . .	109
9.3	integrated charge density around ruthenium . . . . .	112
9.4	Energies of the D-orbitals of different transitions metals . . . . .	112
9.5	$\text{Ru}^{2+}$ bis-terpyridyl complex coupled to leads . . . . .	113
9.6	Excess electron density on Ru-complex (LS) for different gate charge . . . . .	114
9.7	Excess electron density on Ru-complex (HS) for different gate charge . . . . .	115

9.8	Flow of orbital energies for Ru complex . . . . .	116
9.9	Transmission through the Ru complex (different lead size) . .	117
9.10	Transmission through the Ru complex (different $\eta$ ) . . . . .	118

# List of Tables

8.1	Energy dependence for Bipyridine between Gold leads (71 Gold)	82
8.2	Distances for Bipyridine under applied voltage . . . . .	106
9.1	D-orbitals . . . . .	108
9.2	Basis sets used for Ru <sup>2+</sup> bis-terpyridyl complex . . . . .	111
9.3	Bond distances Ru-N . . . . .	111
9.4	$E_F$ of Ru complex for different lead size . . . . .	115
9.5	Bond distances Fe-N . . . . .	119
9.6	Basis sets used for Fe <sup>2+</sup> bis-terpyridyl complex . . . . .	120
9.7	Bond distances Co-N . . . . .	121



# Chapter 1

## Introduction

For four decades the number of transistors in a computer has doubled every four years. This was possible because the computers' functional devices became smaller and smaller. The most important such devices, diodes and transistors, currently have typical dimensions of less than 100 nm. Decreasing the size yet further will inevitably invoke new technological challenges due to approaching the atomic (quantum mechanical) scale. For example, a transistor requires an insulating layer between its gate and its source/drain, which is currently about 10 nm thick, i.e. only about 40 atomic layers of SiO<sub>2</sub>. For smaller widths, however, the tunneling current through the layer will drastically increase. Furthermore, cooling of the devices will become very hard because small and fast switches suffer from substantial local Ohmic heat production, which is already now a considerable problem. Even, if the difficulties within the present technique can be overcome, extrapolating the current trend one finds that in about 20 years the atomic limit (i.e. of the spacer layers) is finally reached.

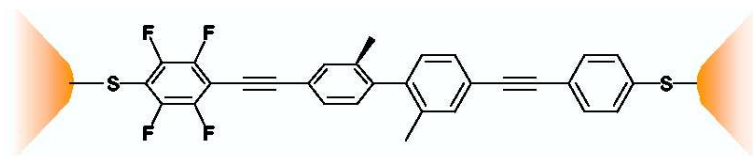


Figure 1.1: Schematic structure of a diode molecule. The Fluorine changes the electronic structure of the Benzene ring on the left side compared to the right ring, thus inducing an on-axis dipole moment on the molecule that affects the transmission. The length of the molecule is about 2.5 nm.

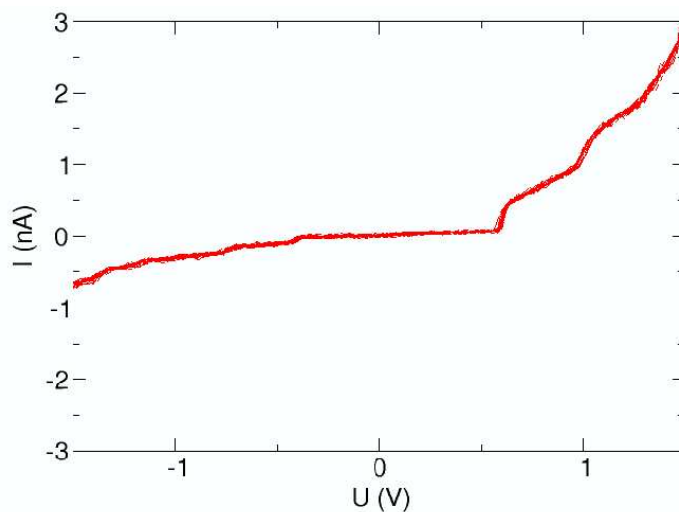


Figure 1.2: The  $I(V)$ -curve of the diode molecule (depicted in Fig. 1.1) shows a clear asymmetry between positive and negative voltages.[2]

The size of the devices that can be produced with currently available semi-conductor techniques is thus limited. But one can think of even smaller devices built from single (metal-)organic molecules. Their size can vary from less than 1 nm to hundreds of nanometers. Variety of the molecules with different physical properties and therefore functionalities is well mirrored in the complexity of living nature. All these aspects make molecular electronics an interesting field both scientifically and technologically[1].

Clearly, we are currently far away from building computers out of molecules, but still good progress has been made in recent years in this field. Single molecules can be synthesized in a fully reproducible fashion, and the functionality of single molecule devices can be thoroughly investigated. Given a set of physical/chemical properties, it is nowadays possible to design and synthesize promising molecules to match these properties, sometimes within only months.

First (still very crude) functional devices have already been built, like a transistor[3] or a diode[2] (Fig. 1.1). As a proof of principle for functionality, single molecules have been contacted to Gold leads with stable chemical bonds, and the current-voltage ( $I(V)$ ) dependence has been measured. These experiments have demonstrated that molecular devices can work as expected.

An experimental  $I(V)$ -curve, as depicted in Fig. 1.2, can show pronounced

steps, probably originating from the individual molecular orbitals. Step height and position depend on microscopic details, and for a thorough understanding a theoretical analysis is necessary.

To show that molecular electronics is a field comprising many phenomena, we shortly present a few experiments that have been done in the last years. The interesting one is about Coulomb blockade, where a gate is used to change the charge state of a molecule. The hopping of single electrons onto the molecule has indeed been observed[3, 4]. This effect is called Coulomb blockade, because the energy difference between the different charge states is determined predominantly by the Coulomb repulsion, i.e. by the fact that molecular orbitals reshuffle when an additional electron enters the system.

In this type of experiments sometimes also the Kondo effect is observed (Fig. 1.3). The molecule with an odd number of electrons always carries a net spin, e.g. spin 1/2. If the direction of this spin is not fixed, Kondo physics can be observed. This can be seen as a increasing zero bias transmission when decreasing the temperature. It indicates resonant transport that remarkably is largely independent of the gate voltage.

Another phenomenon that has been investigated is electron-phonon interaction. At finite bias voltages, the electrons can be scattered by phonons, leading to additional steps in the  $I(V)$ -curve at values, where the voltage is equal to a phonon energy[5].

Not only a molecular diode but also a molecular switch has already been realized. Switching is triggered by applying a bias voltage from a large to a low conductance state (Fig. 1.4). Apparently, the switch works stable for seconds. Only inverting the bias voltage takes the molecule back to the low conducting state[6].

The theoretical prediction of single molecule properties is a challenging task. Exact methods are available only for systems with few electrons, typically smaller than e.g. a Benzene ring (42 electrons). By contrast, molecular devices are usually much larger, often containing hundreds of electrons; therefore approximative methods have to be deployed. In fact, calculations should take a portion of metallic leads into account as well, which increases the size of the molecule even further, thus called “extended” molecule. Treatment of the interaction between the leads and the molecule is important, because a good description of the hybridization between molecular orbitals and the leads is crucial for understanding electronic transport, as will be explained below.

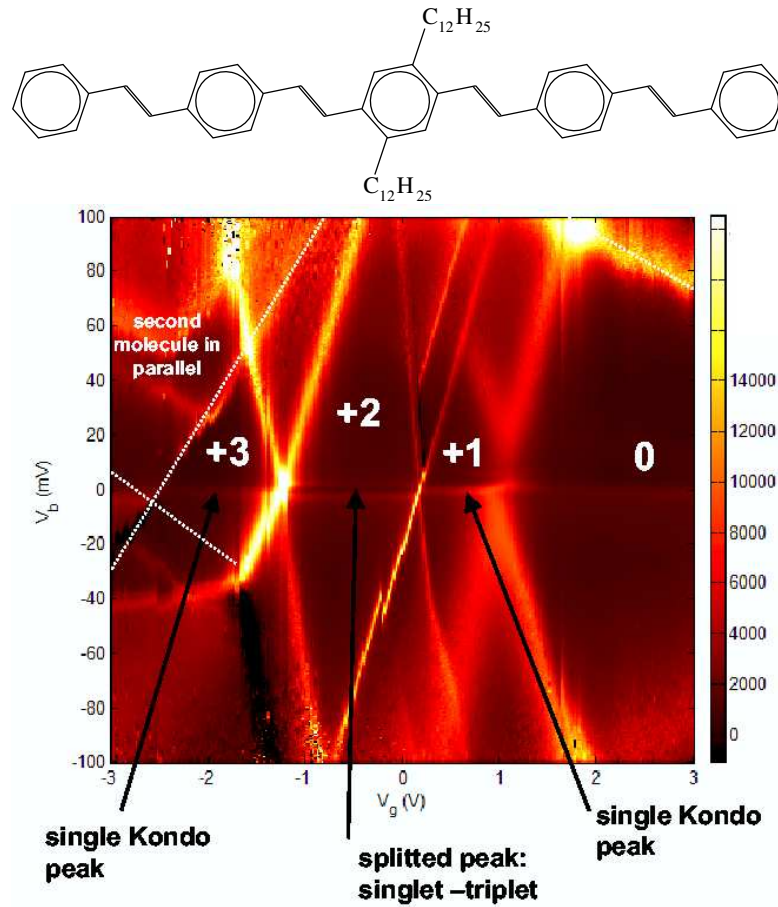


Figure 1.3: Shown is the conductance as color, the gate voltage on the x-axis and the bias voltage on the y-axis. Conductance due to molecular orbitals shows a linear shifting with  $V_G$ , while the Kondo effect is independent of  $V_G$  and appears always for  $V_{\text{bias}} \approx 0$ . (Experiment by H. van der Zant)

**State of the art in theory of molecular transport:** In the zoo of *ab initio* methods, there is only one numerical method known to handle sufficiently large systems, namely density functional theory (DFT) [7, 8, 9, 10]. DFT is very popular, since it is very successful in determining the atomic configuration of molecules or band structures in simple metals with only modest computational requirements. DFT scales almost linearly with the number of atoms [11], compared to an exponential scaling for “exact” methods. This allows for the treatment of large molecules with several thousand electrons

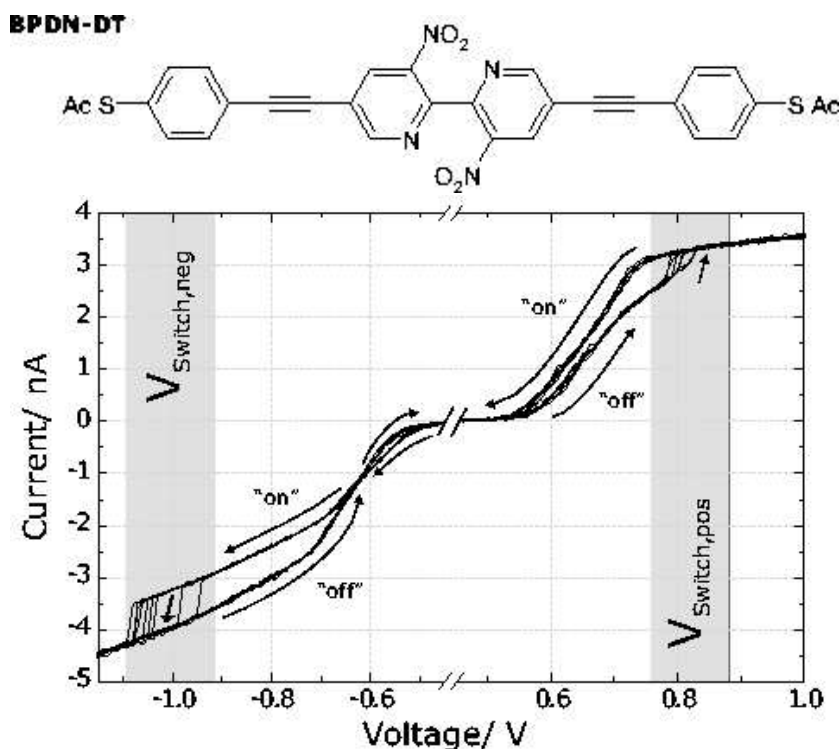


Figure 1.4: Molecule showing hysteresis. When going to 0.8 V, the molecule switches to the “on”-state with higher conductance. This state is stable until the voltage is reduced to -1 V. There it switches back.[6]

on a standard PC.

However, enormous challenges persist. The standard method constructs scattering states from the one-body wavefunctions (“Kohn-Sham-orbitals”) of DFT, and uses them for the usual Landauer-Büttiker formula, which is up to now only justified for non-interacting particles. Lately, very promising attempts for a better justification have been made using time-dependent (TD-)DFT. But in TD-DFT[12, 13, 14, 15] there seems to be no agreement in the community whether or not the appropriate the time-dependent functional is the same as for DFT.

For DFT the exact functional is as well not known, but approximations exist. Phonon frequencies can be calculated with these, often with a high accuracy. By contrast, charge densities and the response to external fields are plagued by inaccuracies. The resonance positions and shapes are uncertain.

Importantly, the approximations in functionals with local density approximation (LDA) turn out to show a good agreement with experimental results if used for metallic systems. This can be understood, since the density in metallic systems is almost constant and can be approximated by the local value.

The possibility to calculate the electronic structure led to many works on different molecules, predicting the  $I(V)$ -dependence under various conditions [16, 17, 18, 19, 20, 21, 22, 23, 24]. Transport calculations through chains of metal atoms work well, showing a good agreement with experiments [25, 26, 27]. For organic molecules, discrepancies between theory and experiments emerge when calculating magnitudes of currents at a given bias voltage. Most likely this is due to the sensitivity of the conductance to approximations made in the functionals for DFT. The qualitative current-voltage dependence is however fairly robust, sometimes even leading to good quantitative predictions e.g. for step positions in the  $I(V)$ -curve [2]. Current research tries to improve the approximations in an effort to reproduce the experimental  $I(V)$ -curves quantitatively[28].

**What is novel in this work:** In this thesis a detailed analysis of effects of gating and non-equilibrium on the  $I(V)$ -curve will be presented. The gating effect, where a charged gate is used to switch the physical properties of a molecule, is especially interesting for transistors. Non-equilibrium effects can be useful for non-linear devices like diodes.

To calculate such effects, leads have to be introduced into the calculation. However, the enormous size of the contacts makes a direct treatment untractable. In our work we shall introduce a very fast and accurate way of treating the coupling of the molecule to the leads in a quantum chemistry calculation. In its regime of applicability, the method gives essentially exact results. A particular aspect is that it allows to replace a tedious and sometimes imprecise numerical spectral integration by a simple analytic expression. To achieve this, only the molecule together with a certain number of lead atoms, the “extended molecule”, need to be treated directly. The clear advantage of our method in comparison to the other available ones[28, 29] is that the transport calculations become more transparent and easier to implement. A disadvantage is that sometimes very large extended molecules have to be introduced in order to make our approach applicable.

Our method is not restricted to investigation of transport phenomena. In

fact, it opens up the door for a new field of quantum chemistry calculations for molecules in effective/embedding media. For instance, it can be insightful for studying adsorption of molecules on surfaces. With coupling included, the part of the substrate that has to be explicitly taken into account is greatly reduced, especially if there is charge transfer between the molecule and the surface.

In this thesis, the new approach has been implemented in the program package TURBOMOLE[30] and applied to various molecular transport problems. As a first application, we consider the effect of a gate voltage,  $V_G$ , on the zero bias conductance of Benzene di-thiol (BDT), which has evolved into the most important test system for DFT based transport calculations. The motivating idea for this particular investigation is that in principle DFT should give the exact evolution of the total molecular charge with gate voltage. In particular, it should capture the stepwise increase of the electron number with  $V_G$ , the so called ‘‘Coulomb blockade’’. However, in reality the exact ‘‘exchange correlation’’ (XC) functional that would appear in the proper DFT calculation is approximated by a ‘‘local density approximation’’ (LDA), and it is important to investigate the consequences of this. As this investigation will show, the mean field character of LDA has a dramatic impact on the description of charging phenomena within practical DFT calculations.

Charge reorganization not only underlies the Coulomb blockade, it is also important in order to understand the effect of a finite bias on the molecular transmission function. We shall see that the same LDA-artifact entering the Coulomb blockade can also spoil the theoretically determined  $I(V)$ -curve in a qualitative way. To give an example, explicit calculations for the Bipyridine molecule will be presented. Bipyridine has been investigated as a promising candidate for a molecular switch in a recent series of experiments and therefore is a very relevant testing system.

Using the approach in non-equilibrium is very important for many experiments. Especially true is this fact for non-linear devices, e.g. diodes, which show non-linear effects even at small voltages. These effects can be calculated with this formalism to within the limits by the functionals available.

As a third application of our method, we have investigated metal-organic complexes. These systems are interesting for various reasons. For example, they have been used already in experiments in order to generate Kondo-scattering of transport electrons at a single atom held inside a molecular cage. In our work we would like to address the question whether the spin state of that atom may be controlled by applying an external gate voltage

(“high-spin - low-spin” transition). If so, a possibility may exist to switch externally from a Kondo system into a Coulomb-blockade situation and back.

**The outline:** To start with, in Chap. 2 a short overview over the well established experimental techniques will be given [3, 4, 2, 31, 32, 33], followed by a description of the theoretical methods used in the thesis in Chap. 3. Namely, there will be an introduction into standard quantum chemistry calculations and density functional theory, as well as a short description of transport calculations starting from DFT results. Since these issues have been outlined already by many previous authors, we take the freedom to be very brief at this point. There will, however, be an extended description of how to couple molecules to reservoirs within a DFT calculation in Sec. 3.2. In Chap. 4, the coupling of a molecule to (infinite) leads will be presented along with the specifics of our model coupling. In Chap. 5, test calculations will demonstrate how well the method works inside its regime of applicability, but also what its limits are.

As a realistic application we present the Benzene molecule in Chap. 6. It is a commonly used test molecule, mainly due to its smallness and therefore modest computational requirements[16, 24, 21, 28, 34, 35, 36, 37, 38, 39, 40, 41, 42]. With this molecule we want to show the problems of the approximations used within DFT, e.g. the derivative discontinuity problem[43, 44] becomes transparent. In Chap. 7, the effect of a finite bias voltage on the BDT molecule is addressed.

In the following chapter (Chap. 8), the Bipyridine molecule, a candidate for an externally controlled switch[45], will be analyzed. We illustrate the switching of the geometry by calculations of the shifting of the orbitals due to the gate voltage. The evolution of the molecular orbitals under applied bias voltage, the “non-equilibrium Stark effect”, is demonstrated. Our investigations show that transport calculations for this species, reporting quantitative agreement with experiment[46], are likely plagued by functional artifacts. But also, we shall see, that many qualitative features remain valid.

The last application in Chap. 9 will be a calculation of a metal-organic complex, where one transition metal atom from the 3d or 4d series is put between two organic molecules. The focus was kept on Ruthenium[47], Cobalt (Kondo effect[4]), and Iron (diamagnetic,  $S=0$  – paramagnetic,  $S=2$  switches).

## Chapter 2

# Experimental techniques contacting single molecules

In order to measure transport properties of single molecule, one has to connect the molecule to leads. Before starting any measurement, one has to assure that the molecule has indeed formed a chemically stable bond to the contacts, and that there is exactly one molecule between them.

It is very difficult to directly determine the contact geometry, since it is formed in a self-organizing process (well established in e.g. organic chemistry) and thus cannot be visualized via electron microscopy or comparable methods. However, it is at least possible to determine whether there is a stable chemical bond between the leads and the molecule. A direct proof can be achieved by e.g. pulling at the junction. In a stable contact this will affect the current very little, while in a tunneling regime (missing contact at one side) the current depends exponentially on the distance. An indirect proof is the observation of reproducible steps in the current[2], when sweeping the voltage. If the bond is not stable, the step positions will not be fully reproducible.

To determine the properties of a contact, one needs to know what happens on the chemical side. To couple a molecule to a lead, a contact group able to form a stable bond to lead metal is necessary. Usually, one uses Sulfur, because Sulfur-metal bonds are very stable[48]. To ensure that the molecule couples only to the lead and nothing else, this Sulfur is protected by a methyl-group. In solution, this group prevents coupling to other molecules; however, it is split off as soon as the molecule approaches the lead. The lead material is typically Gold, or Cobalt if ferromagnetic leads are required. Gold is

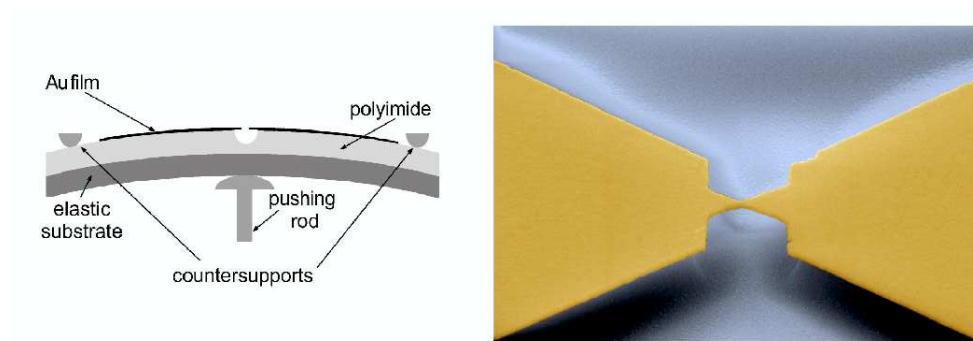


Figure 2.1: Mechanically controlled break junction (MCBJ): schematic description of the experimental setup. The left picture shows the three point bending mechanism, allowing for a very precise change in the distance of the two contacts. The right picture shows the junction before the breaking, as created with e-beam lithography.

preferred, since it forms more stable bonds to Sulfur. In addition, Gold can form monoatomic chains[49], thereby allowing for a contact to a single Gold atom. By this, as we will see below, one can assure that there is only a single molecule contacting each of the leads, and since the methyl-group hinders molecule-molecule coupling, the molecules cannot form chains between the contacts. Together this ensures that only a single molecule is located between the contacts.

In the following the most commonly used techniques for contacting molecules will be briefly addressed.

## 2.1 Mechanically controlled break junction

An important type of experiment is the mechanically controlled break junction (MCBJ, [31]). Fig. 2.1 shows the experimental setup. There is a thin layer of Gold on top of a substrate, created by e-beam lithography[50]. The “three point bending mechanism” allows for bending the substrate, leading to tensile stress on the Gold junction. To prevent contamination of the setup, the whole experiment is done in a vacuum.

The contact is build by pulling the Gold junction apart until it breaks. Pulling slowly, the Gold will first form a chain of atoms before it breaks. This leaves a bump on the surface, which is of crucial importance for contacting

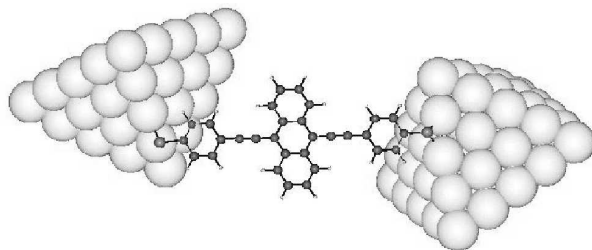


Figure 2.2: A stable Gold-molecule-Gold contact. This is one possible configuration of a stable contact between a molecule and two leads, as used in numerical calculations.

single molecules. On a flat surface, many molecules will couple at the same time. On a bumpy surface, however, the different molecules will have to bridge different distances and thus allowing for contacting of single molecules. The main advantage of this method is that the distance of the two tips can be adjusted very precisely, in the order of 0.01 nm.

After the tips are formed, the vacuum chamber is filled with Nitrogen to prevent contamination when opening it. Then, a droplet of the molecule in solution is brought into the junction. One chooses the distance of the tips to be larger than the size of the molecule, so that they can form a bond only to a single lead. Now the rest of the solution with unbound molecules is removed by rinsing the junction with Tetrahydrofuran (THF) and the chamber is evacuated again.

To form a stable contact between both leads, one applies a finite bias voltage. In the strong electric field close to the junction the molecules align in direction of the opposite electrode. Now the lead distance is slowly reduced until there is a plateau in the current. At this point one assumes that only a single molecule has formed a stable bond between both leads (see Fig. 2.2). However, the molecule will not form a bond to the leads at low temperatures, because bonding is a thermally activated process; therefore, the system temperature can only be reduced after the formation of the contacts.

To check the stability of the contact, the distance of the leads is changed a bit. A stable molecule-Gold contact will not show a remarkable difference in the current, since for small distances the molecule will bend somewhat and Gold will be drawn out of the surface, but it will not strongly affect the current. This is completely different from the tunneling behavior that is

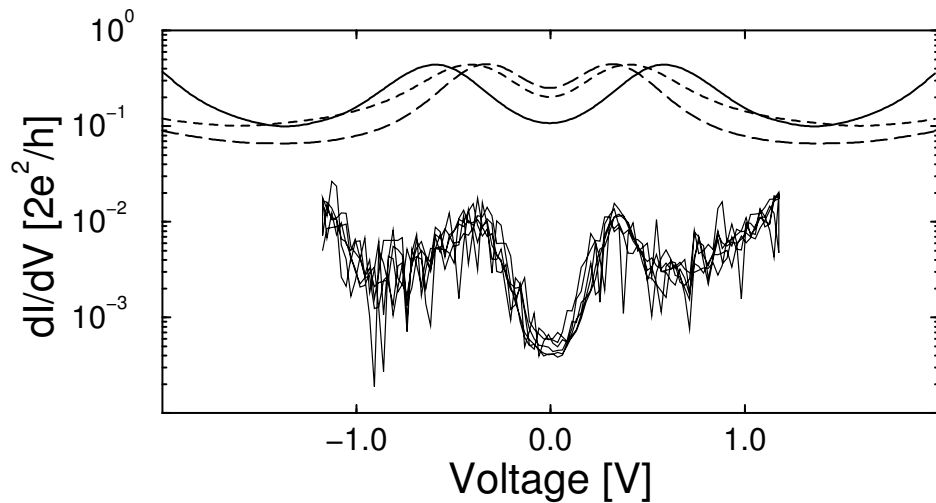


Figure 2.3: Experimental data (lower curve) from MCBJ for the conductance of the molecule depicted in Fig. 2.2. The different theoretical curves (upper curves) represent a change in the coupling between the molecule and the Gold. As one can see, the prediction of the peak positions is quite good, but the conductance is vastly overestimated.[53]

expected if only one rather than two stable contacts exist. In such a case the current will show an exponential suppression with increasing distance.

After the Gold-molecule-Gold junction has formed, one can sweep the voltage and measure the current many times for a single geometry, because the BJ keeps its configuration very well in time. Opening and closing the junction again will lead to a different configuration, but it usually does not have a major effect on the  $I(V)$ -curve, at least not on a qualitative level. The MCBJ technique very popular by now and *de facto* standard in the field of single molecule electronics, e.g. [51, 52]

Fig. 2.3 shows the differential  $I(V)$ -curve for a single molecule as well as the theoretical prediction. The experimental curves show, that sweeping the voltage back and forth does not change the  $I(V)$ -dependence dramatically, illustrating that a stable contact is indeed formed. The theoretical prediction shows the same peak positions in the differential  $I(V)$ -curve. Unfortunately, the conductance is overestimated by two orders of magnitude, as already indicated in the introduction.

The major disadvantage of the MCBJ technique is that it appears to be

difficult to do experiments with a metallic gate. Since the size of the full contact is very large compared to the molecule, the leads will completely screen any externally applied gating field. And it is also not possible to put an electrode close to the molecule, because the position of the junction is not known due to its formation by breaking the metal film.

## 2.2 STM experiments

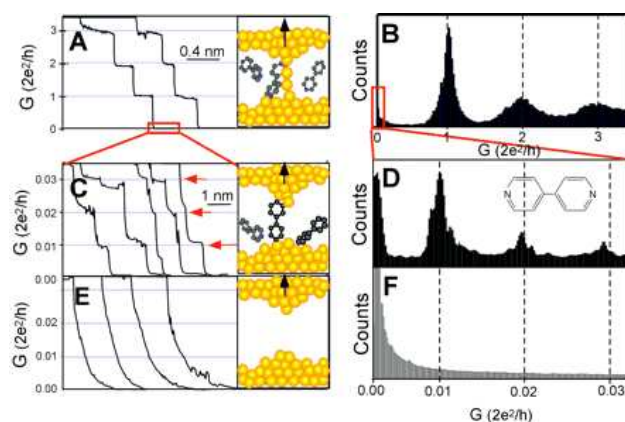


Figure 2.4: Schematic view of a STM experiment with Bipyridine molecules directly coupled to the Gold. The top pictures show the formation of a Gold chain; the conductance is a multiple of  $G_0$  (the conductance of a monoatomic Gold Chain). Below, the conductance-scale is reduced by two orders of magnitude. Still, plateaus can be observed, but at a conductance around  $0.01G_0$ . This corresponds to stable Gold-molecule-Gold contacts. On bottom of the plot the control experiment without molecules is shown. No steps can be seen, only the exponential tunneling of the broken Gold chain. [33]

Another method of contacting molecules is using a scanning tunneling microscope (STM) tip [32]. Here one electrode is the surface and the other the tip. The molecules can be placed on the surface as a self-assembled monolayer (SAM). Alternatively, simple molecules can be deposited on the surface keeping surface and tip in a solvent or electrochemical solution. By moving the tip up and down under a constant bias voltage, stable contacts between the tip and one or more molecules can form.

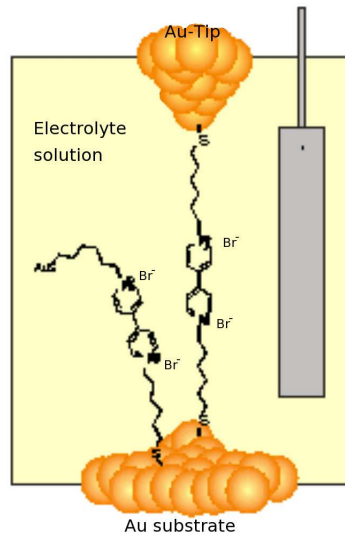


Figure 2.5: Schematic view of a STM experiment with Bipyridine molecules coupled to alkane chains on a surface. The surrounding solution is used as an electrochemical gate by applying a voltage to a third electrode in the solution. [45]

The conductance is recorded under constant applied voltage while the tip moves up and down. Tip motion is programmed in the following fashion: first, the tip is pushed into the Gold layer to form a Gold-Gold contact. Pulling the tip slowly out of the surface will reduce the current since the contact becomes thinner, until the Gold starts to form chains of the width of a single atom, as mentioned in the previous section. Therefore the conductance will show a clear plateau at  $G_0$ , the conductance of a gold chain. When pulling further, this chain will break and leave a single Gold atom lead on the surface and the tip.

If no molecules are in the junction, the STM will enter the tunneling regime after the chain is broken, and the conductance will drop exponentially with the distance. On the other hand, if molecules are in the junction, the conductance will frequently drop to smaller values, but still show plateaus. These plateaus correspond to the transmission of a single or few molecules. Clear plateaus indicate a stable contact [33] (see Fig. 2.4).

This procedure is repeated many times, and the conductance of a single molecule at the given bias voltage is extracted from a statistical analysis[54].

To measure a  $I(V)$ -curve, this procedure has to be repeated at different voltages.

If the experiment is performed in a solution and not with a SAM, one can introduce a third electrode, the gate (see Fig. 2.5). This will create an electric field surrounding the molecule by charging the solution, as known from electrochemistry[45]. This electric field will change the transport properties of the molecule by shifting the orbital energies. The disadvantage of this method is, that in comparison to the MCBJ these experiments cannot be done at low temperatures.

Due to the speed at which one can form a stable lead-molecule-lead contact, this type of experiment has also become very popular, see e.g. [55, 45].

## 2.3 Electromigration

An alternative gating technique, which allows for cooling, is electromigration. The first step in an electromigration experiment is to create a small Gold wire of around 10 nm in width by e-beam lithography [56] on a  $\text{SiO}_2$  insulating layer [57]. Below this layer one can use a doped Si-substrate as a gate electrode.

The junction is formed by applying slowly increasing voltages, leading to a strong electric field along the wire. This field polarizes the Gold atoms, which move along the electric field, thereby slowly decreasing the size of the wire. The electric field is strongest at the thinnest part of the wire, weakening this part even further. Eventually, the wire will break and form a gap. This usually happens around 1-2 V. As soon as there is a gap of  $\approx 2$  nm [4], which can be seen as a clear drop in the conductance, the voltage is turned off and the molecules will be added to the junction using the same procedures described for the MCBJ method.

The full experiment is usually done at low temperatures (4.2 K for the electromigration and the conductance measurement, and 100 K for the coupling of the molecules to the leads), but recently the method has been successfully applied at room temperature as well[58].

This type of experiment is very popular due to the possibility of using the doped Si-gate as a gate electrode. This allows to study e.g. Coulomb blockade [3], where a single electron can jump onto the molecule and then prevents additional electrons from getting into the molecule due to the repulsive Coulomb interaction.

Since this method is very successful for experiments with a gate electrode, many different molecules have been analyzed, e.g. [59, 60, 61], reporting Coulomb blockade or the Kondo effect[4].

## Chapter 3

# Electron Transport calculations with *ab initio* methods

While experiments allow the measurement of electron transport properties of specific molecules, they are quite time consuming. Ideally, theoretical or numerical calculations would allow to screen a large number of candidate systems thus reducing the experimental effort. In addition, they are also very important to gain a deeper insight into the underlying physical processes, of course. Especially for understanding the basic mechanisms of transport, *ab initio* methods can be extremely useful. However, the leads used in transport experiments are too big to be modeled directly by such methods; a more clever method is needed, which is able to calculate the electronic structure of a molecule in presence of the leads without taking the leads explicitly into account.

Let us first discuss why the leads are important for the transport characteristics of the molecule. In a molecule in vacuum one can think of electronic orbitals with well defined energies<sup>1</sup>. Coupling the molecule to leads will change this structure. An electron can hop from the molecule into the lead and back, and therefore has a finite lifetime in the molecule. This leads to a broadening of the molecular orbitals in energy.

Finite lifetime is a direct consequence of hybridization of orbitals. The molecular orbitals hybridize with the lead orbitals, forming new hybrid orbitals at shifted energies. Details of hybridization will determine the broaden-

---

<sup>1</sup>The single particle picture is only true for non-interacting electrons, strictly speaking. Effects not coming from strong correlations can be understood within this picture as well, at least qualitatively.

ing and shifting of the orbital energies and thus are crucial for understanding the transmission through the molecule in a profound manner.

In order to properly describe hybridization it is mandatory to include at least parts of the contacts in the *ab initio* treatment. To deal with a large number of electrons, one can use effective non-interacting quasi-particles instead of the full interacting many-body problem. This is for example done in density functional theory.

### 3.1 Calculations for large molecules: Density functional theory

In this section, only a short overview over the DFT formalism, i.e. mainly the definitions, will be given. For an explanation the reader is referred to literature, e.g. [7].

Density functional theory (DFT) [8, 9, 10] is a well established method for calculating the structure of molecules. DFT calculates the ground state electron density, as well as the ionization energy and total energy of the molecule. The strong point is, that these quantities are determined not by solving the full interacting many particle problem, but instead by using effective non-interacting quasi-particles. The Hohenberg-Kohn theorems [62, 63] tell us that there is a unique single particle Hamiltonian,  $H = T + v_{\text{eff}}$ , which carries an effective “XC-functional” (exchange correlation functional that only contains the electron density) that will give us the exact energy. The ground state electron density can be found by solving the Kohn-Sham equations:

$$\left(-\frac{1}{2}\nabla^2 + v_{\text{eff}}(\mathbf{r}) - \epsilon_j\right) \phi_j(\mathbf{r}) = 0 \quad (3.1)$$

with

$$v_{\text{eff}} := v_{\text{ext}}(\mathbf{r}) + \int d^3\mathbf{r}' \frac{n(\mathbf{r}')}{|\mathbf{r} - \mathbf{r}'|} + v_{\text{xc}}(\mathbf{r}) \quad (3.2)$$

with first term the externally applied potential, second term the Hartree potential and last term the exchange correlation potential:

$$v_{\text{xc}} := \frac{\delta}{\delta \tilde{n}(\mathbf{r})} E_{\text{xc}}[\tilde{n}(\mathbf{r})] \Big|_{\tilde{n}(\mathbf{r})=n(\mathbf{r})} \quad (3.3)$$

Importantly, the XC-functional,  $E_{xc}[\tilde{n}]$  depends only on the electron density.

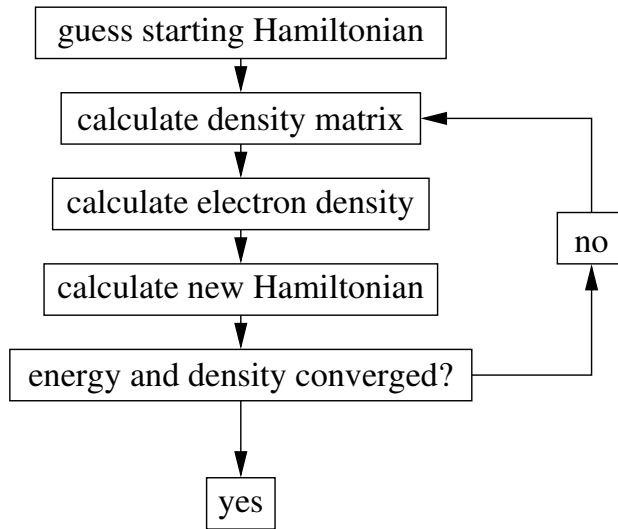
Unfortunately, this XC-functional is not known exactly for realistic systems. Only approximations are available, like BP-86 [64, 65], PBE [66] or B3-LYP [67, 68]. While BP-86 and PBE are GGA functionals, where GGA is a gradient corrected version of LDA, B3-LYP is a hybrid functional, containing both a GGA and a HF part (thus including a portion of exact exchange). It is not always clear which functional will give the best result for a given molecule. In general, only such results can be trusted, which do not depend on the specific choice of the functional.

As mentioned before, the Kohn-Sham method works with a set of non-interacting quasi-particles. The electron density can be calculated from the Kohn-Sham (KS) orbitals,  $|\Phi_\alpha\rangle$ , which are the eigenstates of the Hamiltonian (only occupied orbitals contribute):

$$D = \sum_{\alpha}^{\text{occ.}} |\Phi_\alpha\rangle\langle\Phi_\alpha| \quad (3.4)$$

$$n(\mathbf{x}) = \langle\mathbf{x}|D|\mathbf{x}\rangle .$$

Finding the density with the lowest energy is done in a self-consistent way: starting from a guess for the Hamiltonian, a density matrix is calculated (Eq. 3.4). From this density matrix, the electron density is extracted and a new Hamiltonian constructed. For this step it is important, that the effective pseudopotentials do only depend on the electron density (that we just calculated) This new Hamiltonian is used as the next guess. This process is then repeated until self-consistency is reached, i.e. until the density matrix and the energy of the system change less than a predefined limiting value. Typically, the relative change of both quantities is supposed to be smaller than  $10^{-6}$ .



**Leads in DFT:** As explained before, the leads have a strong influence on the molecule and the transport characteristics of the system. The full leads cannot be included even in the DFT calculation, because of their macroscopic size. In principle, it is possible to calculate the molecule in vacuum without explicit coupling to the leads. Then the leads are taken into account in the transport calculation via a self-energy, which describes the coupling of the molecule system to the surrounding medium, the leads (see Chapter 4).

Including the leads in the self-energy makes the calculation of the molecule numerically very cheap at a first glance, but the self-energy is a very complex operator since it has to contain all information about the interaction between the molecular orbitals and the leads. An exact self-energy for realistic systems is not easily constructed, and approximations often lead to artifacts in the transmission function. Therefore, this method is currently not successfully used for transport calculations for realistic molecules.

Instead of ignoring the leads in the self-consistent (SC) calculation, one can deal with the hybridization by including a finite number of lead atoms in the DFT calculation, introducing the so called “extended molecule” (see Fig. 4.1, and then only couple the extended molecule to leads via a self-energy. The advantage of the extended molecule in comparison of the molecule in vacuum is that hybridization is explicitly included in the DFT calculation. The self-energy of this extended molecule can be shown to be (almost) independent of the molecule, if enough lead atoms are included in the extended

molecule, usually about 50 atoms. In this case reliable approximations for the self-energy are available[69].

## 3.2 Coupling molecules to leads: Quantum chemistry with open boundaries

The coupling of a molecule to a reservoir introduces additional degrees of freedom. Particles can leave the subsystem and disappear in the thermodynamic bath; the system boundaries are now open, and time evolution is no longer unitary. In technical terms, the resolvent operator  $G$  describing the dynamics on the molecular subspace has the structure

$$G^{-1}(E) = G_0^{-1}(E) - \Sigma(E) \quad (3.5)$$

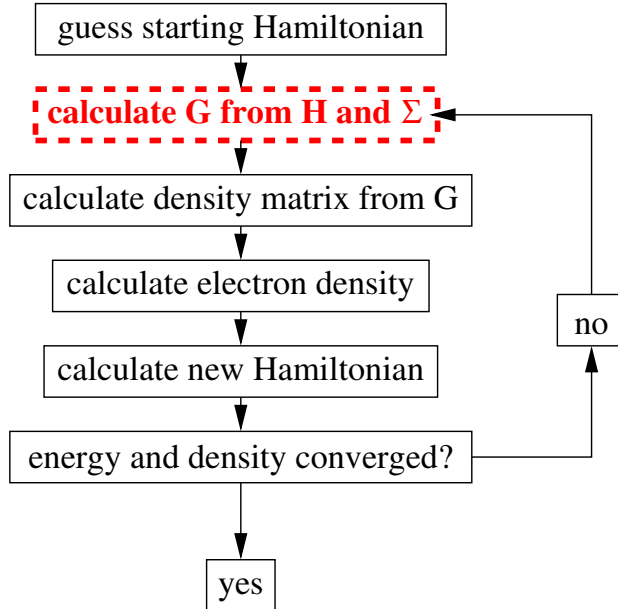
with  $G_0 = E - H + i0$  describing the uncoupled extended molecule[70]. As  $H$  the KS-Hamiltonian is used. This equation is a definition of the self-energy  $\Sigma$ , describing the coupling between the subsystem and the reservoir. At this point, we do not need to know how to calculate  $\Sigma$ , this will be explained in Chapter 4.

If the molecule is coupled to a reservoir, the calculation of the density matrix,  $D$ , cannot exclude the self-energy. Therefore, one can no longer use Eq. (3.4). Instead, one has to use:

$$\begin{aligned} n(\mathbf{x}) &= \sum_{i,j} \langle \mathbf{x}|i \rangle D_{ij} \langle j|\mathbf{x} \rangle \quad (3.6) \\ D &= \frac{1}{2\pi i} \int_{-\infty}^{E_F} [G(E) - G^\dagger(E)] dE \\ &= \frac{1}{\pi} \int_{-\infty}^{E_F} \text{Im}\{(E - H - \Sigma(E))^{-1}\} dE \quad (3.7) \end{aligned}$$

Here,  $i$  and  $j$  are the basis functions in which the density matrix,  $D$ , is expressed, and  $\mathbf{x}$  the location where the density,  $n$ , is evaluated. If the coupling  $\Sigma$  is set to  $i0$ , one gets exactly the result for the molecule in vacuum.

Compared to the calculation for closed boundaries (vacuum, see previous Section), the algorithm for the construction of the density matrix has been changed:



Numerically this procedure is complicated, since now we have to integrate Green's function, a complex matrix, over the energy (see Eq. 3.7). How this integration can still be done is explained e.g. in Ref. [29]. But we want to present a different way in the following.

**Model self energies:** Up to now it has been just explained the formalism for including open boundaries into the self-consistency cycle of e.g. DFT. Now we want to explain how one uses a model self-energy to simplify the calculations. The Green's function contains the self-energy, which in general depends in a nontrivial way on the energy. Integrations are simplified dramatically if simple model self-energies can be used. The most important simplification is that model self-energies can be constructed which are independent of the energy, so that the inverse Green's function will again be linear in energy and can be integrated analytically. Such models can deliver essentially exact results if used with care, as presented shortly below.

We diagonalize the complex Matrix  $H + \Sigma$  and calculate Green's function from the eigenstates and -energies. The eigenvectors are independent of

the energy, so only the eigenvalues of Green's function,  $\frac{1}{E-Z_k}$  have to be integrated over energy (this calculation is done at  $T = 0^2$ ):

$$\begin{aligned} G(E)^{-1} &= E - H - \Sigma \\ V &\hat{=} \text{matrix of right eigenvectors of } H + \Sigma \\ Z_k &\hat{=} \text{eigenvalues of } H + \Sigma \end{aligned} \quad (3.8)$$

$$D_{ij} = -\frac{1}{\pi} \sum_k V_{ik}^{-1} V_{kj} \int_{-\infty}^{E_F} \frac{dE}{E - Z_k} \quad (3.9)$$

$$= -\frac{1}{\pi} \sum_k V_{ik}^{-1} V_{kj} \log(E - Z_k) \Big|_{-\infty}^{E_F} \quad (3.10)$$

This density matrix is now used as the new density matrix inside the self-consistency loop of DFT. As in standard DFT, a diagonalization of the Hamiltonian is needed (which is, depending on the functional, often a dominating part). However, here the matrix is complex, thus increasing the effort by a factor of three.

### 3.3 Applying bias voltages: non-equilibrium calculations

In the previous section, it was presented how to couple a molecule to a single reservoir with open boundaries. The reservoir is in equilibrium with itself as well as with the molecule. An extension of the formalism can also be applied to the case of two reservoirs, where each reservoir is by itself in thermodynamic equilibrium, while the combined system does not have to be. Each reservoir has its own chemical potential,  $\mu_L$  and  $\mu_R$ , leading to a finite bias voltage between the reservoirs.

---

<sup>2</sup>The effect of a finite temperature in the leads would be a finite smearing of the orbital energies. In the molecules we studied, the temperature smearing was at least one order of magnitude smaller than the life time broadening  $\Gamma$  of the orbitals we were interested in, so  $T = 0$  is justified.

One can use this method to simulate a finite voltage applied to a molecule coupled to leads. This allows to analyze the transmission function,  $I(V)$ -curve and change of the orbitals due to the bias voltage.<sup>3</sup>

In case of two reservoirs, where each contributes with its own self-energy  $\Sigma_L$  and  $\Sigma_R$ , the Green's function can be evaluated as:

$$G^{-1} = G_0^{-1} - \Sigma_L - \Sigma_R \quad (3.11)$$

This expression is exact because it can be understood as a definition of the self-energies  $\Sigma_{L/R}$ ; but the exact calculation of  $\Sigma_L$  and  $\Sigma_R$  is tedious. The coupling will be explained in more detail in Chapter 4.

Calculation of the density matrix in the non-equilibrium regime is carried out within the Keldysh formalism for non-interaction electrons [70].

$$D = \frac{i}{\pi} \int dE G^<(E) \quad (3.12)$$

$$G^< = G \Sigma^< G^\dagger \quad (3.13)$$

$$\Sigma^< = if(\mu_L)\Gamma_L + if(\mu_R)\Gamma_R \quad (3.14)$$

$$\Gamma_{L/R} = \frac{i}{2}(\Sigma_{L/R} - \Sigma_{L/R}^\dagger) \quad (3.15)$$

Here, we have two different self-energies for the left and right reservoir,  $\Sigma_L$  and  $\Sigma_R$ , and  $f(\mu)$  the Fermi function.

Let us proceed with the derivation of the equations we are using to calculate the density matrix in a non-equilibrium situation. Starting from the Keldysh Green's function (Eqns. (3.13)-(3.15)):

$$G^<(E) = iG(E) (f(\mu_L)\Gamma_L + f(\mu_R)\Gamma_R) G^\dagger(E) \quad (3.16)$$

one can calculate the density matrix:

$$D(\mu_L, \mu_R) = \frac{i}{\pi} \int_{-\infty}^{\infty} G^<(E) dE \quad (3.17)$$

---

<sup>3</sup>Including the bias voltage into the self-consistency loop of DFT will give a steady state. In this calculation no external electric field appears, and the E-field near the molecule is produced by the Hartree field at the lead electrons. This is a technical advantage as compared to methods based on periodic boundary conditions (like TranSIESTA [71]), since there an external electric field has to be explicitly included [29] due to an implicit constraint of  $\mu = \text{const.}$ .

The calculations are done at zero temperature,  $f(\mu) = \Theta(\mu - E)$ . The density can be calculated as the sum of two parts. In the first part, below the chemical potential of both leads, all states are occupied. In the other part, only the states of one lead are occupied, while the other lead is empty. Let us now assume  $\mu_L < \mu_R$ :

$$D(\mu_L, \mu_R) = -\frac{1}{\pi} \int_{-\infty}^{\mu_L} G (\Gamma_L + \Gamma_R) G^\dagger - \frac{1}{\pi} \int_{\mu_L}^{\mu_R} G \Gamma_R G^\dagger \quad (3.18)$$

$$= D_{\text{eq}}(\mu_L) + D_{\text{neq}, R}(\mu_L, \mu_R) \quad (3.19)$$

The first integral is already known from the equilibrium situation, while the second part is more complicated:

$$D_{\text{eq}}(\mu_L) := -\frac{1}{\pi} \int_{-\infty}^{\mu_L} \text{Im}(G(E)) dE \quad (3.20)$$

$$D_{\text{neq}, R}(\mu_L, \mu_R) := -\frac{1}{\pi} \int_{\mu_L}^{\mu_R} G(E) \Gamma_R G^\dagger(E) \quad (3.21)$$

In the non-equilibrium situation, we have two parameters, namely the chemical potentials of the two leads. The applied bias voltage corresponds to the difference in the chemical potential,  $\mu_R - \mu_L$ , but the average chemical potential,  $\frac{1}{2}(\mu_R + \mu_L)$ , still has to be adjusted so that the full system, including the leads, is charge neutral, just as for the equilibrium case above. This global charge neutrality condition fixes the average chemical potential. Note, that since the density of states (DoS) of the lead material does not have to be energy independent, the average chemical potential can change even if large leads are included in the extended molecule.

For practical calculations, the easiest way (as well as fastest in computation time) is to fix the average chemical potential and check the electron number of the extended molecule after convergence. One then adjusts the average chemical potential and repeats the calculation until charge neutrality is reached.<sup>4</sup>

---

<sup>4</sup>However, this will only work for small bias voltages and a symmetric molecule and lead. In other cases, one has to adjust the electron number “on the fly” in the self-consistency loop: at each iteration, the average chemical potential is adjusted in order to retain charge neutrality of the molecule. This increases the calculation time, but reduces the steps

For a self-energy independent of  $E$  one can do the integration analytically, see Eq. (3.24) and (3.25) below. The diagonal Green's function, Eq. (3.8), from the equilibrium calculation enters here again:

$$\begin{aligned} D_{\text{full}} &= D_{\text{eq}} + D_{\text{neq}} \\ &= D_{\text{eq}}(\mu_L) + D_{\text{neq}, R}(\mu_L, \mu_R) \\ D_{\text{neq}, R} &= -\frac{1}{\pi} \int_{\mu_L}^{\mu_R} G(E) \Gamma_R G^\dagger(E) \end{aligned} \quad (3.22)$$

$$= -\frac{1}{\pi} \int_{\mu_L}^{\mu_R} V^{-1} G_{\text{diag}}(E) V \Gamma_R V^\dagger G_{\text{diag}}^*(E) V^{\dagger-1} \quad (3.23)$$

$$=: -\frac{1}{\pi} V^{-1} M V^{\dagger-1} \quad (3.24)$$

$$M_{ij} = (V \Gamma_R V^\dagger)_{ij} \int_{\mu_L}^{\mu_R} \frac{1}{E - Z_i} \frac{1}{E - Z_j^*} dE \quad (3.25)$$

Now we can use this density matrix inside the DFT-SC loop. From this we will get the electron density under finite bias in a fully self-consistent way.

### 3.4 Transport from density functional theory calculations

Now knowing how to calculate the electronic structure of molecules coupled to leads, let us continue and have a look at ways of obtaining the transmission function from this data. As explained before in Sec. 3.3, the molecule is coupled via the self-energies  $\Sigma_{L/R}$  to infinite leads, [72], and Green's function was presented in Eq. (3.11).

The transport through the molecule is calculated within scattering theory [73, 74]. Here we assume that the timescales of relaxations are much slower than the time an electron needs to travel through the system (coherent regime). An electron that enters with an energy  $E$  will either be transmitted or reflected, but it will keep its energy  $E$ . For each energy, the

---

needed until convergence. Thus it can be faster, if the voltage drops not symmetrically, i.e. the average chemical potential differs from the equilibrium value.

transmission of a particle through the molecule can be calculated with an incarnation of the Landauer formula [75]:

$$T(E) = \text{Tr} \Gamma_L(E) G(E) \Gamma_R(E) G^\dagger(E) \quad (3.26)$$

with  $\Gamma_{L/R} = \text{Im} \Sigma_{L/R}$ .

If one wants to determine the current-voltage behavior of a molecule, one has to calculate for each bias voltage a new transmission from the DFT result including the bias, as explained above.

To calculate the  $I(V)$ -curve from the transmission function, one only has to integrate  $T(E)$  in the voltage window between the different chemical potentials:

$$I(V)_{\text{non-SC}} = \int_{\mu_L}^{\mu_R} T(E) dE \quad \text{with} \quad V = \mu_R - \mu_L \quad (3.27)$$

However, this will only give a non-SC  $I(V)$ -curve, where the feedback of the bias voltage on the transmission function is not included, which works well in linear response. To include the feedback, one has to repeat the calculation of the transmission function for every bias voltage:

$$I(V)_{\text{SC}} = \int_{\mu_L}^{\mu_R} T(E, V) dE \quad (3.28)$$



# Chapter 4

## Coupling of molecules to leads: Self-energies

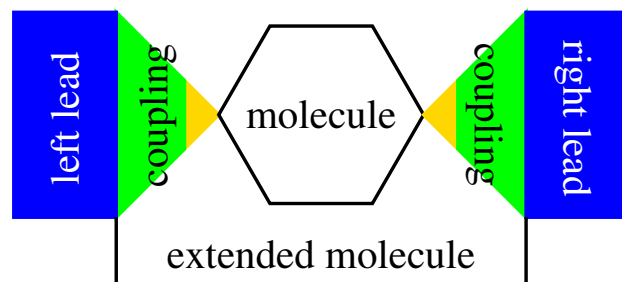


Figure 4.1: Schematics of coupling of molecules to leads. The contact has been partitioned into tractable sections: the leads and the extended molecule. Part of the extended molecule is the coupling region, where a finite part of the lead is coupled to infinite leads.

In Chap. 3, Eq. 3.5, a self-energy in order to describe the coupling of a molecule to external reservoirs with an eye on transport calculations was introduced. Its exact explicit definition is given below, in Eq. 4.2. Since this expression is difficult to evaluate for realistic systems, model self-energies are a very important tool for practical calculations. In order to motivate their construction, we will explain in detail what the self-energy of interest means in physical terms.

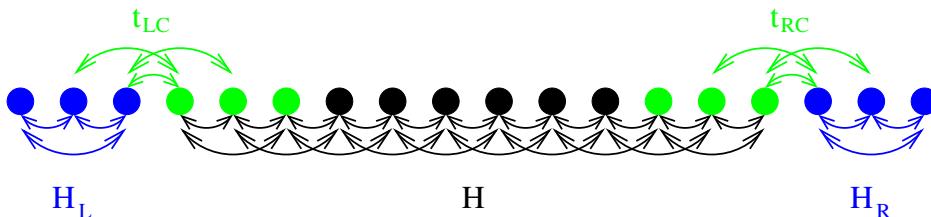


Figure 4.2: Extended molecule as realized in a tight binding chain. The left and right leads (blue dots) and the extended molecule (green and black dots) each have their own Hamiltonian. The extended molecule contains a coupling region (green dots) which is coupled via hopping matrix elements to the leads,  $t_{LC}$  and  $t_{RC}$ .

## 4.1 Basic formalism

Now let us proceed with the formal construction of the self-energy. Since we are only able to deal either with finite or periodic systems, we have to partition the full system into numerically tractable sections. An appropriate partitioning has been depicted in Fig. 4.1.

The part of the molecule, that enters explicitly the *ab initio* calculations, is called the “extended molecule”. It contains the molecule itself and a finite part of the leads, the so called coupling region, and is described by the Hamiltonian  $H^{\text{eM}}$ . We have to combine the partial systems to get the Hamiltonian of the full system,  $H_{\text{full}}$ :

$$H_{\text{full}} = \begin{pmatrix} H_L & t_{LC} & 0 \\ t_{LC}^\dagger & H^{\text{eM}} & t_{RC}^\dagger \\ 0 & t_{RC} & H_R \end{pmatrix} \quad (4.1)$$

with  $H_{L/R}$  the Hamiltonians of the leads,  $H^{\text{eM}}$  the Hamiltonian of the extended molecule, and  $t_{LC/RC}$  the hopping from the leads to the extended molecule and back. The direct hoppings from the left to the right lead (and back) can be neglected (see Fig. 4.2).

To calculate transport properties we need Green’s function of the full system, including the leads. However, the transport theory is set up in such a way, that only the part of the full Green’s function located on the extended molecule enters explicitly. The leads enter only as a shift of the

bare molecular Green's function,  $G_0^{-1} = E - H^{\text{eM}} + i0$ , which defines  $\Sigma$ :

$$G^{-1}(E) = G_0^{-1}(E) - \Sigma(E) = E - H^{\text{eM}} - \Sigma(E) \quad (4.2)$$

A straightforward calculation shows, that

$$\Sigma_X(E) = t_{XC}^\dagger G_X(E) t_{XC} \quad \text{with} \quad X = L, R \quad (4.3)$$

with  $G_{L/R}^{-1} = E - H_{L/R} + i0$  and the hopping matrix elements from lead to the extended molecule,  $t_{LC}$  and  $t_{RC}$ .

Direct evaluation of Eq. (4.3) to calculate  $\Sigma$  is challenging. What is needed is  $G_{L/R}^{-1}$  in the presence of an interface to the extended molecule. We know how to calculate the Hamiltonian of each subsystem, but the couplings are quite complicated to obtain with high accuracy, because hopping is not a short range process<sup>1</sup>. Therefore, in our opinion, it is highly desirable to keep the cluster size sufficiently large for a well controlled calculation of the hybridization matrix elements  $t_{LC/RC}$ . If this condition is satisfied, the calculations are indeed simplified dramatically because  $t_{LC/RC}$  becomes independent of the details of the molecular junction<sup>2</sup>. In this case the hopping matrix elements  $t_{LC/RC}$  can be extracted from a separate large cluster calculation again[72].

## 4.2 Role of the self-energy

Self-energies define the coupling between the molecule and the lead. In this section we explain how the self-energy affects the local spectral function (local DoS) and the transmission of the extended molecule.

We already learned in the previous section, that one does not calculate the isolated molecule, but rather an extended molecule with a part of the leads included. If such a procedure is followed, the hybridization between the molecular orbitals and the leads is already included in the DFT calculation (if the hybridization is not included, it has to be added via the self-energy, making simple approximations for  $\Sigma$  inappropriate).

---

<sup>1</sup>For an extraction of the band structure, e.g., one needs at least 10th order hopping to obtain the infinite cluster limit[72].

<sup>2</sup>The precise meaning of ‘‘sufficiently large’’ depends on the lead material, geometry and the molecule itself. The rule of thumb is that the level spacing on the extended molecule should be much smaller than any other physically relevant energy scale.

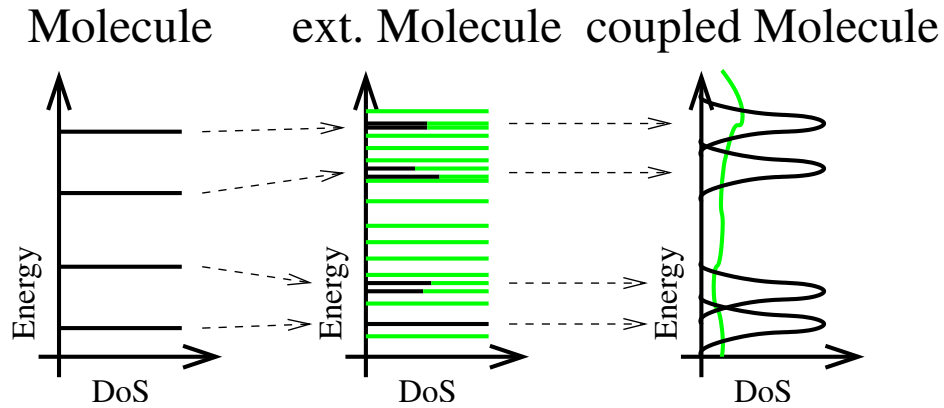


Figure 4.3: Scheme of the DoS for coupled molecules. The left graph describes the molecule in vacuum with only a few isolated molecular orbitals. Center: in the extended molecule there are additional orbitals localized on the lead (green). The energies of the orbitals shift a bit and the levels hybridize with the leads. Right: in the fully coupled molecule the leads form the DoS of the lead material (green), the orbital energies of the molecular orbitals are broadened (black).

Let us assume that we are in the limit, where increasing the extended molecule by adding more lead atoms does “not affect” the molecular orbitals any more. For e.g. the Benzene molecule, the limit can be reached at  $\sim 14$  Gold atoms per lead, which can easily be calculated within DFT. Note, that in many cases, a lot larger leads have to be taken into account, often around 50 Gold atoms and more.

Within this limit, one can use a simple model for the self-energy and still get the (in principle) exact spectral function. This is essentially because hybridization is already included in the DFT calculation and thus does not have to appear in the self-energy again.  $\Sigma$  only provides a small level broadening, which makes the spectrum smooth, with the physical meaning of inelastic effects in the leads, like coupling to phonons. Fig. 4.3 shows the schematic difference between the isolated molecule, the extended molecule and the molecule coupled to a reservoir. In the extended molecule, the molecular orbital energies of the uncoupled molecule are shifted, and hybridize with the additional lead orbitals. Due to the (infinitesimal) inelastic broadening, the DoS finally becomes smooth.

The width of the peaks in the transmission function is not directly related

to the level broadening of the orbitals on the lead. If the level spacing of the extended molecule is smaller than lifetime broadening of the molecular orbitals, this broadening is due to hybridization with many orbitals of the extended molecule. On the other hand, if the level width is comparable to or smaller than the level spacing, this model self-energy cannot be used reliably. But it will be shown further below that for the molecules we are interested in it is applicable. In terms of energies, we have a clear hierarchy:

$$\Delta E^{\text{eM}} \ll \eta \ll \min \{ \Gamma, \Delta E^{\text{M}} \} \quad (4.4)$$

where  $\Delta E^{\text{eM}}$  is the level spacing in the *extended* molecule,  $\eta$  is the level broadening,  $\Gamma$  the width of molecular orbitals, and  $\Delta E^{\text{M}}$  is the level spacing on the molecule itself. The lowest energy scale on the molecule itself (in cases we are interested in) is  $\Gamma$ .

### 4.3 Understanding self-energies as absorbing boundaries

The formalism described in Chap. 3 has been developed for non-interacting particles, meaning we can understand the electrons moving through the molecule as waves. A wave traveling through the molecule will enter at the left lead and then leave through the right lead. Importantly, there should be no reflection from the right boundary, because there the *extended* molecule couples to a perfectly transmitting metal.

To mimic wave propagation in infinite systems using only a finite one, we have to ensure that the wave is completely absorbed within the outer coupling region (see Fig. 4.4(bottom) and compare to Fig. 4.4(top), where the boundaries do not absorb). As known e.g. from optics, this can be obtained by adding a finite imaginary part to the Hamiltonian (optical potential), leading to a finite lifetime of the particles in the orbitals. Time evolution is no longer unitary, because particles can leave the system into the bath, where they are fully absorbed.

This is incorporated in the anti-hermitean piece of the self-energy, see Eq. 4.3. This piece is confined to the interface, where it absorbs all incoming waves. Therefore, we can use a model, the “absorbing boundary conditions”, that takes care of the absorption of waves in the interface region.

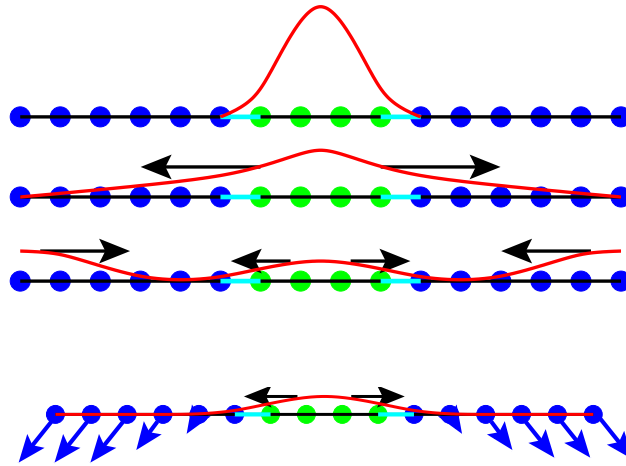


Figure 4.4: Reflecting (top) and absorbing (bottom) boundaries. In the reflecting case, a wave propagating in the molecule will be reflected at the boundaries, creating a standing wave solution to our wave propagation problem, which will be seen in the transmission function as additional (and completely artificial) resonance peaks. In the absorbing case, the wave is completely absorbed.

### 4.3.1 Model self-energy

To construct a model self-energy one has to ask: what do we have to include in our model self-energy and what is already included in the extended molecule?

The coupling to the leads causes a shift in the molecular orbitals due to hybridization with the lead orbitals, which is included in the extended molecule. Depending on the surface of the leads and the molecule itself, the shift will converge quite fast, i.e. the levels will not move in energy as a function of the number of Gold atoms,  $N_{\text{Au}}$ . The DoS of the leads is included, too. For large  $N_{\text{Au}}$ , the DoS will be close to the DoS of an infinite system<sup>3</sup>. The major contribution that is not included in the extended molecule is a finite broadening of the levels, which originates in reality from inelastic processes in the leads.

Up to now we only discussed adding an imaginary part to the Hamiltonian, meaning a purely imaginary self-energy. But what about a real part?

<sup>3</sup>The DoS is not smooth, because the number of orbitals is still finite. But a small broadening will lead to the smooth DoS of the infinite system.

This part mainly shifts the orbital energies<sup>4</sup>. In a non-SC calculation of the transmission function, where the self-consistency loop of DFT does not know about the coupling to infinite leads, this real part will only deform the local DoS in the leads.

However, in a fully self-consistent calculation, where the coupling is included in the DFT loop, this shift is crucial for fixing the local DoS in the coupling region. Without this shift, the imaginary part will deform the local DoS dramatically, and thus charge neutrality of the leads is no longer guaranteed. The real part has to be adjusted such that the full extended molecule is charge neutral.

There are many different model self-energies that can be used, because the smooth form of the spectral or transmission function is ignorant to details of the level broadening. We will use a particularly simple one: a local energy shift and level broadening in the defined coupling region. The self-energy will only have diagonal elements, independent of the energy, in a representation in coordinate space:

$$\Sigma(x, x') = \begin{cases} 0 & \text{if } x \notin \text{coupling region} \\ (i\eta + s)\delta(x, x') & \text{if } x \in \text{coupling region.} \end{cases} \quad (4.5)$$

One has to always check whether the limit is reached, in which the results e.g. for  $T(E)$  do not depend on the size of the extended molecule or the details of the level broadening. In the following sections we will show how that can be checked.

### 4.3.2 How to check the convergence of the results

There are several different parameters in our model:

- $N_{\text{Au}}$ : number of Gold atoms included in the extended molecule
- $N_{\text{S}}$ : number of Gold atoms in the surface region coupled to the infinite leads
- $\eta$ : broadening of energy levels
- $s$ : shift of orbital energies

---

<sup>4</sup>The orbitals will be deformed as well, but does not strongly affect the transport properties.

To still have an *ab initio* calculation, one has to ensure, that there is a plateau in the parameter space, where the results, for e.g.  $T(E)$ , are essentially independent of any of the parameters.

**Number of Gold atoms and flow analysis:** The convergence in  $N_{\text{Au}}$  is very important. Luckily, this check is fairly straight forward to perform by repeating the calculation for the molecule with different lead sizes and geometries. We usually use tetragonal pyramids, because the symmetry eventually allows for the treatment of larger pyramids.

The fastest way to find the interesting orbitals for transmission is to do a Mulliken analysis of all orbitals. In this analysis, the orbitals are projected on the basis functions of the molecule, which gives the relative weight  $A_\nu$  of each orbital on the molecule. Values close to 0 are localized on the Gold leads, while values close to 1 are localized on the molecule. Orbitals contributing to the transmission usually lie in between.

This analysis can be repeated for different lead sizes. Fig 4.5 shows the result for BDT in  $D_{2h}$ -symmetry; the flow of the orbital energies can be clearly seen. The relative energy compared to  $E_F$  is almost converged for  $N_{\text{Au}} = 14$  Gold atom leads. From this point on the calculation of the transmission can give good results. To illustrate the effect of the hybridization, two orbitals are shown in Fig.4.6. The upper orbitals do not show any hybridization, while the lower orbital strongly hybridizes with the leads.

In the flow analysis (lower part of Fig. 4.5) an important effect for finite clusters can be seen: some Gold clusters are charged  $\pm 1$  in ground state. In this case, the finite cluster will charge the molecule in order to get a stable electron configuration. The change of the number of electrons on the molecule shifts all orbital energies. This will only happen for a few magic clusters, while cluster with neighboring sizes will not show this effect. This is a real physical effect of small Gold clusters, but complicates the extrapolation to the thermodynamic limit.

There is more information contained in this flow analysis. The flow presents the hybridization of orbitals with the leads. The molecular orbitals split into hybridized orbitals with less weight on the molecule, but the total weight is still one. E.g. an orbital fully localized on the molecule can split into two orbitals with half weight each on the molecule and the leads. Due to coupling to different lead orbitals, the energy of the two new orbitals will be different, while the wave function on the molecule will look the same.

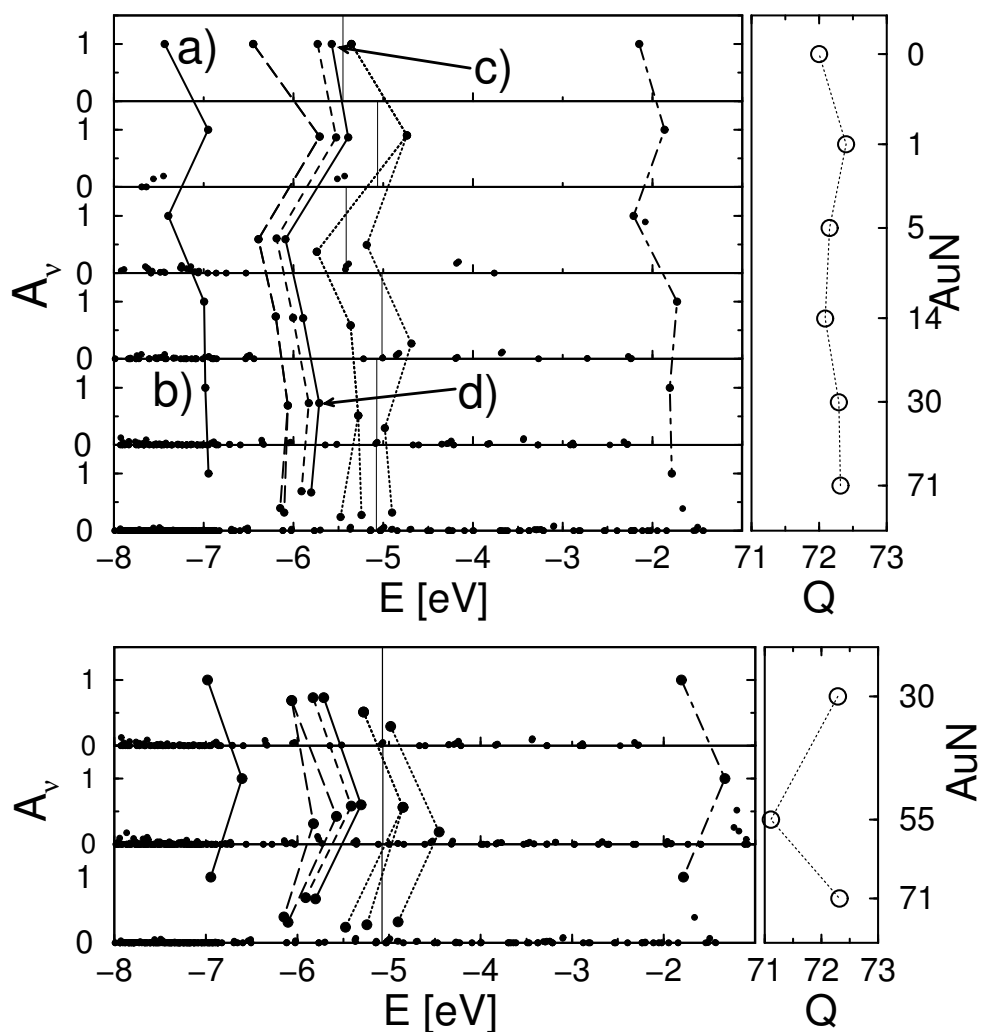


Figure 4.5: Flow of Benzene di-thiol (BDT) orbitals. The lead geometries are tetragonal pyramids of different sizes. The upper plot shows the convergence of the orbital energies as a function of  $N_{\text{Au}}$ . The left part presents the relative weight  $A_v$  of the orbitals on the molecule. Values close to 0 are orbitals located on the Gold, while values close to 1 are located on the molecule. The right part of the plot shows the number of electrons on the BDT. The lower plot shows the result for the 55 atom pyramid, where the Benzene ring is charged +1 and all orbitals are shifted. This is an effect specific to this special geometry. In Fig.4.6 the orbitals a)-d) are shown.

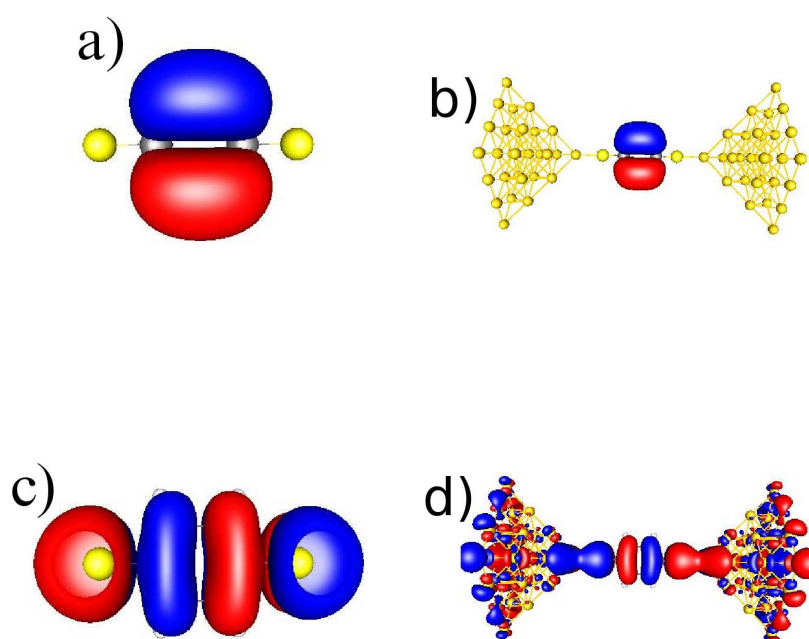


Figure 4.6: Orbitals of Benzene di-thiol. Presented is the hybridization of two different orbitals with 30 atom Gold leads. While one orbital stays completely localized on the molecule, the other one shows a strong hybridization.

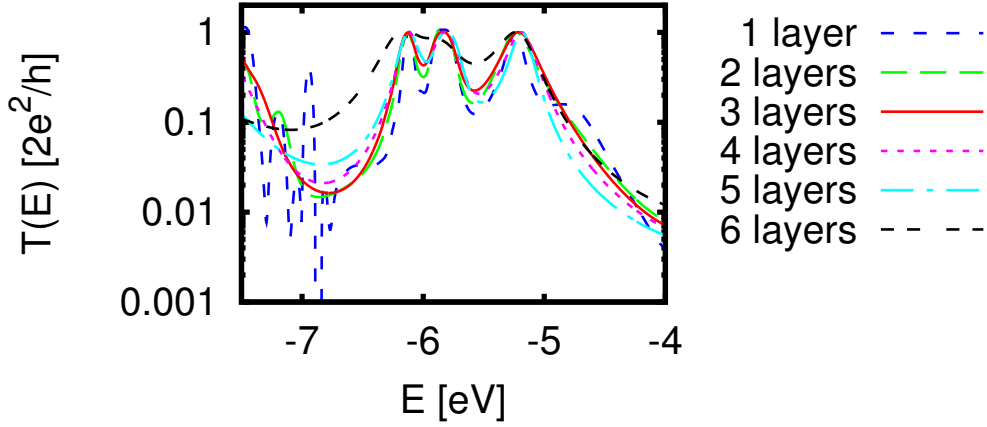


Figure 4.7: Transmission of BDT for different  $N_S$  (BDT coupled to pyramid with 6 layers,  $4 \times 4$ ,  $5 \times 5$ ,  $4 \times 4$ ,  $3 \times 3$ ,  $2 \times 2$ ,  $1 \times 1$ ). Only full layers of Gold are coupled. The broadening was chosen such that the total leakage ( $N_S \eta = 2.85$ ) is constant. The plot shows that one layer is not enough, resulting in large oscillations. On the other hand, if there is not enough Gold between the coupling and the molecule itself, the leakage onto the molecule is too large, while between 2 and 4 layers the calculations present comparable results, the peak position and width is almost the same.

The energy difference between those orbitals is an estimation of the width  $\Gamma$ . There are orbitals localized on the molecule even for large leads, which do not show any hybridization.

Another really important information can be found in the analysis: the level spacing of the extended molecule. As one can see in this plot, Gold does not provide a constant DoS (the dots with only very few weight on the molecule); close to  $E_F$  the level spacing is a lot larger than at -8 eV. The broadening of the molecular levels by the model self-energy has to be larger than this local spacing.

**Number of coupled Gold atoms:** The next step is the convergence in  $N_S$ . If the number is too small, the absorption will be too weak. But if the coupling region is chosen such that there is no spatial separation between the coupling region and the molecule itself, the interaction between the molecule and the coupling region is too strong, leading to an overestimation of the

level broadening. Basically, one has to repeat the calculation for different numbers of coupled Gold atoms in order to test the convergence. If the lead included in the extended molecule is small (e.g. 14 or less atoms for Benzene), we cannot expect our model to be robust under variation of the parameters. There is only one way to couple for the transmission: 2 layers (13 atoms) to prevent reflections and leading to a transmission function comparable to larger leads. But this is just because 14 atoms is the lower limit for the model to be applicable. Increasing  $N_{\text{Au}}$  will allow for a greater variation.

Fig. 4.7 shows the convergence for the 71 atom gold lead. For this calculation the total absorption  $N_C \times \eta = 2.85 \text{ H}$  was chosen constant in order to get comparable results, where  $\eta$  is the local absorption rate. The result shows that coupling of only one layer is not enough, leading to strong unphysical oscillations. Between two and four layers the result is hardly changing at all. But if five or six layers are coupled, the broadening is much too strong, due to a direct overlap onto the molecule as explained before.

**The broadening  $\eta$ :** The check for convergence in the broadening  $\eta$  is easy, as well. The calculation has to be repeated for different  $\eta$ . There will be a region of the broadening in which the transmission is independent of  $\eta$ , provided that the extended molecule is in the regime, where the energy hierarchy Eq. (4.4) holds. The larger this region is, the better the result is converged. Fig. 4.8 shows this for Benzene di-thiol coupled to 14 Gold atoms, and Fig. 4.9 the same for  $N_{\text{Au}} = 71$  and  $N_C = 66$ . The larger pyramid shows a clearly better convergence for varying  $\eta$ .

**The level shift  $s$ :** The energy shift has to be adjusted in a manner providing that the leads remain charge neutral. This parameter is needed, because the imaginary part of the self-energy changes the local DoS on the coupling region. Note, that it is only needed due to the finite size of the coupling region. In an infinite coupling region, the broadening is infinitesimally small and thus the local DoS unchanged.  $s$  is not a free parameter at all, so the results do not have to be independent of it.

## 4.4 Test calculation: a tight binding chain

To demonstrate that the absorbing boundary condition can give exact results in the proper limits, we employ a model that we can solve analytically. For

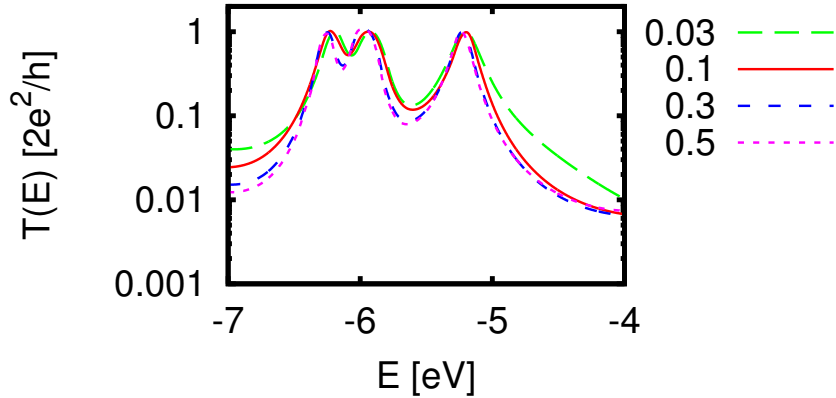


Figure 4.8: Dependence of the transmission on the parameter  $\eta$  [H]. The lead is a 14 Gold atom pyramid. The last 2 Layers (13 atoms) are coupled with our model self-energy. Close to the peaks the result does not depend on the parameter  $\eta$ , but in the regions with small transmission (like in this case the HOMO-LUMO gap), the numbers are not reliable. In this regions, calculations with much larger clusters are needed (see Fig. 4.9). Self-energies calculated from large gold clusters will often fail in these regions because of the large level spacing. The self-energy has to be almost exact in order to get the correct answer, resulting in failure of many approximations.

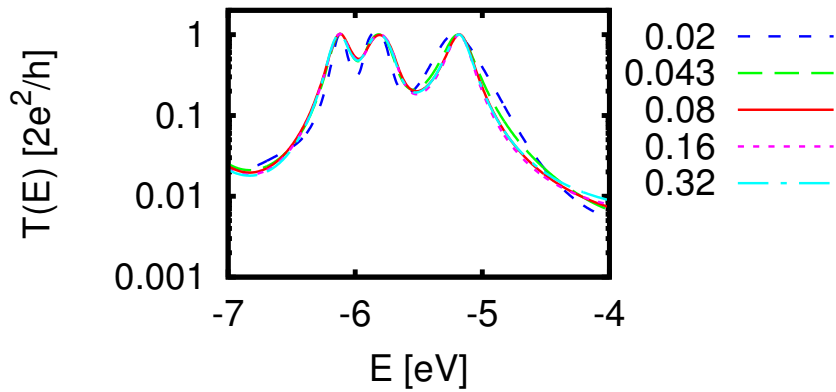


Figure 4.9: Dependence of the transmission on the parameter  $\eta$  [H] for a 71 atom Gold pyramid. This is the same as Fig. 4.8, but 66 out of 71 Gold atoms were coupled for the calculation of the transmission.  $\eta$  can be changed by more than an order of magnitude without influencing the transmission.

this model, we can compare numerical and analytical results in order to explore the limits of the model assumptions. The model that we consider is a tight binding chain with a triple barrier, see Fig. 4.10.

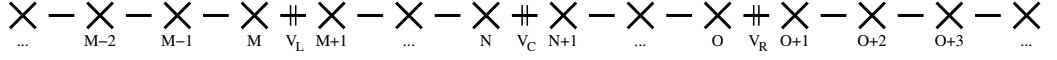


Figure 4.10: A triple barrier tight binding chain.  $M$ ,  $N$  and  $O$  are the positions of the barriers,  $V_L$ ,  $V_C$  and  $V_R$  are the hopping probabilities at the barriers. The hopping outside the barriers is unity,  $t = 1$ .

For  $M = 0$ ,  $N = 2$  and  $O = 4$  the transmission will show a double peak at an energy close to the hopping  $t$  due to having a symmetric and an antisymmetric wave function. The width of the peaks is controlled by the left and right barrier heights,  $V_{L/R}$ , and the splitting of the peaks is governed by the central barrier,  $V_C$ .

#### 4.4.1 Absorbing boundaries

For the numerical calculation of the transmission using the apparatus introduced in Chap. 3.4 we have to specify the molecule, the extended molecule including the coupling region, and the choice of  $\eta$ . The molecule is the triple barrier, containing sites  $M$  to  $O + 1$ . For the extended molecule, we increase the length of the chain to  $L$ , where the barrier at site  $N$  is located in the center. The coupling region consists of all sites outside the ‘‘molecule’’.

The coupling parameter  $\eta$  should not be kept constant in this simple model, because it would lead to reflections at the surface of the coupling region. This is an effect, that is particularly significant in low dimensional systems and becomes less important in 3d electrodes. So, we modulate  $\eta$  to a smoothly increasing absorption inside the coupling region

$$\begin{aligned} \Gamma_L(x, x') &= \eta \delta(x - x') f(x - x_L) \Theta(M - x) \\ \Gamma_R(x, x') &= \eta \delta(x - x') f(x_R - x) \Theta(x - (O + 1)) \end{aligned} \quad (4.6)$$

where  $f(x)$  is the Fermi function. There are a lot of parameters: the inverse ‘‘temperature’’  $\beta$ , which defines the width of the crossover region, the distance  $x_{L/R}$  of the absorption zone, the absorption strength,  $\eta$ , and of course the size of the extended molecule  $L$ .

Now we are able to calculate the transmission of the model using the formalism explained in Chap. 3.4:

$$\Sigma = i(\Gamma_L + \Gamma_R) \quad (4.7)$$

$$G^{-1} = E - H - i(\Gamma_L + \Gamma_R) \quad (4.8)$$

$$T(E) = \text{Tr} \Gamma_L G(E) \Gamma_R G^\dagger(E) \quad (4.9)$$

The level spacing of the “lead orbitals” is of the order of  $\frac{1}{L}$ , while the splitting between symmetric and anti-symmetric solution is in the order of  $V_C$ . The width of the two peaks is in the order of  $(V_{L/R})^2 \rho_F$ , where  $\rho_F$  is the DoS at the Fermi energy. For a barrier height of 0.1, the energetic hierarchy Eq. (4.4) needed for our model self-energy is satisfied for a length of the system of  $L = 100$ , which is easily reached. Fig. 4.11 shows the result in comparison to the analytical calculation (see Appendix C).

The deviation of the numerical and analytical result for different length of the chain is shown in Fig. 4.12. Even for the smallest system size  $L = 64$ , the relative deviation between the numerical and analytical result is smaller than 2%. For larger systems, which satisfy the hierarchy, the relative error drops to below  $10^{-4}$ .

The model self-energy is a good approximation, if one can vary the parameters in a broad range without changing the transmission function. This was done for  $\beta$  between 0.01 and 1 (Fig. 4.13) and  $\eta$  between 0.1 and 10 (Fig. 4.14). The length of the chain was fixed to  $L = 128$  for these tests (which leads to a level spacing only slightly smaller than  $\Gamma$  of the “molecular orbitals”) to show the failure of the approximations as well. The range for  $\beta$  has to be adjusted such that the crossover is smooth, i.e. “adiabatic”. For values smaller than 0.1 and the given parameters,  $\eta$  will jump at the barrier, while for values of 1 or larger  $\eta$  will change abruptly from 0 to 1. The variation of  $\eta$  shows that for too small absorption reflections on the boundaries appear, leading to strong (unphysical) oscillations in the transmission function. For the other values (1 and 10) the relative error is again in the order of  $10^{-4}$ . Importantly, for all calculations the peak position is nearly exact, even if the model self-energy shows a clear breakdown in the regions of small transmission.

Additionally, we changed the self-energy from the diagonal form to a full coupling between all atoms in the coupling regions without a noticeable effect

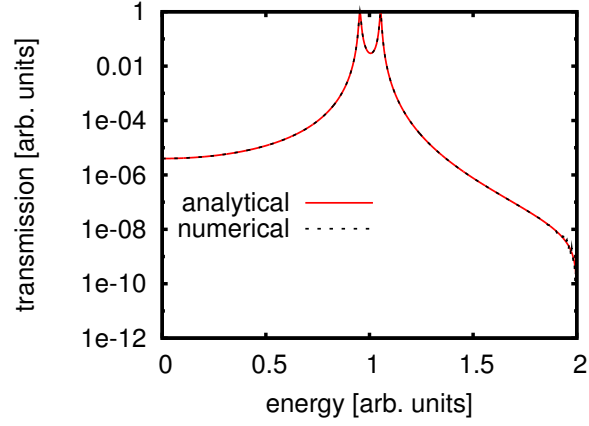


Figure 4.11: Transmission of the tight binding chain, numerical and analytical results. For the optimal values of  $\eta = 1$ ,  $\beta = 0.3$ ,  $x_L = 32$ ,  $x_R = L - 32$ , and  $L = 128$ , no difference can be seen. Note, that the absolute value of the transmission function above an energy of  $1.8 t$  is close to the numerical limits, resulting in large relative errors even for a correct coupling.

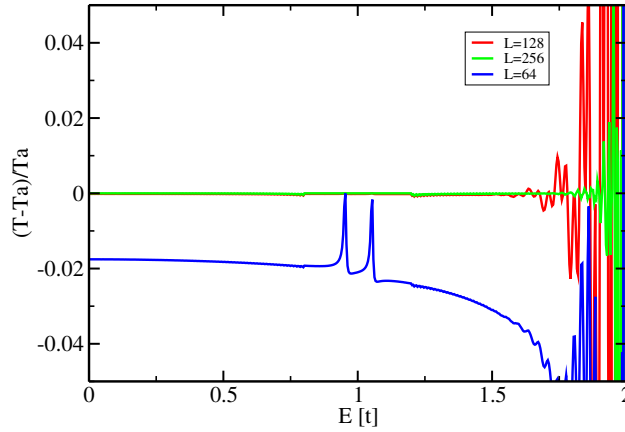


Figure 4.12: Error in the transmission for different  $L$ . Shown is the relative error  $(T - T_a)/T_a$ . For  $L = 64$  the hierarchy (Eq. 4.4 is not fully satisfied.)

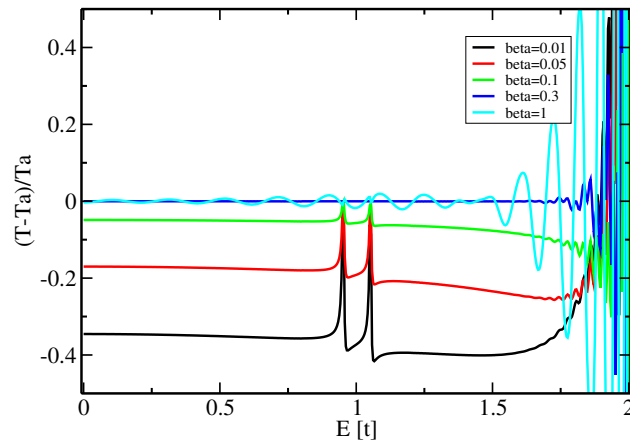


Figure 4.13: Error in the transmission for different  $\beta$ . Shown is the relative error  $(T - T_a)/T_a$ . Small values of  $\beta$  lead to a large broadening directly at the barrier and thus to reflections, increasing the relative error. For large values, the self-energy changes abruptly and thus oscillations appear.

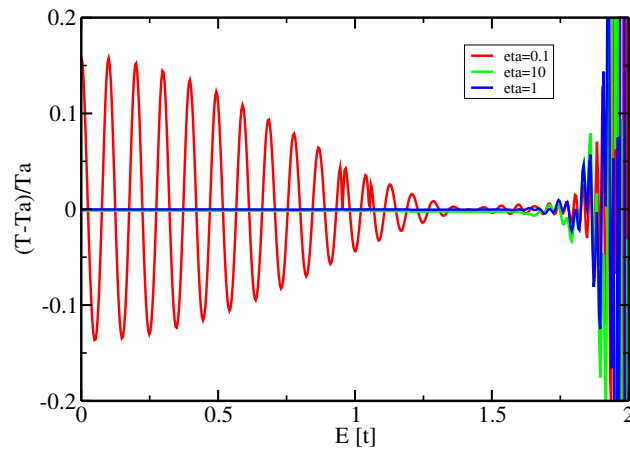


Figure 4.14: Error in the transmission for different  $\eta$ . Shown is the relative error  $(T - T_a)/T_a$ . For small values of  $\eta$  the absorption is not perfect, there is partly reflection from the boundary.

on the transmission.

$$\Sigma(x, x') = \begin{cases} 0 & \text{if } x \notin \text{coupling region} \\ i\eta(x)\delta(x, x') + i(1 - \delta(x, x')) & \text{if } x \in \text{coupling region} \end{cases} \quad (4.10)$$

# Chapter 5

## Test of algorithm for reservoirs in equilibrium

### 5.1 Screening of the electric field on metal electrodes

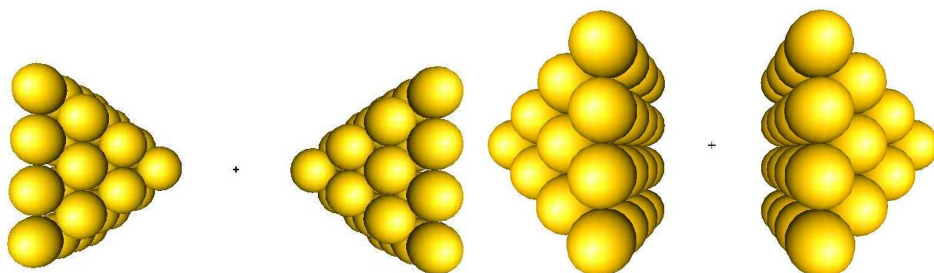


Figure 5.1: Geometry of a point charge between two gold tips. Distance  $d$  between electrode (layer of Gold closest to center) and point charge (+) is 10 au and each tip has 30 atoms. Left: tip-on-tip geometry; Right: back-on-back geometry.

We have introduced a model self-energy in Chapter 4. Now we want to use this model self-energy to couple the extended molecule to leads during the self-consistency loop of a DFT calculation, using Eq. (3.7), and test how the method will perform. As a molecule we want to use a dummy charge,  $Q$ , between Gold electrodes. This dummy charge does not provide (Gaussian)

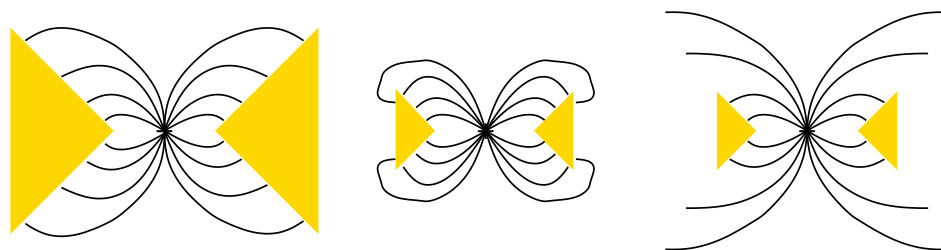


Figure 5.2: Screening of metal electrodes. Left: an infinite system, where the central charge is completely screened.

Center: a finite isolated and charge neutral system. The screening charge accumulates at the surface and corners of the finite lead, increasing the electric field on the finite part of the electrode and shifting the orbital energies.

Right: the calculation is performed with open boundaries. In this case, no artificial charge accumulates at the surface of the pyramid. The field that is not screened by the excess charge on the electrodes goes to infinity.

basis functions, only an electric field.

In this model we analyze the effect of screening of an electric field on a metal surface. In an infinite system the dummy charge would be fully screened by counter charges on the electrodes, meaning that the full system is charge neutral. This screening cloud will be, depending on the geometry of the leads, more or less extended. On the other hand, in any finite sub-system, charge neutrality is not exactly realized. The charge induced on the portion of the included leads,  $Q_L$ , does not exactly counter  $Q$ . The “screening cloud” on the metal electrodes can be large, often more than 15 au, i.e. 4 layers of Gold.

In an isolated system (calculated with closed boundaries) the counter charges have to be added by hand. In a big system with perfect screening one only has to ensure global charge neutrality. But for a system that is smaller than the screening cloud, one does not know how many charges have to accumulate in the extended molecule. Ensuring charge neutrality in the extended molecule will result in additional charges that accumulate on the surface of the lead, as shown in Fig. 5.2. This can shift the Fermi energy of the system, often by few eV.

Systems that are coupled via the self-energies are in a better shape, because here the Fermi energy is fixed. The charge on the extended molecule will adjust such that the local electric field is screened and no additional

charge accumulates on the surface.

For large systems, exceeding the size of the screening cloud, both methods will, of course, lead to exactly the same result. For a fixed electron number the Fermi energy will not shift<sup>1</sup> and for a fixed Fermi energy the excess electron number will exactly counter the point charge. But in small systems with only partial screening, the open boundary calculation is expected to converge faster in the number of lead atoms.

In the following, we will study screening in fixed  $\mu$  calculations with different lead geometries and sizes. The distance between the dummy charge and the tip,  $d$ , will be changed as well. We were using pyramids only, both in tip-on-tip (Fig. 5.1 left ) or back-on-back geometry (Fig. 5.1 right).

Fig. 5.3 shows the screening of the tip-on-tip geometry for  $d \approx 10$  au. In this case, the two Gold atoms closest to the dummy charge can form an orbital surrounding the charge,  $Q$ , leading to almost perfect screening.

For  $d \approx 15$  au the surrounding orbital cannot form,  $Q$  has to be screened at a larger distance, leading to a reduction of the screening to about 85% (Fig. 5.4). Increasing the size of the pyramid has only a small effect. This is because the distribution of the screening charge, shown in Fig. 5.6, falls off very slowly with increasing distance. Tip-on-tip is showing bad screening, because there is only one Gold atom close to the dummy charge that can supply screening charge.

The back-on-back geometry shows a much better screening (see Fig. 5.5). The charge distribution shows, that the screening charge is only located on the first Gold layer closest to the point charge. It falls off much faster than for the tip-on-tip geometry. If the distance of the tips is very small, again a charge cloud around the central point charge is formed (see Fig. 5.6).

## 5.2 Open vs. closed boundaries: charge density

In Sec. 3.2 we derived a method for coupling molecules to leads in the self-consistency cycle of DFT. In the last Section we have seen how this can be used to charge leads. Now we analyze the effect of the coupling on the electron density of a full *ab initio* calculation with a real molecule between

---

<sup>1</sup> $E_F$  of the infinite system may change, if the surface dipole of the leads is changed.

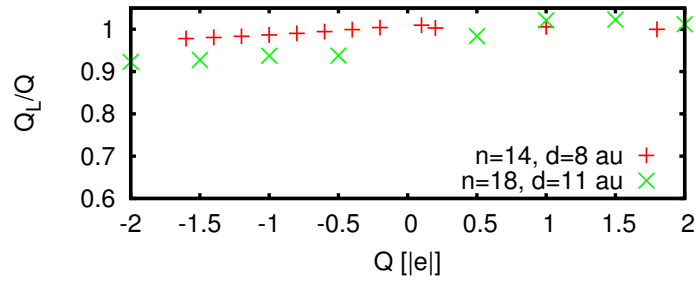


Figure 5.3: Screening of gold pyramids. Shown is the relative induced screening charge  $Q_L/Q$  over the dummy charge  $Q$  for different lead sizes. The distance  $d$  (as defined in Fig. 5.1) is in the order of the size of a Gold atom.

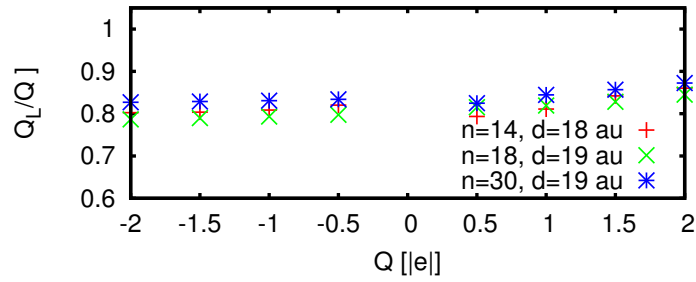


Figure 5.4: Same as Fig. 5.3, but the distance is larger than the size of a Gold atom.

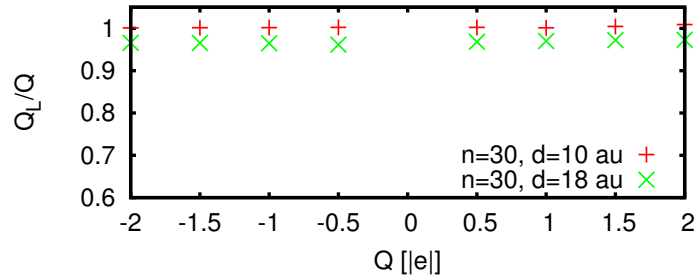


Figure 5.5: Screening of back-on-back gold pyramids. Shown is the relative induced screening charge  $Q_L/Q$  over the dummy charge  $Q$  for different distances  $d$ . The size of the pyramid is fixed.

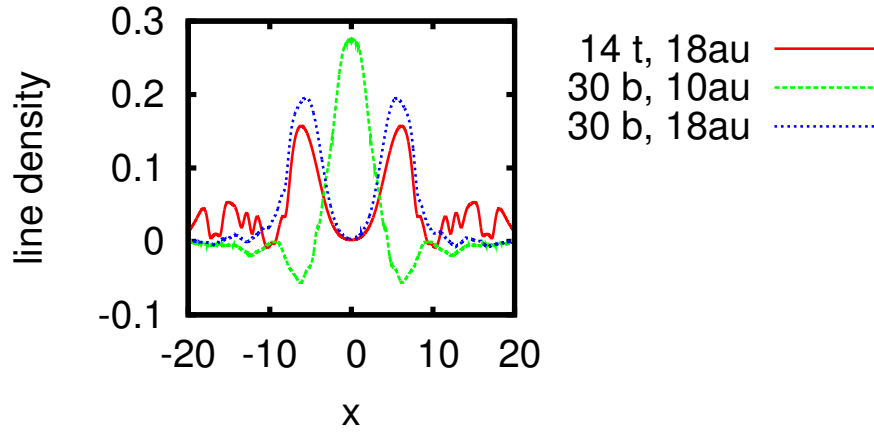


Figure 5.6: Excess electron density on the gold cluster for different geometries. The plot shows the excess line density (excess electron density integrated in the  $y$ - $z$ -plane) for a charge of  $2|e|$  in the center. The different geometries are the 14 atom tip-on-tip pyramid (red) and the 30 atom back-on-back pyramid for two different distances (10 au: green and 18 au: blue). The back-on-back pyramid shows a good screening, meaning the excess electron density falls off fast. For the 14 atom pyramid the density still oscillates at  $10 < |x| < 20$ , which explains why the electron number is still not exactly the number of charges in the center.

One can clearly see that for  $d = 10$  au in the back-on-back geometry the excess electrons form a cloud directly around the point charge in the center, and that is not possible for  $d = 18$  au.

the leads, the benzene di-thiol (BDT, see Fig. 5.7)<sup>2</sup> by comparing the open with the closed boundaries.

For the two different methods the densities on the molecule should not differ, if we are in the limit where hybridization is fully included. The flow analysis of the orbital energies (Fig. 4.5 on page 37) shows, that this should be the case for 14 or more Gold atoms.

Now let us compare the difference in the ground state electron density for the Benzene coupled to 14 Gold atoms with open and closed boundaries respectively. We plot the electron line density (density along the S-S-axis integrated in the orthogonal plane) in Fig. 5.8. The difference is shown in Fig. 5.9 and only on the atoms coupled with the self-energy, there is a sizable difference. This is not unexpected, because on the surface Gold tends to change its electronic structure.

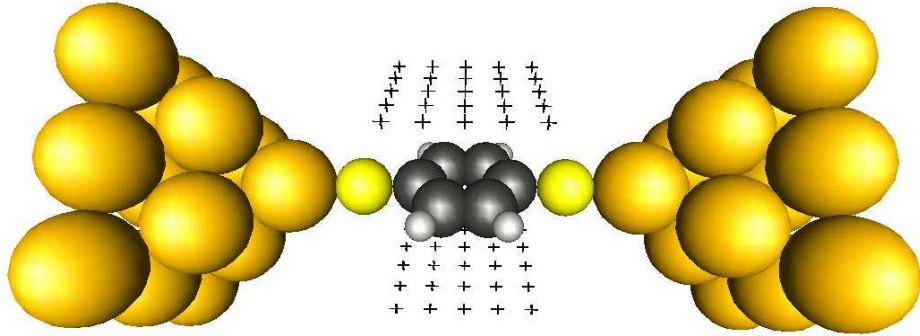


Figure 5.7: Geometry of Benzene between 14 atom leads and the gate. Gray are the Carbon atoms, white the Hydrogen, yellow the Suluf and orange the Gold atoms. The gate electrode, modeled by point charges, can be seen as +.

### 5.3 Transmission function

In Sec. 4.3.2 we already showed the convergence of the transmission function for the model self-energy constructed with the formalism derived in Chapter 4. Varying  $\eta$  does not change the transmission function (c.f. Fig. 4.8

<sup>2</sup>For this calculation, we are using a angle of  $180^\circ$  for the Au-S-C bond for calculational reasons.

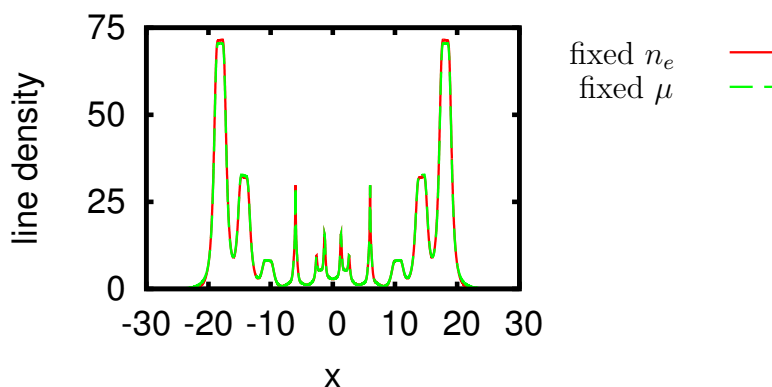


Figure 5.8: Ground state density of Benzene di-thiol, plotted along the S-S axis. The density is integrated along the plane orthogonal to the S-S axis. The sharp peaks about  $\pm 6$  au are the Sulfur atoms, and in between is the Benzene ring.

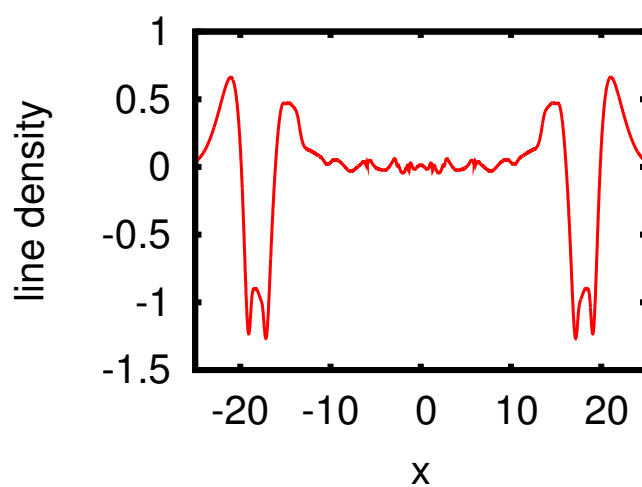


Figure 5.9: Difference of the density (shown in Fig. 5.8) between open and closed boundaries. On the molecule, between  $-8$  and  $+8$ , the charge density of the model system is almost identical for closed and open boundaries. Only on the last Gold layer, at  $\pm 18$ , the densities differ substantially.

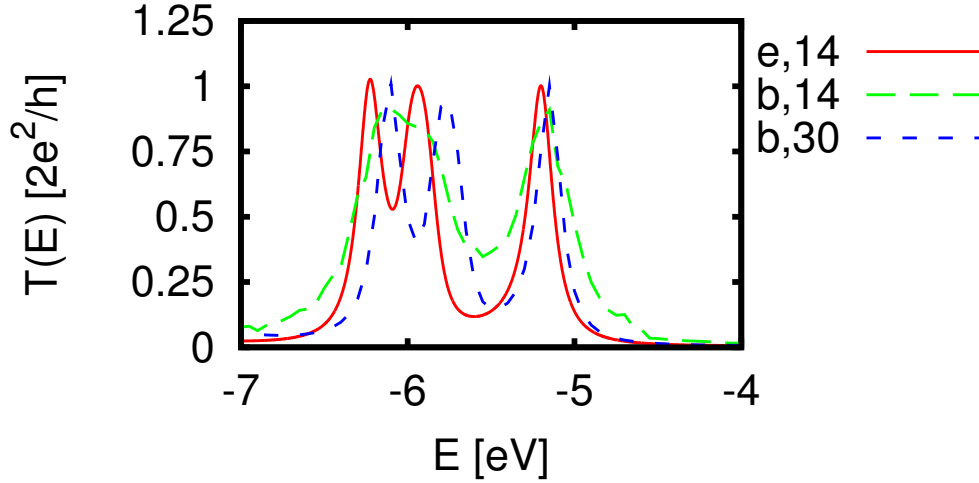


Figure 5.10: Transmission of BDT, comparison of bulk and model  $\Sigma$ . The test system is  $\text{Au}_n\text{-BDT-Au}_n$ . Shown are the transmission functions for the model self-energy with  $\eta = 0.1 \text{ H}$  and two bulk calculations with  $n = 14, 30$ , where the self-energy is calculated with Eq. 4.3.

and Fig. 4.9). Now we compare this result to previous calculations, where the self-energy was derived by direct evaluation of Eq. 4.3 from a large Gold cluster (184 atoms).

Fig. 5.10 shows, that the shape of the transmission function is in agreement between the 14 atom model self-energy and the 30 atom bulk calculation. The shifts of the peak positions are the finite size effect for the tiny pyramid. But the 14 atom bulk calculation shows a different shape. Here, the approximations for the bulk self-energy fail.

For the second test we have to perform a DFT calculation with open boundaries. The transmission function extracted from this calculation should coincide with the results obtained from the uncoupled molecule. Fig. 5.11 shows the result of a 14 atom fixed  $\mu$  calculation in comparison to between 14 and 71 atom fixed  $N_e$  calculations. The transmission functions are quite similar, the peaks only shift in the order of the mean level spacing on the extended molecule,  $\Delta^{\text{eM}}$ .

BDT is a good test molecule, because there are a lot of different works using this as a test system, too. The molecule itself is very small, so the calculational effort is not a major problem. [16, 24, 21, 28, 34, 35, 36, 37, 38,

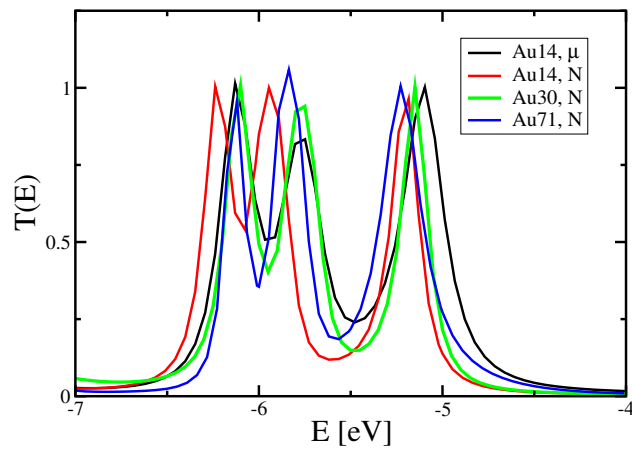


Figure 5.11: Transmission of  $AU_n$ -BDT- $Au_n$  for fixed  $\mu$  ( $n = 14$ ) and fixed  $N_e$  ( $n = 14, 30, 71$ ). In all calculations 2 layers are coupled with  $\eta = 2.7$  eV.

39, 40, 41, 42]

Since we were using the artificial  $D_{2h}$  symmetry, we can compare only to those calculations with this contact geometry [16, 38]. The peak positions in the zero bias transmission are comparable to our result (both open and closed boundaries).



# Chapter 6

## Coulomb blockade with DFT

In this Chapter we study the effect of gating a molecule. To be specific, we are interested in resonance situations where the charge on the molecule changes. This leads to interesting physics, the “Coulomb blockade”.

The origin of this Coulomb Blockade is the interaction between the electrons. If an electron is added to a molecule, all other electrons will feel the Coulomb repulsion. This will lead to an increase of all orbital energies by the interaction energy,  $U$ .

When one electron is added to the molecule, all levels shift, including the (new) LUMO. The next electron needs at least  $U$  more energy. Therefore the transmission curve as a function of the gate voltage has resonances with separation  $U$  (rather than  $\Delta_{\text{eM}}$ ). This is the essential feature of the Coulomb Blockade, it is fully developed only if  $U \gg \Delta_{\text{eM}}$ .

### 6.1 Coulomb blockade and density functional theory

Understanding Coulomb blockade is important because it is seen in many experiments [3, 4]. Therefore, one would like to study this phenomenon with *ab initio* methods, which would allow to extract the interesting parameters, like  $U$  or the HOMO-LUMO gap.

There is a big problem in DFT calculations, originating from the approximations in the functionals currently being used. To understand this, we have to learn about the approximations and exact exchange methods, like Hartree-Fock. On Hartree-Fock level the unoccupied orbitals interact with

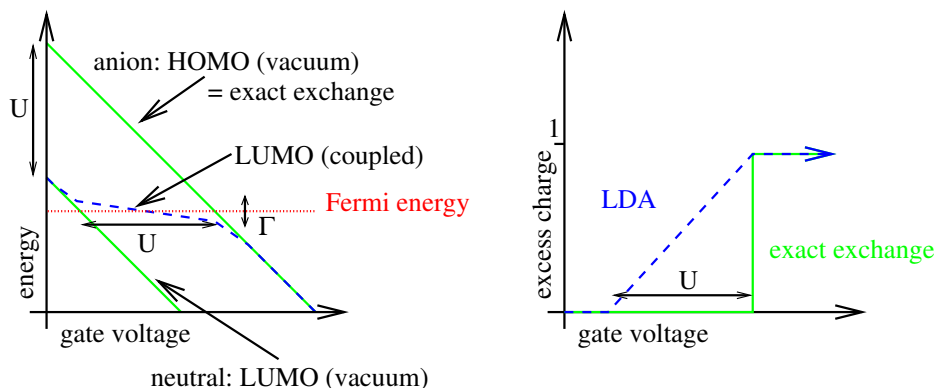


Figure 6.1: Left: Schematic picture for the shifting of orbital energies. The green lines are fictitious non-interacting orbitals that move linearly in the energy, their energy difference is  $U$ . The LUMO of an exact exchange calculation will show this effect, too. The dashed line shows the energy of the LUMO in an LDA type calculation. The Fermi energy is marked red. Right: the excess charge for exact exchange and LDA type calculations.

the total electron density (made from the  $N$  occupied states), while occupied orbitals only interact with the other occupied orbitals, meaning  $N - 1$  electrons, but not with itself. Importantly, the self-interaction in the Hartree part is exactly canceled by the Fock part. By definition, this cancellation is maintained by all those methods with exact exchange functionals.

In DFT functionals one uses another approximation, the local density approximation (LDA). The exchange correlation energy is replaced by the energy  $e_{xc}$  of a uniform electron gas<sup>1</sup>, which works well if the density varies only slowly<sup>2</sup>. In this approximation the self-interaction does not cancel. Occupied orbitals as well as unoccupied ones interact with the full electron density. This leads to artifacts, e.g. underestimation of the HOMO-LUMO gap by  $U$ .

Fig. 6.1 shows schematically what happens if a molecule is charged with a gate. The effect of a gate voltage,  $V_G$  on an non-interacting orbital is a linear shift in energy. This is also true for the LUMO of an exact exchange calculation. When this orbital is pulled below the Fermi energy it is occupied, but this will not effect its energy because even if it is occupied, it will still

<sup>1</sup> $E_{xc}^{LDA}[n(\mathbf{r})] = \int d^3r n(\mathbf{r})e_{xc}(n(\mathbf{r}))$

<sup>2</sup>GGA is a gradient corrected version of LDA

interact with  $N$  particles, not with  $N + 1$  (no self-interaction).

In an LDA type approximation this is no longer true. When the occupation increases (while crossing the Fermi energy) the orbital starts interacting with itself. This increases the orbital energy, while the gate voltage pulls the orbital down. In this window of  $V_G$  the occupation of the LUMO changes, but its energy is almost constant.

This leads to a dramatic effect in the excess electron number. While in an exact exchange calculation the excess electron number will show a sharp step when the LUMO crosses  $E_F$ , for a LDA type calculation this step will be smeared by  $U$ . This is a problem, because the step width is also in the scale of  $U$  and thus Coulomb blockade is totally hidden in a LDA calculation.

## 6.2 Charging the molecule with a gate: flow of orbital energies

Now we show this effect on a test molecule, the BDT, Fig. 5.7. In this figure, one can see the planar gate on both sides, modeled by dummy charges. We apply a gate voltage by increasing the charge,  $Q_G$ , located on the grids. The charge is evenly distributed over all grid points.

The induced charge on the extended molecule,  $Q_{eM}$ , for different gate charges is shown in Fig. 6.2.  $Q_{eM}$  changes such that the electric field is at least partially screened. As we already know from Chapter 5.1, the screening of the pyramid is not perfect, in this case  $Q_{eM}/Q_G \approx 80\%$ .

Fig. 6.3 shows the excess electron number on the molecule,  $Q_M$ . The plot does not show any step-like features, i.e. Coulomb blockade is absent. That is as expected, because we are using a functional with GGA approximation (BP-86). Since the smearing of the steps is of the same scale as the step distances, namely, the Coulomb blockade steps are completely smeared out.

The effect of the self-interaction can be seen directly if the orbital energies are plotted at different  $Q_G$  (see Fig. 6.4). In the window  $-1 < Q_G < 1$  the LUMO is close to the Fermi energy. The orbital energies shift only in the order of  $\Gamma \approx 0.2$  eV (see Fig. 6.5) and do not follow  $Q_G$ , if the gate charge is increased. For the occupied orbitals this is not unexpected. As the LUMO becomes occupied, all other orbitals start interacting with the new electrons on the molecule. This interaction increases the orbital energies by  $U$ . At the same time, the gate charge tries to shift the orbitals to lower energies as well.

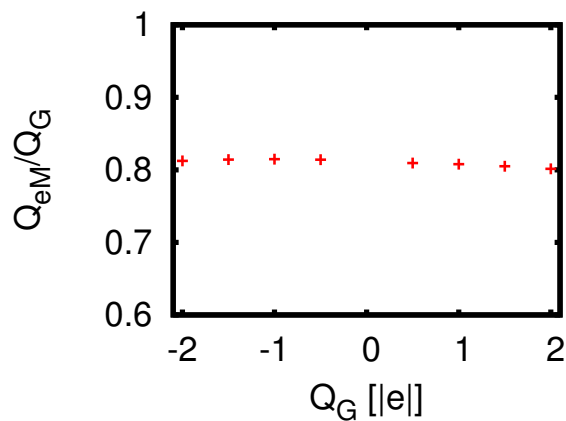


Figure 6.2: Screening of the 14 atom pyramid for Benzene di-thiol. Shown is the relative induced charge on the extended molecule  $Q_{eM}/Q_G$  over the  $Q_G$  (see Fig. 5.4).

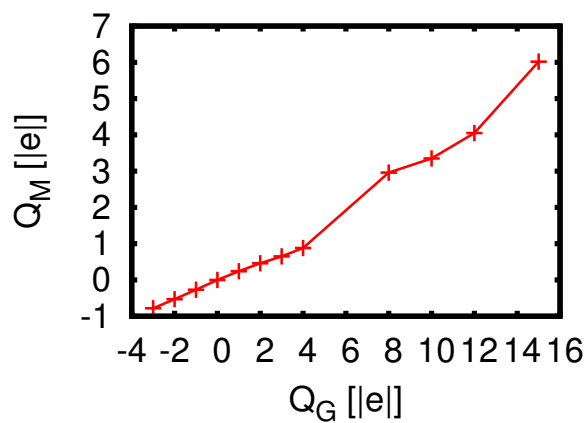


Figure 6.3: Charge on BDT over gate charge. The sharp steps of a Coulomb blockade one would expect are smeared by the LDA functional.

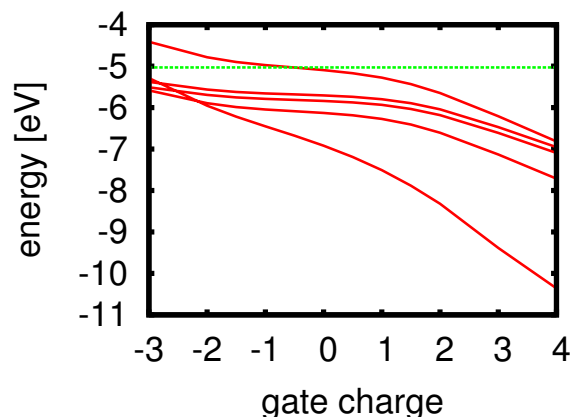


Figure 6.4: Orbital flow of BDT for different gate charge. All orbitals shown here are partly localized on the BDT. The orbital with the lowest energy is fully localized on the BDT and therefore closer to the gate and thus changing the energy much faster. Between -1.5 and +1 gate charges, the LUMO crosses  $E_F = -5.032$  eV.

The sum of both is the energy of the orbital we can see here. In an exact exchange calculation, the LUMO should move down (almost) linearly, even when crossing  $E_F$ , because it should not interact with itself. But in DFT functionals without exact exchange, this is not true. The HOMO-LUMO gap is too low in energy when not fully occupied due to a self interaction.

For  $Q_G < -1.5$  and  $Q_G > 1.5$ , the LUMO is fully occupied or fully empty. At this point, the orbitals move linearly with the applied gate voltage. Note, that the charge on the molecule can change, even if there is no orbital crossing the Fermi energy, see Fig. 6.3. This can happen if the hybridization is very strong, so that the level broadening exceeds the energy difference to  $E_F$ . In case of BDT, charge accumulates on the Sulfur, which is closest to the gate due to being larger than Carbon.

The different orbitals do not shift exactly the same. The orbitals that shift faster in energy are more localized on the Sulfur and thus closer to the gate, screening the gate field for the other particles.

The shift and width of the orbitals can be seen in the transmission plot (see Fig. 6.5). The shape of the transmission does not change a lot for different gate charge, only the position of the resonances. This is in agreement with the level shift seen in Fig. 6.4, where the shown orbitals move parallel.

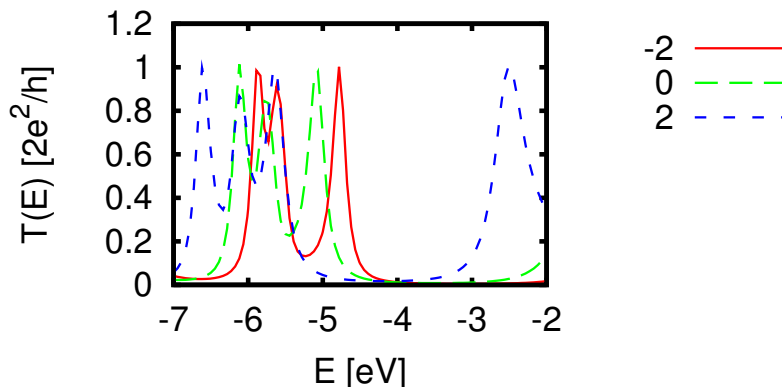


Figure 6.5: Transmission of BDT for different gate charge. The peaks shift with the gate charge, like the orbital energies (Fig, 6.4). The width is constant and the relative position of the peaks does not change a lot. The plot shows that it is possible to shift the LUMO below the Fermi energy using this gate geometry.

Let us now compare the results to those of other groups. The effect of a gate on the conductance has been analyzed already in Refs. [76, 38]. In these papers, the same linear shift of molecular orbitals with the gate voltage that we observed is reported Ref. [38] uses the same geometry and molecule as we do. Here, the transmission curve at  $V_G = 0$  is quantitatively in agreement with ours. However and somewhat mysteriously, the feedback of the gate voltage on the shape of the transmission is not observed in that work. This implies, that there is no change of orbital energies due to the different number of electrons, which seems to be unphysical.

Ref. [76] observes, as we do, that while the LUMO is pulled by  $V_G$  below  $E_F$ , the energy of the HOMO does not follow  $V_G$  but stays approximately constant. This is what one would expect since the (repulsive) Coulomb interaction between the newly occupied LUMO and the other orbitals drives up the energy of the previously occupied states.

# Chapter 7

## Applying a finite bias voltage: non-equilibrium Stark effect

Instead of fixing the Fermi energy and shifting the orbitals by gating we now apply a finite bias voltage between the leads and study non-equilibrium effects. We investigate, how the bias voltage induced level flow of KS-orbitals feeds back into the  $I(V)$ -characteristics.

To start with, we explore the Stark shift of a molecule in a constant electric field. We will see, that qualitatively the same physics can be observed in a molecule under finite bias. From this we will be able to calculate the transmission function and thus the  $I(V)$  characteristics of our test molecule, the BDT.

### 7.1 The Stark effect

Let us recall the Stark effect for a molecule in a constant electric field first. This is a phenomenon familiar from introductory methods on quantum mechanics. We will here only illustrate, how Stark physics reflects in our basic “observables”, the level flow and orbital deformations.

The Stark effect discriminates two types of orbitals: such with and such without dipole moment. Orbitals without a dipole moment will show a quadratic shift, because for interaction the electric field first has to induce a dipole moment on them. On the other hand, orbitals with an intrinsic dipole moment will move linearly in energy, because this dipole moment couples directly to the applied electric field.

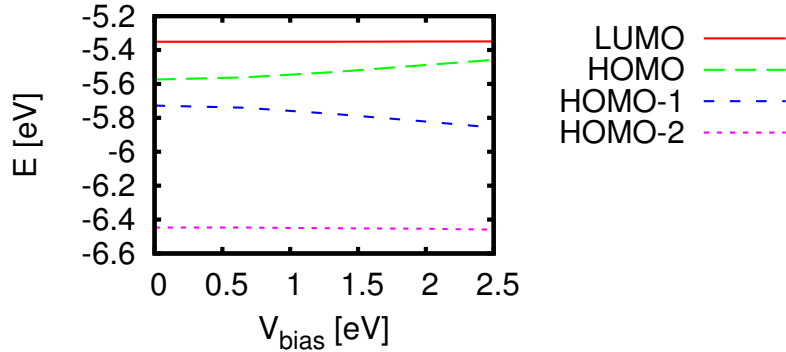


Figure 7.1: Flow of BDT orbitals (without leads, in vacuum) in a constant electric field. Plotted are the orbital energies around  $E_F$  over the electric fields, which here are given as effective bias voltages. The bias voltage is the electric field times the tip-to-tip distance ( $d = 12$  au) of the imaginary Gold leads. There are only two nearly degenerate orbitals that can form left/right localized orbitals, HOMO and HOMO-1. Then localized orbitals show a linear shift. The other orbitals, LUMO and HOMO-2, do not have an intrinsic dipole moment, and the level flow is of second order in  $V_{\text{bias}}$ .

We apply an electric field in direction of the S-S-axis. Fig. 7.1 shows the evolution of the orbitals around the Fermi energy under a constant electric field. HOMO and HOMO-1 will form hybrid orbitals localized on either the left or the right half of the Benzene ring. These orbitals show a linear shift. On the other hand, LUMO and HOMO-2 show a very weak quadratic Stark shift. The induced dipole moment is very weak. Fig. 7.2 shows the orbitals with and without electric field.

## 7.2 Stark effect induced by finite bias

Now we add leads and apply a finite bias voltage with the method presented in Sec. 3.3. Scattering electrons enter the molecule from one lead and leave into the other, if the orbital energy is between the two chemical potentials. The average occupation of these transmitting orbitals changes. We can now study the excess electrons due to this change of the occupation.

The calculation was done with the same parameters as in Chapter 6, but in this case the average chemical potential was fixed. As a test that

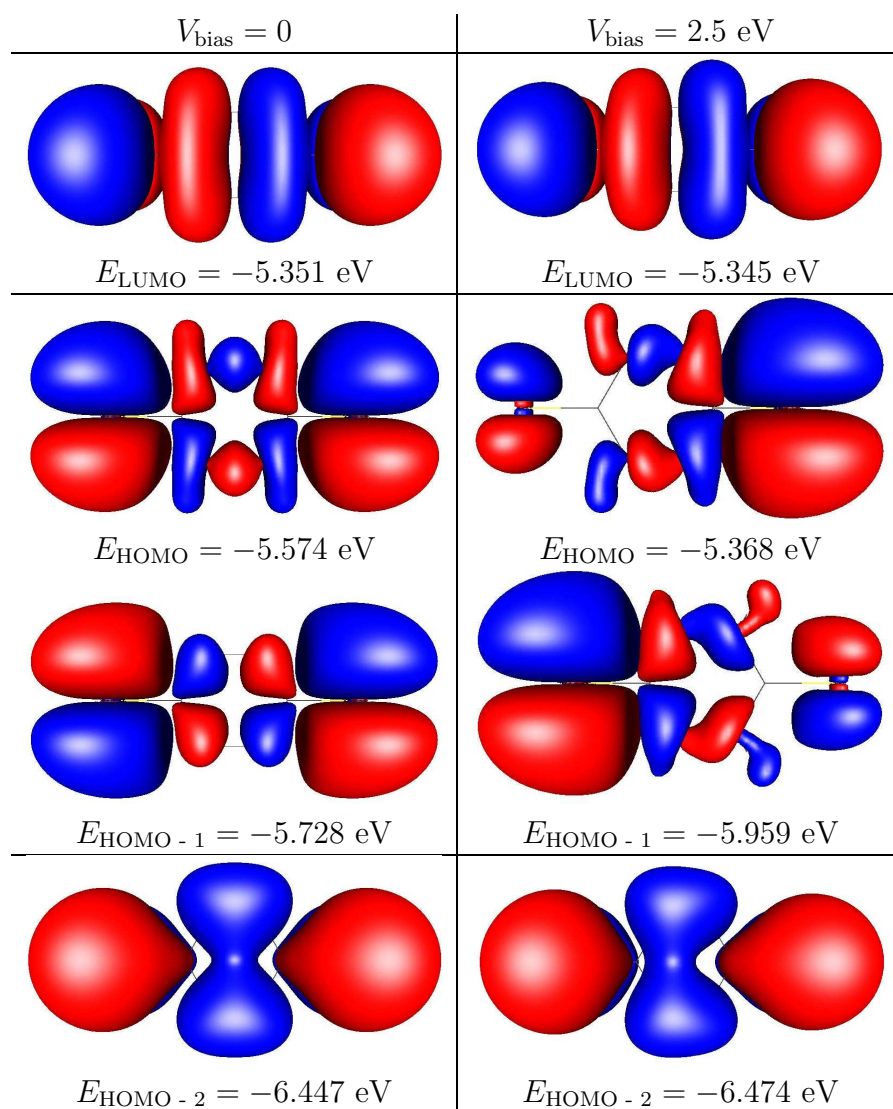


Figure 7.2: Orbitals of BDT in vacuum and an electric field, orbital energy flow shown in Fig. 7.1. HOMO and HOMO - 1 form almost left/right localized orbitals, while LUMO and HOMO-2 show only an induced dipole moments

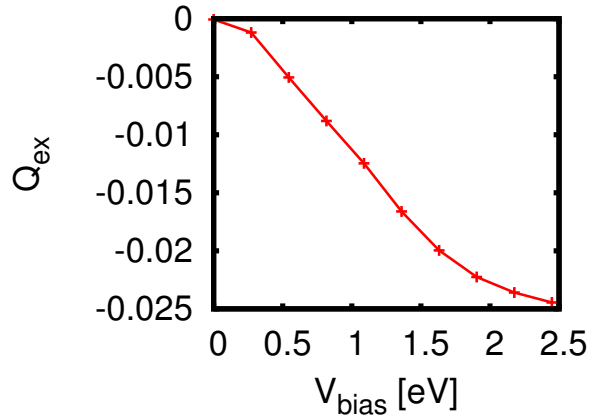


Figure 7.3: Electron number on the extended molecule (BDT and leads) for different applied bias voltage  $\mu_R - \mu_L$  at a constant average chemical potential  $1/2(\mu_L + \mu_R)$  of 5.032 eV. This picture rather nicely if the leads are big enough. For infinite leads the electron number would be constant.

parameters have been chosen well, we show in Fig. 7.3 the total electron number of the molecule. It changes by only 0.025 electrons in our voltage window, showing that the approximation is good enough.

We extracted from the calculation with bias voltage the energies and wave functions of the same orbitals as for the vacuum calculation. Fig. 7.5 shows the orbital energies. At first sight, they look qualitatively different. As we already learned in Chap. 6, the excess charge on the molecule  $Q_M$  will shift the orbital energies. The excess charge is shown in Fig. 7.4, which explains the strange shift of orbital energies. The LUMO and HOMO-2 follow  $Q_M$ , while the HOMO and HOMO-1 show a linearly increasing energy difference.

When subtracting the orbital shift due to  $Q_M$ , one finds qualitatively the same Stark physics as in vacuum. Since the voltage, that drops on the molecule, cannot be extracted easily due to a not constant field, the bias voltages in both calculations cannot be directly compared, so the energy splittings between HOMO and HOMO-1 differ by a factor of two. In Fig. 7.6 the absolute square of the orbital wave functions is plotted, showing the same result as observed in vacuum (c.f. Fig. 7.2).

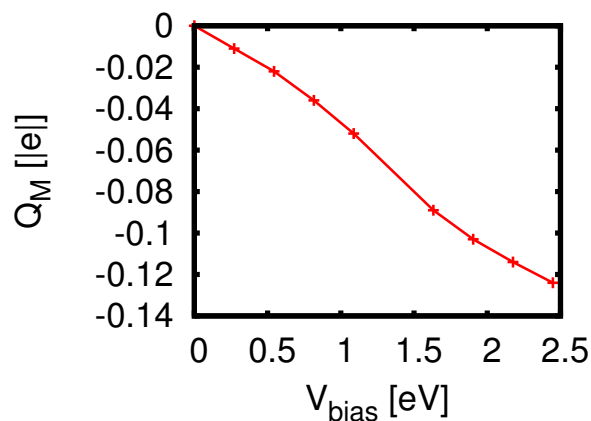


Figure 7.4: Electron number on the Benzene ring for different applied bias voltage  $\mu_R - \mu_L$  at a constant average chemical potential  $1/2(\mu_L + \mu_R)$  of 5.032 eV. The change in the electron number explains the orbital shift of all orbitals close to the Fermi energy.

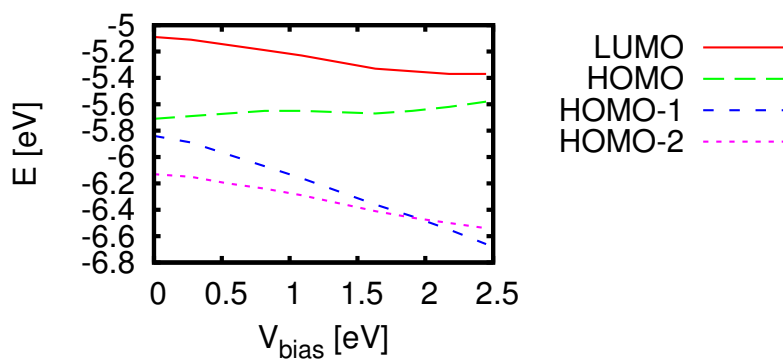


Figure 7.5: Flow of Benzene orbitals under applied voltage. Plotted are the molecular orbital energies around  $E_F$  for different applied bias voltages. The result is qualitatively similar to a constant electric field, but here the orbitals all show an additional shift because of charge transfer from the leads to the molecule. The electron number on the molecule is not constant, explaining the reason for the bending at higher voltages.

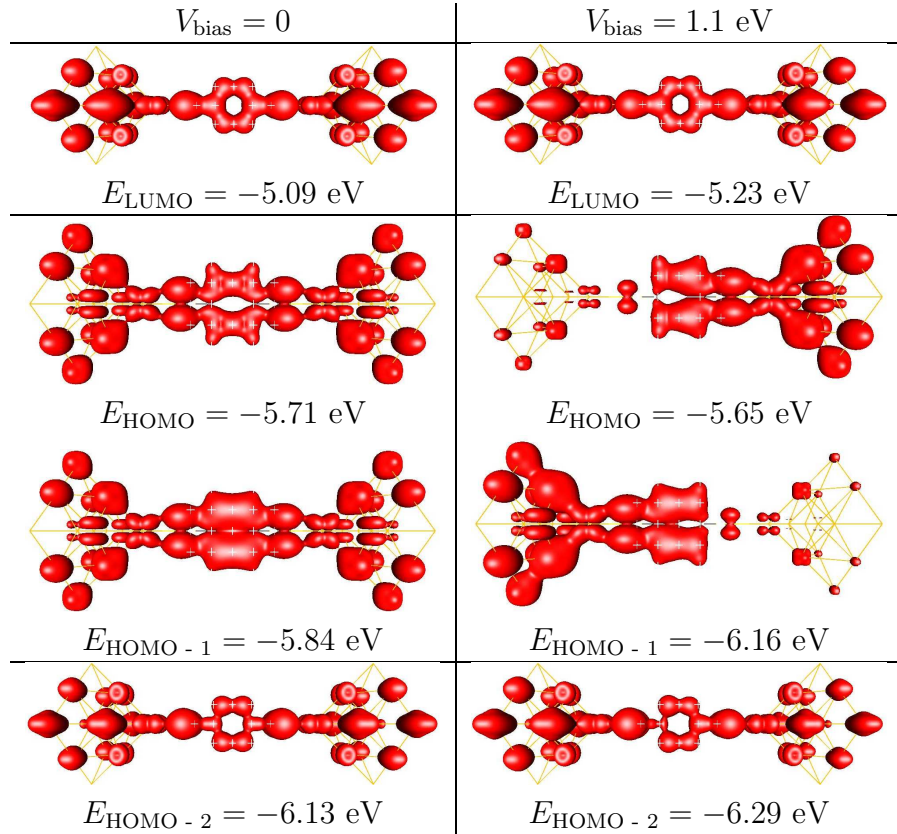


Figure 7.6: Orbitals of Benzene di-thiol under applied bias voltage. The plot shows the absolute square of the orbitals shown in Fig. 7.2, but coupled to gold leads. The hybridization shifts the levels. The Stark effect is qualitatively similar to the isolated molecule, but there is an additional energy shift coming from the charge transfer with the leads.

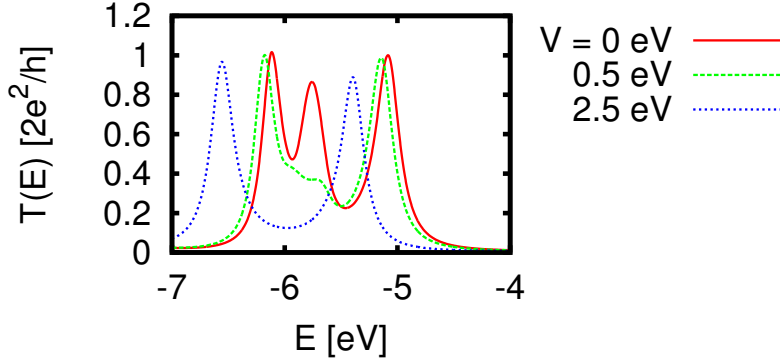


Figure 7.7: Transmission function for BDT molecule, see Fig. 5.7, at different bias voltages. At zero bias, three peaks can be seen close to the Fermi energy. For 0.5 eV bias voltage, the middle peak has almost disappeared. For even larger voltages it completely “vanishes”.

### 7.3 Transport including the bias voltage

Calculations from the preceding section also allow us to compute the transmission function for a finite bias voltage. One can now repeat this calculation for many different voltages to extract the  $I(V)$ -curve. That is done by integrating the transmission function in the voltage window between the left and right chemical potential:

$$I(V) = \int_{\mu_L}^{\mu_R} T_V(E) dE, \quad V = \mu_R - \mu_L \quad (7.1)$$

Here is  $T_V(E)$  the transmission at the energy  $E$  for an applied bias voltage  $V$ . The formula just states, that each electron in the left lead tunnels through the “barrier” with a probability  $T$  to the right lead, if the left side is occupied and the right side not. There are no contributions from above the higher or below the lower chemical potential, because either there are no electrons which can tunnel or all states are occupied so there is no place to tunnel to.

Fig. 7.7 shows the transmission function of the BDT molecule for different bias voltages. The splitting of the HOMO and HOMO-1 can be clearly seen at small voltages. At larger voltages the peak disappears. That can be

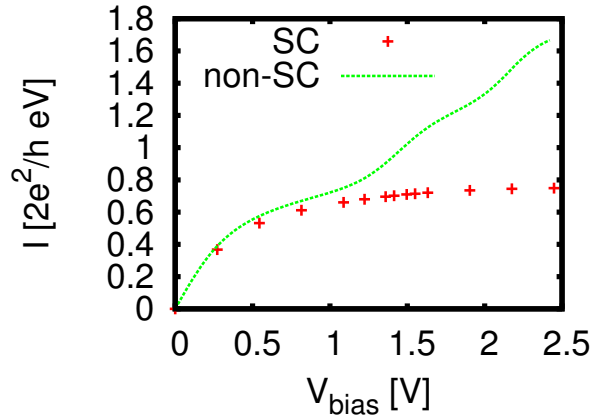


Figure 7.8:  $I(V)$ -curve for Benzene. Shown is the difference between the non self consistent calculation, where the  $I(V)$ -curve is the integrated zero bias transmission, and the self-consistent calculation, where for each bias voltage a new self-consistent calculation with applied bias was used for the transmission.

understood from a look at the orbitals. HOMO and HOMO-1 hybridize and form a left and a right centered orbital with only little weight left on the other half. This reduces the transmission through the orbitals, because the current has to tunnel through half of the Benzene ring. The other peaks show only a second order Stark effect with a very weak polarization, having no big effect on the transmission.

The  $I(V)$ -curve can be seen in Fig. 7.8. As expected from the transmission function, the overall conductance is reduced by a factor of 3 as voltage increases to 2.5 eV. This is mainly due to the missing HOMO and HOMO-1 peak. The HOMO-2 peak shifts to larger voltages (from 2.5 eV to around 3 eV) and cannot be seen in this voltage window.

Now let us compare the previous results of other groups to our findings. The effect of a finite bias voltage has been investigated [34, 35, 41, 42, 77] and a decrease of the conductivity compared to the zero bias prediction was observed. But differences in the detailed changes of the transmission function for finite bias voltages persist. To the best of our knowledge, a detailed explanation in terms of the Stark effect has not been given before. Ref. [42] explains the linear shift of *all* orbitals close to the Fermi energy with symmetry arguments. But from a comparison with our result one attributes

this linear shift to the accumulating charge on the molecule. Apart from this difference in interpretation of their data, both calculations lead to the same qualitative result.

## 7.4 Addendum: Artificial symmetries and their effect on transport

Many molecules, like the BDT, have a rich symmetry group. Coupling the thiol groups to a single Gold atom each one finds an angle of around  $110^\circ$  between Au-S-C. This angle reduces the symmetry of the molecule in vacuum, because it eliminates a mirror plane.

In some publication it is argued, that by stretching the molecule the angle of this coupling might change to  $180^\circ$ [16, 38]. But at this angle the overlap between the Gold and the Sulfur orbitals is only very small. This leads to a dramatic increase in the energy, which makes this configuration unstable. The issue is very important, since it has been suggested that the change in the angle could be a major reason for the fact that the experimentally observed zero bias conductance is so much smaller than the theoretical value (depending on the experiment and calculation a factor of 5 to  $10^{-3}$ ).

To analyze this we optimized the structure of the BDT with coupling to a single Gold atom (see Fig. 7.9 upper structure). The starting angle is not exactly  $180^\circ$ , because then there would be no force acting on the angle (exact cancellation of all forces). To show that even under stretching this angle evolves and deviations from  $180^\circ$  grow large, we enlarged the distance of the  $2 \times 2$ -Au-layers in a second “control experiment”. Fig. 7.9 lower structure shows the result of this optimization. In this first calculation the distance of the two  $2 \times 2$ -Au-layers was fixed to 39 au. Increasing this distance by 2 au resulted in a change of the angle by  $7^\circ$  from  $149^\circ$  to  $156^\circ$  (c.f. the full distance of 2 Au-atoms is 5.4 au). The distance of the two single Gold atoms changed by about 0.1 au, while the size of the full Benzene ring changed by less than 0.1 au. The energy difference between the starting structure and the relaxed one is 1.8 eV, the energy cost for increasing the distance by 2 au is 1 eV. This differences are close to the binding energy of Gold.<sup>1</sup>

This numbers show clearly that the angle of the Au-S-C bond will not change to  $180^\circ$  by applying tensile stress. The energy cost for forming a chain

---

<sup>1</sup>The binding energy per bond of Gold is 1.5 eV when in a chain and 0.5 eV in bulk[49]

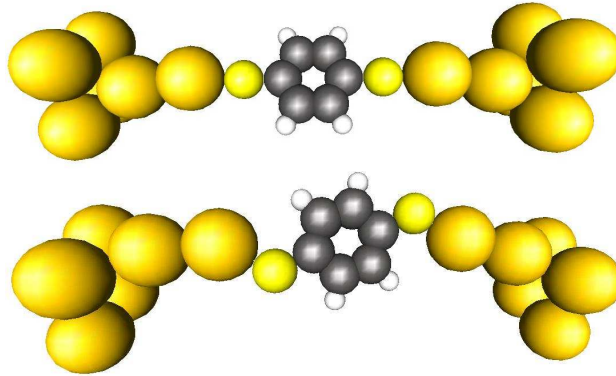


Figure 7.9: Structure for the relaxation of the BDT molecule between leads. The upper structure is the one we started the relaxation with, the lower one the resulting structure. The bond angle between Gold, Sulfur and the Benzene ring changed a lot, as well as the structure of the Gold pyramid. The Benzene ring itself did not change. For the relaxation, the coplanar  $2 \times 2$  layers were fixed.

of Gold atoms is much smaller.

We know now that the sometimes introduced  $D_{2h}$ -symmetry (i.e.  $180^\circ$  angle) is not physical. Let us now show its effect on transport calculations. Quite generally, additional symmetries might change the hybridization with the leads. This may lead to an electron exchange between the molecule and the leads.

This can be seen for the BDT, too. The HOMO of the molecule couples strongly to an orbital close to the Fermi energy, which leads to an energy shift. It is almost independent of the coupling if chosen physical and about 1 eV below the Fermi energy. For couplings to a single Gold atom with an angle larger than the optimal one ( $110^\circ$ ) the HOMO shifts to higher energies.

This artificial level shift is not the only effect on the transmission through the molecule. Since the coupling is much weaker due to a decrease in overlap matrix elements, with the increased bond angle the width of all orbitals is a lot smaller (the width is defined by the coupling to the leads). Fig. 7.10 shows the difference in the transmission for the different coupling. Both effects can be clearly seen.

The calculation shows that the transmission is dependent on the angle of the Au-S-C bond. But within the constraint of a stable molecule the

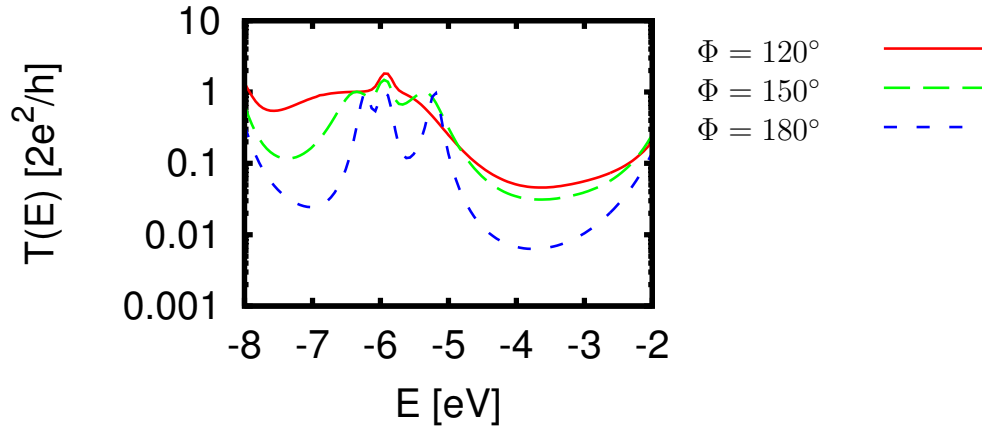


Figure 7.10: Transmission through BDT for different coupling angle, calculated for a 14 atom Gold pyramid coupled with a different angle  $\Phi$  to the BDT. One can clearly see the shifting of the HOMO to higher energies for larger bond angles as well as the decreasing width of all orbitals. Around  $E_F = -5$  eV, the difference between  $120^\circ$  and  $150^\circ$  is much smaller than between  $150^\circ$  and  $180^\circ$ .

difference is quite small, not larger than a factor of two. Only by going far away from the stable bond angle towards  $180^\circ$ , the difference becomes one order of magnitude.

Another effect of this artificial symmetry is, that if one puts another Gold atom between the molecule and the lead, the conductance drops by one order of magnitude, because of the weaker and weaker tunneling from the lead to the molecule. But in the physical coupling, this does not happen.



## Chapter 8

### Application: Bipyridine – candidate for a molecular switch?

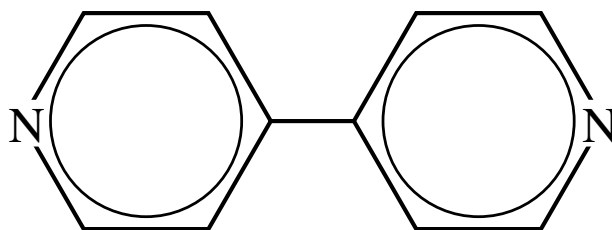


Figure 8.1: 4,4'-Bipyridine

Bipyridine (see Fig. 8.1) is a very interesting molecule. The two rings are separate  $\Pi$ -conjugated systems, that couple through a C-C bond. Steric interaction between the Hydrogens forces the molecule to have a torsion angle between the ring planes of about  $30^\circ$ .

The properties change if additional electrons are added. In this case the  $\Pi$ -electrons form a single conjugated system. The bond length between the two rings increases by 5%, enough to reduce the steric effects of the hydrogen. The molecule becomes flat. This has been observed in experiments [45].

The change in the electronic structure can be understood from Hückel's rule. The rule is, that only  $2 + 4n$  electrons can form an aromatic system. A short motivation for this rule is, that in an aromatic system the lowest

orbital is completely symmetric and carries 2 electrons, while higher orbitals are double degenerate, thus carrying 4 electrons. If one orbital is not fully occupied, one gains energy by breaking the symmetry. For a detailed explanation see e.g. [78].

In the charge neutral Bipyridine one has exactly 6  $\pi$ -electrons per ring. The 12 electrons can only form 2 separate stable  $\pi$ -systems, for a fully conjugated system 10 or 14 are needed. Adding two electrons to the Bipyridine molecule will therefore lead to a fully aromatic system. Note, that removing two electrons will not work, because the HOMO is the free electron pair of the Nitrogen.

The switching between the flat and the tilted configuration will result in significantly changed transport properties of the molecule. At first sight, the molecule looks like a good candidate for realization of molecular switches, because the switching can be controlled by a third electrode, the gate.

On the theoretical side, we want to analyze more closely, why the Bipyridine becomes flat. In experiments the molecule is charged with an electrochemical gate. We calculated a system custom tailored to model this situation and study the effect of the gate voltage on the molecular orbitals. In fact, it turns out that the configurational change can already been seen in a calculation with the Bipyridine in vacuum, not coupled to leads.

Another motivation to study transport in Bipyridine are the two electronically almost separated Pyridine rings. From that fact we would expect, that orbitals can easily split into left and right localized orbitals. As explained before, the LUMO forms a fully conjugated system out of the two rings, so one expects this orbital to not localize. This makes non-equilibrium calculations for applied bias voltages very interesting. The polarization driven by  $V_{\text{bias}}$  should be much larger than for the Benzene molecule. Charge may localize on one of the two rings, which can have a big effect on the  $I(V)$ -curve.

As we have already seen in Chap. 6, LDA type functionals will lead to artificial level shifts. For Bipyridine, this will show up again in the calculation of the non-equilibrium physics, making the separation of artifacts and real physics very hard.

## 8.1 Tilting of free molecule

We want to analyze, why the Bipyridine becomes flat when charged. The first step is to analyze the molecule in vacuum, because from this calculation we

can find the mechanism for the switching. For an estimation of  $E_{\text{LUMO}} - E_F$ , which turns out to be important for the switching, one has to introduce leads later.

To learn about the mechanism for switching of Bipyridine between a tilted and a flat configuration, we studied the evolution of the molecular energy under variation of the torsion angle  $\Phi$  between the two ring planes (for illustration of the angle, see Fig. 8.8 on page 83). The lowest energy will correspond to the optimal configuration. The mechanism can be explained by studying the evolution of the orbitals under variation of  $\Phi$ . Since the experimental switching occurs under charging, we charged the molecule by adding or removing electrons directly on the molecule and repeating the same calculation. If the molecule switches, the angle of minimal energy will change for a changing number of excess charges.

Figure 8.2 shows the energy variation with  $\Phi$  for different excess electron numbers. For each charge state we can extract the angle  $\Phi$  with the minimal energy, this is the optimal configuration for the given charge. For zero or positive charge (2 electrons removed) the molecule is tilted. The minimum angle  $\Phi$  is only weakly dependent on the occupation. If one adds two electrons to the molecule the angle of the minimal energy drops to zero. However, in this calculation the energy of the HOMO was positive for two additional electrons. That means that this molecule is unstable, and the result cannot be trusted at face value.

In the vicinity of metal surfaces, the di-anion is stabilized by screening. Thus motivated, we tried to add a single Gold atom to each Nitrogen. Fig. 8.3 shows the result, and again the negative charged molecule is unstable, so including many Gold-atoms would be necessary to model the electrode.

However, a cheap alternative is adding positive ions. But this has to be done carefully, because we only want to shift the electronic orbitals in energy, but not disturb their spatial structure. The Nitrogen has a free electron pair, and it can easily couple to positive ions, which is commonly used in chemistry. The smallest ion we can couple to the Nitrogen is  $H^+$ , a single proton. It will be absorbed in the electron cloud of the nitrogen without a strong interaction with the very robust  $\Pi$ -electron system. The protonized Bipyridine has a comparable electronic configuration to the charge neutral unprotonized molecule. Fig. 8.4 shows the energy over  $\Phi$  for different charge states. Indeed, the result for charge neutral molecule and the di-anion is comparable to the previous observation, but the energy of the HOMO is below 0 eV for all cases.

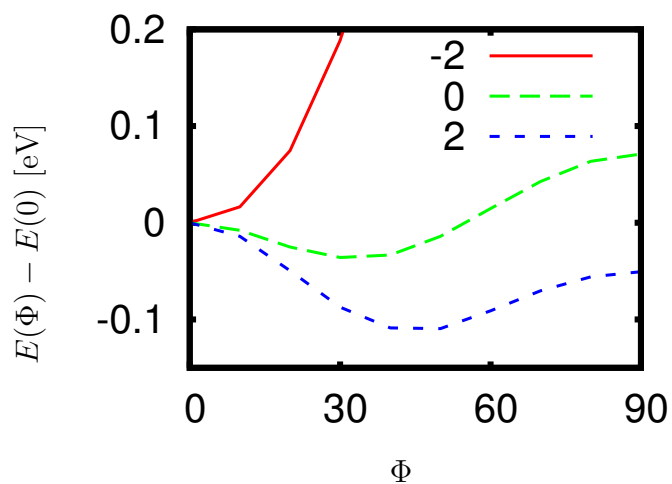


Figure 8.2: Variation of the ground state energy of Bipyridine with the torsion angle  $\Phi$  between the ring planes (illustrated in Fig. 8.8).  $E(\Phi) - E(0)$  for different excess electron number. For positive or zero charge the molecule is tilted. For negative charge the flat configuration has lowest energy.

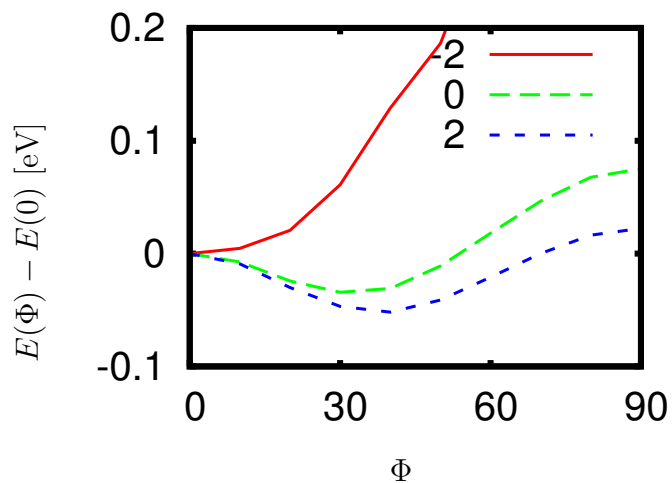


Figure 8.3: Same as Fig. 8.2, but with an additional Gold atom attached to each Nitrogen.

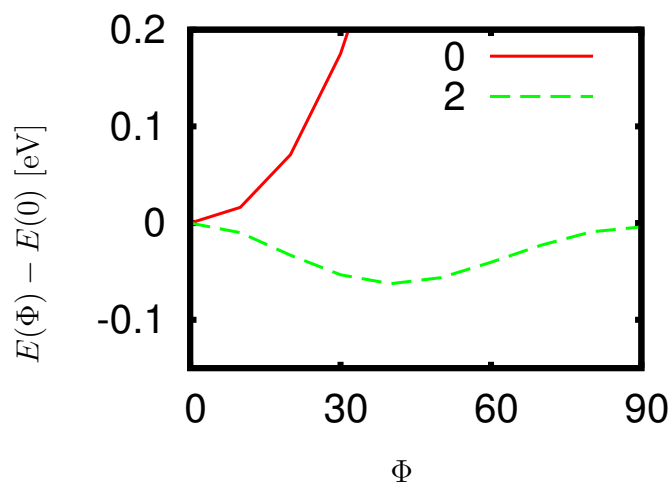


Figure 8.4: Similar to Fig. 8.2, but with a single proton attached to each Nitrogen.

To analyze why the molecule switches from the tilted to a planar configuration we plotted the HOMO and LUMO of the molecule (see Fig. 8.5). The HOMO of the molecule is anti-symmetric between left and right, with zero weight in the center. Therefore, this orbital has an (almost) constant energy under variation of  $\Phi$ . On the other hand, the LUMO, which is filled within the anion, is symmetric with a finite weight in the center. Here, the energy depends strongly on the angle,  $\Phi = 0$  has the lowest energy and  $\Phi = 90^\circ$  is 0.8 eV higher. The Pyridine rings want to form a fully aromatic system, which is only possible if the angle is zero.

So far we used a fixed geometry (only the angle  $\Phi$  was changed) and only one functional for the DFT calculation. Now we confirm that the nonzero tilt angle (in absence of charging) is in fact a robust result under variation of theoretical methods. Fig. 8.6 shows the minimal angle for two additional calculations. First we relaxed the full structure with only the angle  $\Phi$  fixed. As one can see, this does not have any effect on the tilting. To check the robustness under the used functional we performed a MP2[79] calculation<sup>1</sup>. It turns out, that this method yields a tilting angle  $\Phi \approx 40^\circ$ , which is even larger than the DFT result.

<sup>1</sup>MP2 is a Hartree-Fock calculation with a second order correction in the interaction.

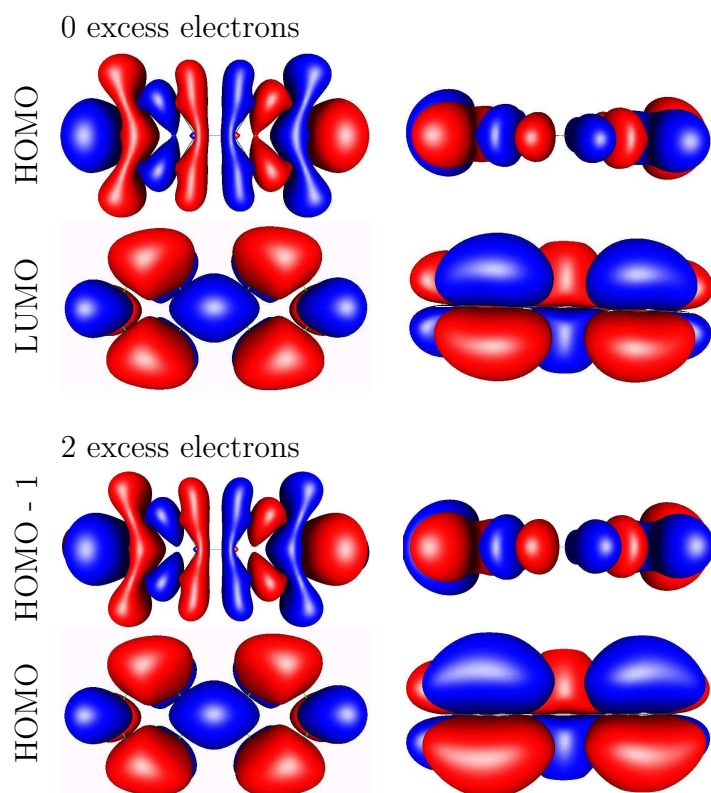


Figure 8.5: Bipyridine in vacuum: HOMO and LUMO for zero excess electrons and HOMO-1 and HOMO for two excess electrons. The HOMO becomes HOMO-1 after adding two electrons. This orbital is invariant under rotation angle  $\Phi$  between the two rings. The LUMO becomes the HOMO, which is not invariant under rotation.

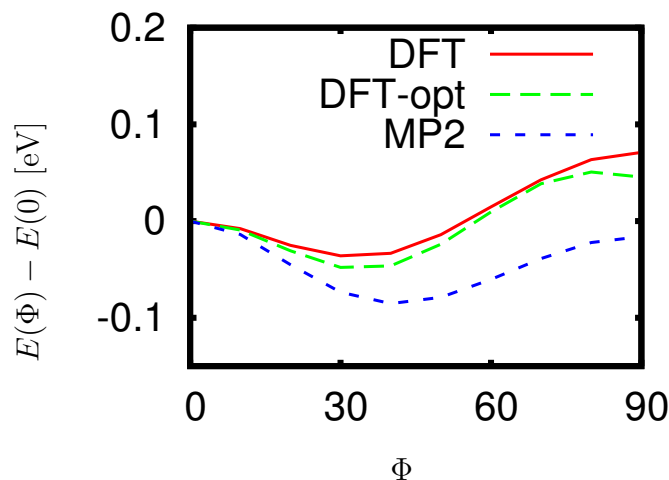


Figure 8.6: Similar to Fig. 8.2, but for different calculations: DFT with fixed structure, DFT with fully optimized structure (only angle  $\Phi$  between the two rings is fixed) and MP2. They all show almost exactly the same angle for the charge neutral calculation.

## 8.2 Bipyrindine between Gold leads: tilting with a gate

The charged molecule in vacuum is not realistic for experiments, where experimentalists have coupled the molecule to leads. The leads will modify the orbital energies on the molecule due to hybridization and screening. The charge on the molecule in these experiments can be controlled by an external gate.

So our next step towards more realistic modeling is to include parts of the leads into the DFT calculation. The gate will be implemented by point charges around the molecule, as already explained in Sec. 6.

In order to find the preferable configuration for a given gate field, we compared the energy of the planar and a tilted configuration at a fixed angle  $\Phi = 45^\circ$ . In the presence of a gate, we cannot easily repeat the analysis that we did in vacuum. Calculation of all  $E(\Phi)$  values is computationally too expensive (about one week for each value). Instead we show that  $E(\Phi = 0^\circ) - E(45^\circ)$  changes sign with increasing gate charge, and this we take as an indication that switching takes place indeed. As configuration for the

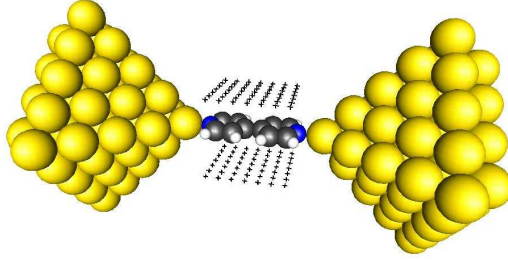


Figure 8.7: Bipyrindine between 71 Gold atom pyramids. The gates are planar on both sides of the molecule, represented by 49 dummy charges each.

$Q_{\text{Gate}}$	planar gate	cylindrical gate
	$E(\Phi = 0^\circ) - E(\Phi = 45^\circ)$ [eV]	$E(\Phi = 0^\circ) - E(\Phi = 45^\circ)$ [eV]
-2	0.218	0.012
0	0.006	-0.039
2	-0.285	-0.285

Table 8.1: Bipyrindine between leads of 71 Gold atoms: energy difference between flat molecule and tilted one. For positive gate charge the flat configuration is preferable. The gate is planar.

Bipyrindine, we used the structure from vacuum with a full  $D_{2h}$ -symmetry. The Au-N distance was optimized with a single Gold atom on top of each Nitrogen.

Two different calculations will be presented. One calculation will have a constant electron number and large leads. The second one will have a constant chemical potential, but smaller leads.

**Planar electrodes and constant  $N_e$ :** The first calculation is a standard DFT calculation with leads of 71 Gold atoms (see Fig. 8.7).<sup>2</sup> The energy difference  $E(45^\circ) - E(0^\circ)$  thus obtained for different number of gate charges  $Q_{\text{Gate}}$  can be found in Tab. 8.1, planar gate.

The result is similar to the findings in the previous section. For positive

<sup>2</sup>The lead Gold atoms all have a def-SV(P) basis set [80] and def-ecp pseudo potentials, the molecule TZVPP basis [81]. The gate is modeled from  $2 \times 7 \times 7$  point charges. The gate is  $12 \times 12$  au wide and the distance from the (flat) Bipyrindine is 6 au. The electron number was adjusted such that the extended molecule (including the gate) remains charge neutral.

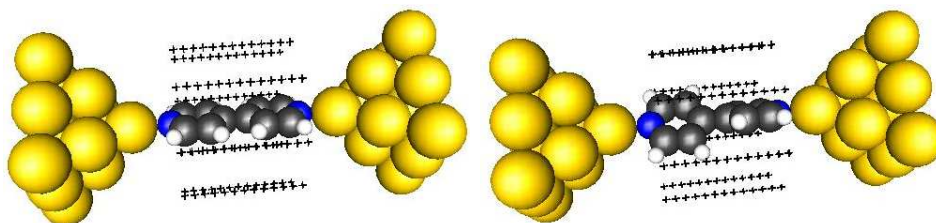


Figure 8.8: Bipyridine between 14 gold atom pyramids for  $\Phi = 0^\circ$  and  $\Phi = 45^\circ$ .

gate charge, electrons are attracted and the LUMO on the Bipyridine ring is filled. The flat configuration is much more preferable. For a negative gate charge, the molecule wants to be tilted.

At zero gate charge, the energy difference between the two angles is almost zero. As we will see later (Fig. 8.15), the LUMO is already partially occupied at zero  $Q_{\text{Gate}}$ . Since the charge transfer is only partial, the energy gain by forming a fully conjugated  $\Pi$ -electron system does not fully overcome steric interaction, and so  $E(0^\circ)$  and  $E(45^\circ)$  turn out to be very similar.

**Cylindrical gate and constant  $\mu$ :** The planar gate is not optimal for a switch. The excess charge is attracted by the gate, thus aligning the molecule in direction of the gate. For a strong electric field this aligning force will be stronger than the steric interaction. Our test calculations show, that for a gate distance of 10 au from the axis two charges on the gate are strong enough to destroy the switching between the two states.

In the experiment where the switching has been reported[45], an electrolyte was used as gate, which is all around the molecule, not just a planar gate. For the next calculation we chose a cylindrical gate, which is closer to the experimental gate geometry. Since this gate is invariant under rotations, there will be no tilting force on the angle  $\Phi$ .

The second calculation is done using the geometry depicted in Fig. 8.8 at a fixed chemical potential of  $\mu = -5.05$  eV.<sup>3</sup> The gate is cylindrical around the Bipyridine. It is modeled from 104 point charges ( $8 \times 13$ ) at a radius of 8 au and a length of 12 au.

<sup>3</sup>The leads are included with def-SV(P) basis set [80] and def-ecp pseudo potentials. The  $3 \times 3$ -layers are coupled with  $\eta = 0.1$  H and  $s = 0.06$  H. The molecule is included with TZVPP basis.

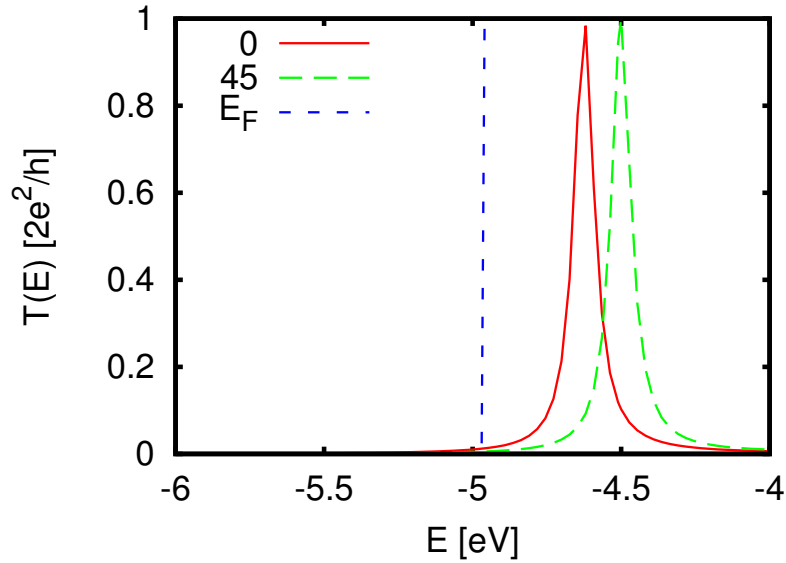


Figure 8.9: Transmission function of Bipyridine between 71 atom leads under variation of  $\Phi$ . Plotted is the transmission over energy for two different geometries: one planar (red) and the other tilted by  $45^\circ$  (green). The resonance above  $E_F$  is the LUMO which shifts up for a finite  $\Phi$ .

Again the energy for  $0^\circ$  and  $45^\circ$  has been calculated and can be found in Tab. 8.1, cylindrical gate. For a positive gate charge,  $Q_G = 2 |e|$ , where charge is attracted by the gate and the molecule is charged negatively, the planar configuration is preferable like in the calculations above. However, for  $Q_G = -2 |e|$  the energy difference is one order of magnitude smaller than in the 71 atom calculation, thus indicating finite size effects. Still, the tilted configuration becomes much lower in energy, suggesting that the crossover takes place in this calculation as well.

Thus we can conclude that the molecule coupled to leads will switch by applying a gate voltage between the planar and tilted configuration. The effect on the conductance of the molecule still has to be investigated. In Fig. 8.9 the transmission function for the two different tilting angles is plotted without changing the gate charge. What can be observed is the shifting of the LUMO to higher energies for  $\Phi = 45^\circ$ . However, the overall change in the conductance is not more than a factor of two close to  $E_F$ .

There are theoretical calculations for this molecule from other groups, too.

In Ref. [46] the effect of the bond length Nitrogen-Gold and the angle between the rings on the zero bias transmission has been investigated. To our best knowledge, they did not try to find the optimal structure for different gate charges. In their calculation, the conductance is independent on the angle between the rings. This is unexpected, because the transmission should depend mainly on the LUMO. In their calculation, the density of states shows no orbitals closer to the Fermi energy than the LUMO. But in the transmission, a very broad peak appears directly at the Fermi energy. It seems to be an artifact of the small lead size, a large number of strong (unphysical) oscillations appear as well. The positions of HOMO and LUMO are comparable to our calculation. The LUMO shifts to higher energies, if the angle between the two rings is increased. This is what we can see as well and should lead to a reduction in the transmission, like it has been observed in experiment [45]. Other calculations, like Ref. [82], find a very weak zero bias transmission, thus confirming our findings.

### 8.3 Effect of a gate: Orbital flow and Coulomb blockade

In the previous sections we learned, that the occupation of the LUMO forces Bipyridine to become flat. In this section we show the relative position of the LUMO with respect to  $E_F$  for different lead geometries and surfaces. From that information, we will show, that Bipyridine indeed shows a dramatic difference in the conductance when the LUMO crosses  $E_F$ , but not only due to tilting. It turns out, that a much more important impact of gating is the shift of the frontier orbitals (HOMO/LUMO) with respect to  $E_F$ . This shift gives the reason for the strong change in conductance observed and not the tilting itself.

**Effect of the lead geometry:** To start with, we want to compare different lead geometries, depicted in Fig. 8.10. The surface structure for  $N_{\text{Au}} = 14, 26, 71$  is (100) and for  $N_{\text{Au}} = 25, 28, 30$  it is (111). For all these lead geometries we calculated the orbital energies, as shown in Fig. 8.13. The first important information from this analysis is the different  $E_F$  for (100) and (111) surfaces (5.0 eV and 5.2 eV), which is a natural consequence of the modified surface dipole. The relative energy of the LUMO to  $E_F$ , however,

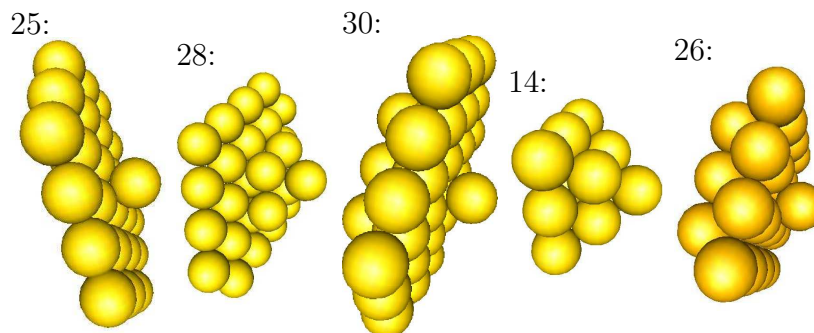


Figure 8.10: Different lead geometries. The numbers represent the total number of Gold atoms. 25, 28, and 30 are (111) surfaces, while 14 and 26 correspond to (100) surfaces.

is very robust under changing the lead geometry.

Now let us analyze the screening of the electric field on the different surfaces. Perfect screening means that in a fixed  $N_e$ -calculation  $E_F$  is constant under variation of the gate voltage.<sup>4</sup> On the other hand, a fixed  $\mu$ -calculation will have a constant number of electrons,  $N_e$ .<sup>5</sup> As we learned already in Chapter 6, the tetragonal pyramid does not show a perfect screening even for large pyramids. Increasing the number of Gold atoms close to the gate improves the screening, as can be seen in Fig. 8.11 (26 instead of 14 Gold atoms). The screening is improved from 72% to 85% by doubling the size of the layer close to the gate. The 71 atom pyramid (also shown in this figure) shows a comparable screening. Note, that for  $N_{\text{Au}} = 14$  the change in  $E_F$  for a fixed  $N_e$  calculation is larger than the orbital width,  $\Gamma$ , and the level spacing of orbital energies,  $\Delta^{\text{M}}$ . In this case, quantitative calculations will fail and open boundaries have to be used.

For positive gate charge the screening is almost 5% higher than for negative gate charge. This is easily explained: for a positive charge, the LUMO is occupied, charge can be accumulated easily on the molecule. On the other hand, for negative gate charge the HOMO has to be depopulated, which is 3 eV below  $E_F$  and thus leading to a reduced charge accumulation on the molecule. Therefore, the leads have to screen a larger field.

The (111) surfaces show a similar behavior, see Fig. 8.12. Since all struc-

<sup>4</sup>To be precise, this statement is true, provided that the screening charge (together with the screened charge) has not modifies the surface dipole of the electrode material.

<sup>5</sup>For all fixed  $\mu$  calculations the last layer was coupled and  $\eta = 0.1$  H

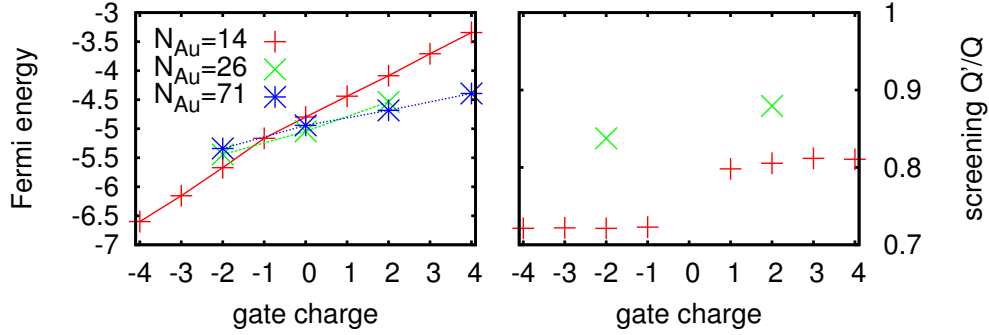


Figure 8.11: Screening of an Au-(100) cluster. Left:  $E_F$  for constant  $N_e$  calculations with different number of lead atoms,  $n$ . Right:  $N_e$  for constant  $\mu$  calculations ( $N_{\text{Au}} = 14$ :  $\mu = -5.05$ ;  $N_{\text{Au}} = 26$ :  $\mu = -5.22$ , extracted from Fig. 8.13).

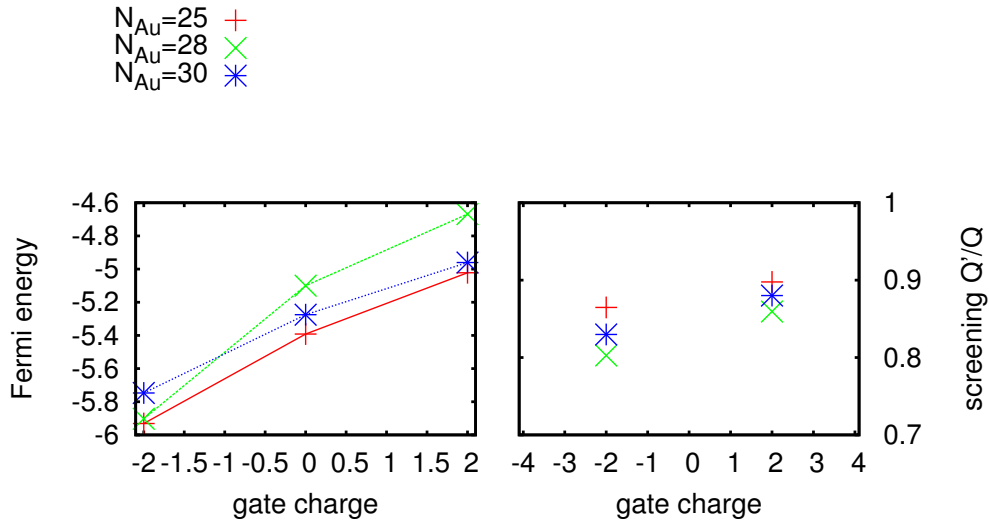


Figure 8.12: Screening of a Au-(111) surface. Left:  $E_F$  for constant  $N_e$  calculations with different number of lead atoms,  $n$ . Right:  $N_e$  for constant  $\mu$  calculations ( $n = 25$ :  $\mu = -5.16$ ;  $N_{\text{Au}} = 28$ :  $\mu = -5.13$ ;  $N_{\text{Au}} = 30$ :  $\mu = -5.22$ , extracted from Fig. 8.13).

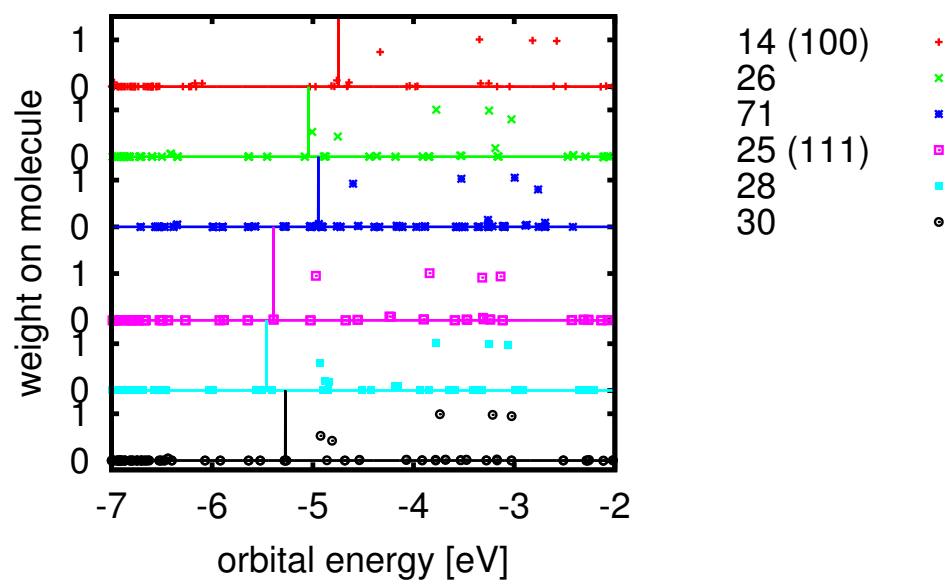


Figure 8.13: Orbital flow for Bipyridine. 14, 26 and 71 are (111) surfaces, 25, 28 and 30 are (100). (111) and (100) surfaces have a different Fermi energy. The relative position of the orbitals compared to the Fermi energy does not change a lot.

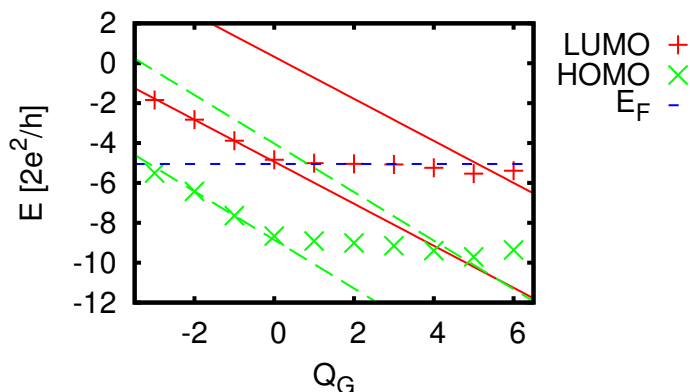


Figure 8.14: Bipyridine: orbital energies for different gate charge. Shown are the HOMO and LUMO as well as straight lines for illustration. For both HOMO and LUMO there are two lines each, one fitted to the orbital between -2 and -1 gate charges, the other shifted up by  $U^{(2)}$  with the same slope.  $U^{(2)}$  is extracted from a vacuum calculation with modeled screening.

tures are almost planar, the screening is better than that of the previous structures, between 85% and 90%. Increasing the distance between the gate and the lead plane reduces the screening (compare 25 and 28 atom structures). Interestingly, the 30 atom lead shows a reduced screening compared to the 25 atom lead in the fixed  $\mu$  calculation. This originates from the different  $\Sigma_{eM}$  and is only a finite size effect.

**Orbital flow:** Now we want to analyze the orbital flow of the LUMO and HOMO under variation of the gate charge. Understanding of the orbital flow is not easy in DFT calculations, see Sec. 6. One would expect, that the LUMO is shifted down in energy proportional to the gate voltage (positive gate charge) until the next orbital is filled. As soon as the LUMO is filled, all occupied orbitals will shift up in energy because of the increased Coulomb interaction.

But in DFT calculations with LDA or GGA functionals, this does not happen. When the orbital is uncharged or fully charged, the shift is exactly as expected. But in between, the orbital is only partly occupied. In this voltage window, we encounter the problem of the missing derivative discontinuity [43, 44]. This has been shown and discussed already in Fig. 6.1 on page 58.

The orbital energy of the LUMO of the Bipyridine (see Fig. 8.14) is

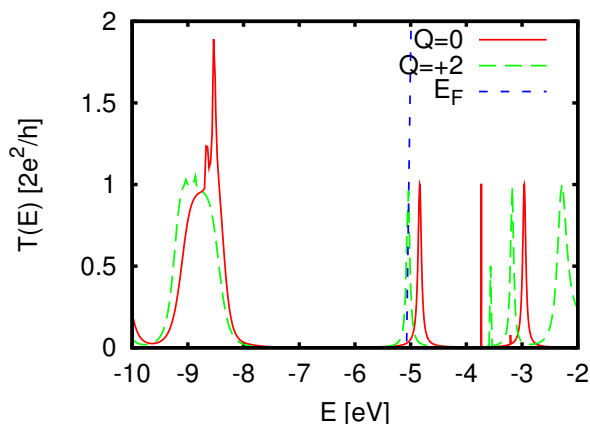


Figure 8.15: Transmission of Bipyridine for two different gate charges,  $Q = 0, +2$ . This indicates, that the main effect on the zero bias conductance is determined by the relative position of the LUMO to  $E_F$  and not by the angle between the two rings.

almost a text book example of the behavior presented in the schematic picture (Fig. 6.1). While the LUMO is unoccupied, the energy decreases linearly with the gate charge. But as soon as the occupation is non-zero, the energy is almost constant, until the orbital is fully occupied. (For bigger gate charge, the LUMO – at this point the HOMO, because the molecule is now charged – should move down linearly again. This cannot be seen for Bipyridine, because at this gate charge filling of the LUMO+1 already intervenes.)

The Coulomb interaction,  $U$ , has been extracted from a calculation of Bipyridine in vacuum with a model screening. This will be explained in more detail in the following section. Using this information, we plot the energy of the LUMO and the HOMO under variation of the gate charge. To show that the energy indeed increases by  $U$  when the LUMO is fully occupied, we plot two straight lines, one fitted to the energy of the HOMO and LUMO resp., the other shifted parallel by  $U$  up in energy. The slope of the fitted lines is the energy change of the orbital for increasing gate charge.

As one can see in Fig. 8.14, the straight lines shifted up by  $U$  cross the HOMO and LUMO resp. at a gate charge of about +5. At this point the LUMO is indeed fully occupied and the LUMO+1 touches  $E_F$ .

As for the BDT molecule, the transmission function of the Bipyridine will shift under applied gate voltage, see Fig. 8.15. In the voltage window, where

the occupation of the LUMO changes, that is the voltage window where the tilting angle will switch, the zero bias conductance will increase dramatically by two orders of magnitude. But this is not the effect of tilting, but only due to the LUMO being directly at  $E_F$  instead of 0.5 eV higher.

## 8.4 Modeling screening of leads with image charges

When charging a molecule in vacuum, orbital energies will be shifted by the Coulomb interaction,  $U_{\text{vac}}$ . The same is true for molecules coupled to leads, but the coupling effectively screens this interaction, thus reducing  $U$ . The reduction can be, depending on lead geometry and molecule, a factor of two or three. Therefore, the leads cannot be ignored when trying to find  $U$  for a coupled molecule. This is not unimportant, since it may imply that  $U$  is no longer much larger than  $\Delta_M$ .

Taking leads into account increases the numerical effort by orders of magnitude. Thus a simple model screening would be desirable.<sup>6</sup> Since our leads are metals, the electric field inside is zero. In this case we can use the model of image charges. Let us assume, that we have planar leads at a distance  $d$  from the center of the molecule at both sides. The excess charge on the molecule is  $q$ . To model a perfect screening on the two planes we have to put alternating counter-charges  $(-1)^n q$  at the distances  $\pm 2n \cdot d$ ,  $n \geq 1$  integer. The spacial distribution of the counter-charges is the same as for the excess charge itself (of course mirrored).

Since the excess charge distribution is not easy to model, the first approximation we make is assuming it is localized in the center. Thus the counter-charges are reduced to point charges. The next approximation is a cutoff parameter. At a finite number  $n_{\text{max}}$  of dummy charges the orbital energies are converged, meaning adding more counter-charges will not shift them anymore. Note, that the last point charges carry only  $q/2$  to ensure a charge neutral system.

For our calculation of the Bipyridine molecule we used as a cutoff  $n_{\text{max}} = 3$  (i.e. 60 au) and as distance of the leads  $d = 10$  au. The interaction energy

---

<sup>6</sup>Ideally, one would like to include screening on metallic half spaces by modifying the boundary conditions for solving the KS-equations. Unfortunately, this opportunity is not a standard option in the TURBOMOLE code and therefore we find another model.

for adding two electrons  $U^{(2)} = 5.2$  eV is screened compared to the vacuum case,  $U_{\text{vac}}^{(2)} = 7$  eV. For a single electron,  $U = 2.5$  eV.

## 8.5 Orbital shift under applied bias voltage

Bipyridine is not only interesting because of the switching. The two electronically almost separate Pyridine rings make it interesting for a case study of finite bias.

As for Benzene, see Chapter 7, we start with a calculation of Bipyridine in a constant electric field, followed by a non-equilibrium calculation with the method explained in Chapter 3.3. We will illustrate the effect of a level crossings under bias, where a “phase transition” occurs.

**Orbitals in a constant electric field:** To get an overview over the phenomena, we start with a presentation of the behavior of a Bipyridine molecule in a static electric field. The electric field is applied in direction of the N-N-axis. Fig. 8.16 shows the orbitals between HOMO-2 and LUMO and their energies. As already known from Chapter 3.3, we encounter two types of splitting, linear, here for HOMO, HOMO-1, and HOMO-2 (the symmetric partner, HOMO-3, is not shown), and quadratic, here for the LUMO.

The orbital energies for increasing bias are given in Fig. 8.17. As already explained, the HOMO and HOMO-1 form a left and right localized orbital and thus splitting up linearly, while the LUMO shows a quadratic Stark effect. We repeated the same plot, but for the single negative charged Bipyridine, see Fig. 8.18. We used the screening presented in the previous section to model the reduction of  $U$  by the leads.

**Level crossing:** In the calculation above at some voltage  $V_{\text{bias}} \approx 11$  eV, the molecule shows a “phase transition”, because the LUMO+4 and the HOMO cross. To analyze the level crossing seen in Fig. 8.18, we plot the LUMO+4 at zero bias, see Fig. 8.19. This orbital shows a strong dipole moment in direction of the electric field and thus reducing its energy a lot<sup>7</sup>, while the LUMO (Fig. 8.18 and LUMO+1 (not shown) show only a weak induced dipole moment. For the anion (Bipyridine<sup>-</sup>), at a voltage of 11 eV,

---

<sup>7</sup>At zero field, the LUMO+4 has an energy of 2.3 eV, which is reduced (almost linearly) by 0.4 eV when increasing the “bias voltage” by 1 eV. The bias voltage is the electric field times a distance  $d = 13.65$  au. At this distance the Gold leads would be.

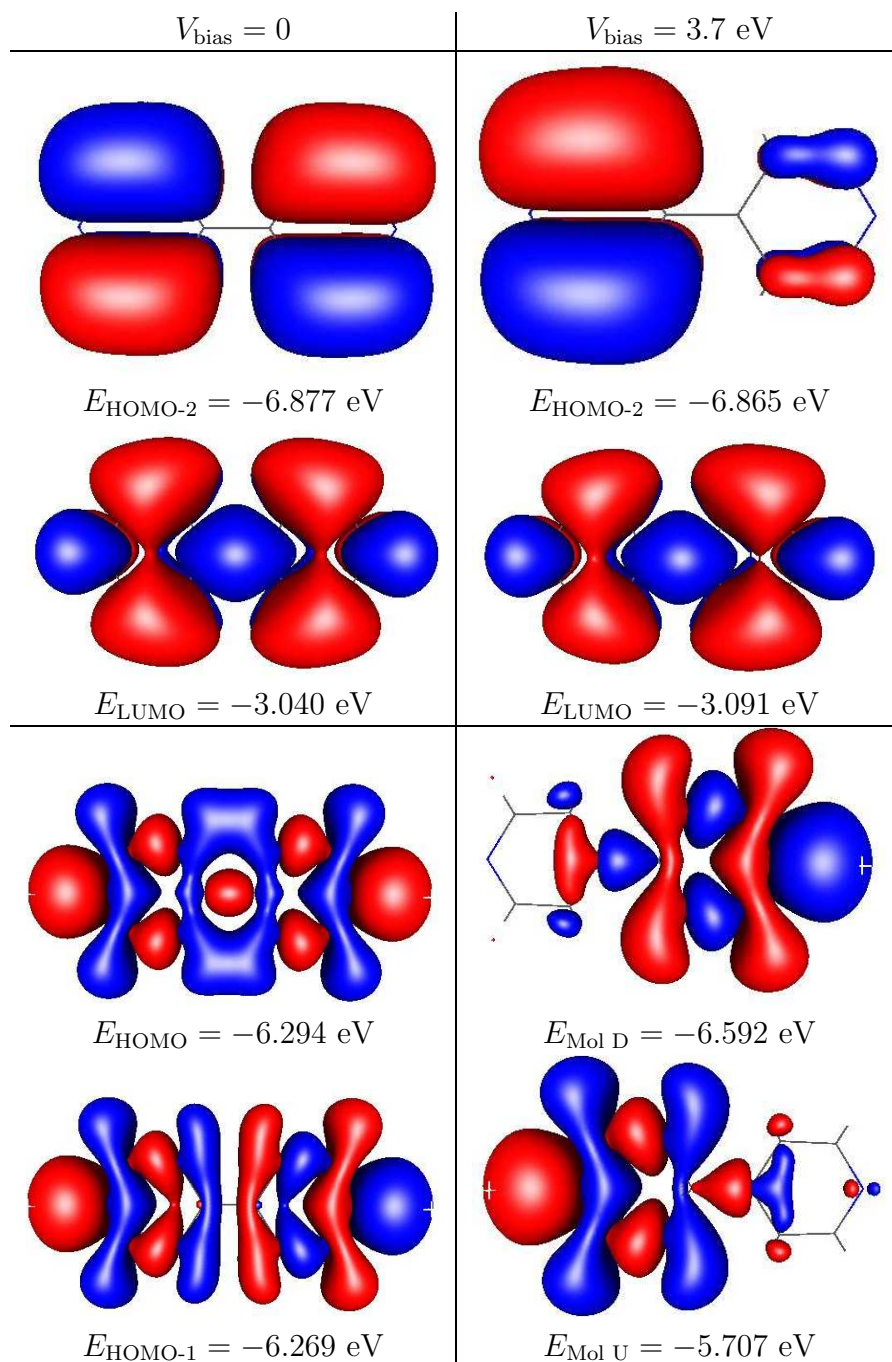


Figure 8.16: Orbitals of Bipyridine in vacuum and an electric field. Shown are the orbitals around the Fermi energy, because they are most important for transport. The LUMO shows only an induced polarization, leading to a quadratic shift in the energy. The HOMO, HOMO-1, and HOMO-2 form localized orbitals on the left and right half of the molecule, leading to a linear shift in the energy, depending on the direction of the dipole moment (The degenerate partner of the HOMO-2 is not shown).

The bias voltage is the electric field times the distance of the (not included) leads, 12 au.

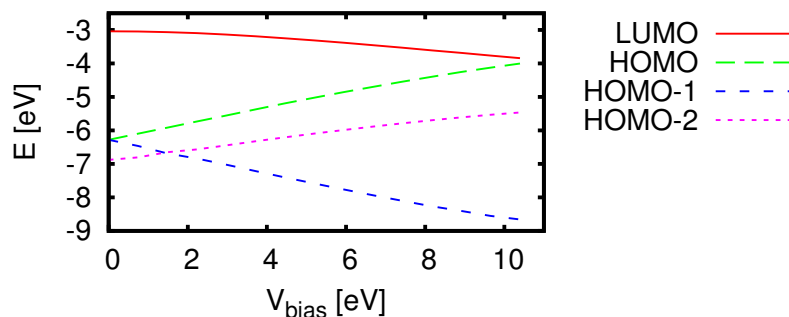


Figure 8.17: Orbital energies (same orbitals shown in Fig. 8.16) for Bipyridine in vacuum and an electric field. The HOMO and HOMO-1 split up into two orbitals localized left/right, leading to a linear splitting. The LUMO shows a quadratic effect. The voltage is the electric field time the distance of the imaginary leads (12 au).

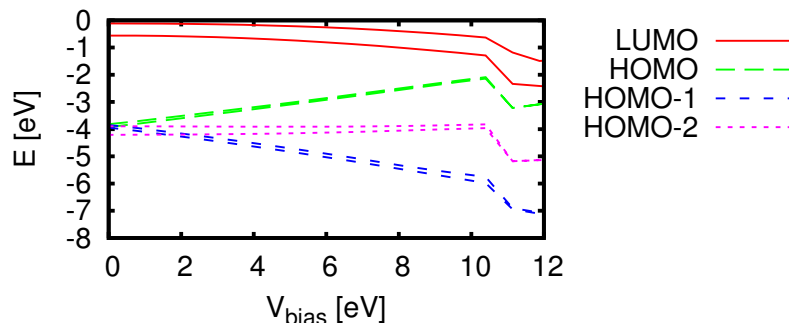


Figure 8.18: Orbital energies (same orbitals shown in Fig. 8.16) for negatively charged Bipyridine in vacuum and an electric field. The orbitals are shifted up in energy due to the Coulomb interaction. Lines appear in pairs, because the orbitals are spin split since only one electron is added. At large voltages (11 eV) HOMO and LUMO cross, causing a “phase transition”.

LUMO+4 falls below the HOMO and thus the occupation changes. The new HOMO is the former LUMO+4. Since the spatial extension of the new HOMO is a lot larger than that of the new LUMO, the Coulomb repulsion is weaker, resulting in a energy shift of around 1 eV to lower energies (see Fig. 8.20).

**Evolution of  $Q_M$  with  $V_{\text{bias}}$ :** Now we include the leads using the mechanism explained in Chapter 3.3. The molecule and the leads are both symmetric, so for small voltages we can assume, that the voltage drops symmetrically. Since the LUMO is close to the Fermi energy (0.5 eV) and the HOMO is far away (-3 eV), one would expect the charge on the molecule to increase for a finite voltage. Indeed, this can be seen in Fig. 8.21, where at small voltages the LUMO is slowly occupied. Above about 4 eV bias voltage the HOMO is depopulated, the charge decreases again.<sup>8</sup> Since the HOMO is 3 eV below  $E_F$ , one would expect a bias voltage of 6 eV for depopulation (two times the energy difference). However, the HOMO shifts up in energy, as we will show in Fig. 8.22, thus reducing the voltage to 4 eV.

The increasing excess charge  $Q_M$  will affect all orbital energies, as explained in Chap. 6. Since we are using a LDA type functional, the LUMO will shift as well, which is unphysical. The slowly increasing  $Q_M$  is an artifact, too, realistic would be a quite sharp step (broadened by  $\Gamma$ ) at a voltage of about twice the distance between LUMO and  $E_F$ . However, we will show shortly below, that even with this artifact disturbing the calculation, we still can recover the Stark shift.

**Orbital flow with  $V$  – bias:** Fig. 8.23 shows the effect of the bias voltage on the orbitals. For zero bias the orbitals localized on Gold are quasi-degenerate, one with even and one with odd parity. On the other hand, at a finite bias voltage they split into a left and a right orbital with orbital energies differing by  $V_{\text{bias}}$ . A Gold orbital on the left side (lower chemical potential) has a lower energy. The Gold orbitals on the right side (higher chemical potential) have a higher energy.

The HOMO and HOMO-1 of Bipyridine show a very strong hybridization

---

<sup>8</sup>def-SV(P) basis [80] and def-ecp pseudo potentials for the Gold atoms and TZVPP basis set [81] for the atoms of the molecule were used once again. The average chemical potential  $\frac{1}{2}(\mu_L + \mu_R)$  was adjusted such that the full extended molecule is charge neutral. Only the last Gold layer ( $3 \times 3$ ) is coupled using  $\eta = 2.72$  eV and  $s = 1.632$  eV.

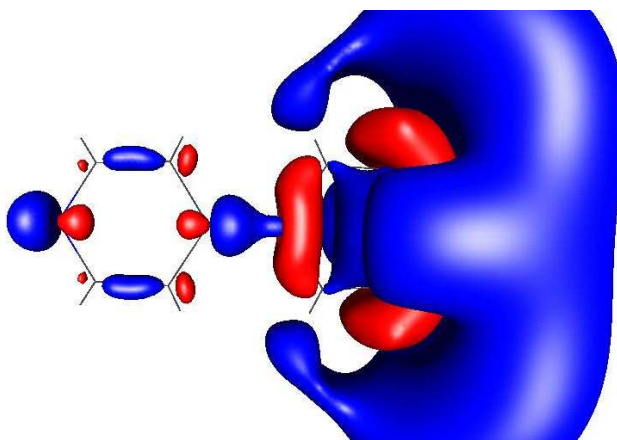


Figure 8.19: LUMO+4 of Bipyridine at a constant electric field that simulates a bias voltage of 11 eV.

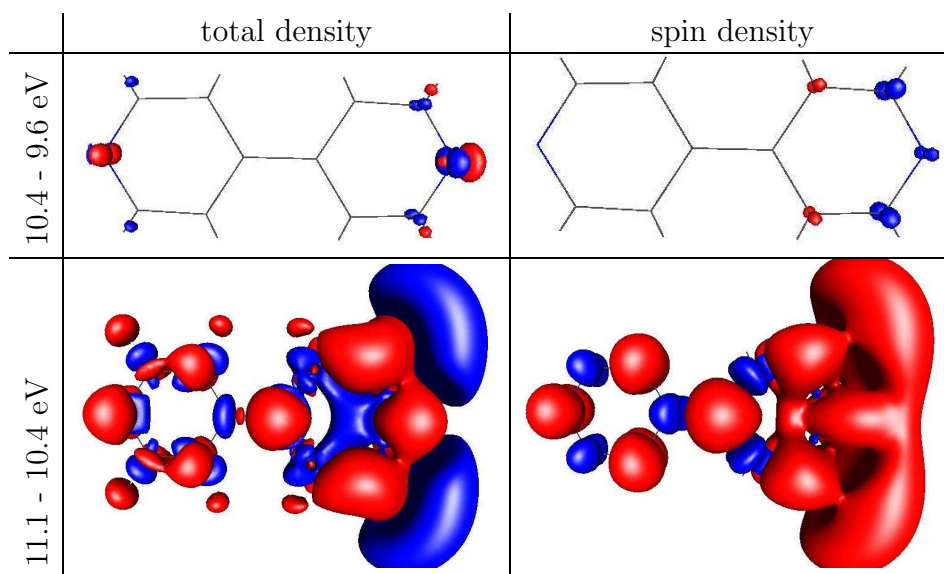


Figure 8.20: Level crossing at high voltages. Shown is the difference in left the total electron density and right the spin density for an increasing electric field. For a better understanding, the electric field is expressed as a bias voltage between the (not included) leads. Top row: change between 9.6 eV and 10.4 eV. Bottom row: change between 10.4 eV and 11.1 eV.

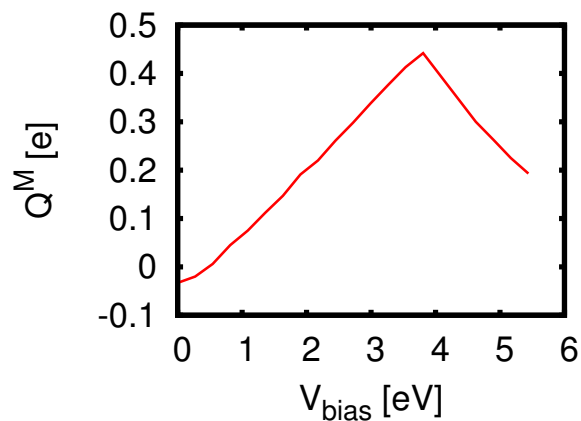


Figure 8.21: Excess electron number on the Bipyridine under applied bias voltage. Between 0 and 4 eV bias voltage, the LUMO is being occupied, at a larger bias voltage, the HOMO crosses the lower chemical potential and is depopulated.

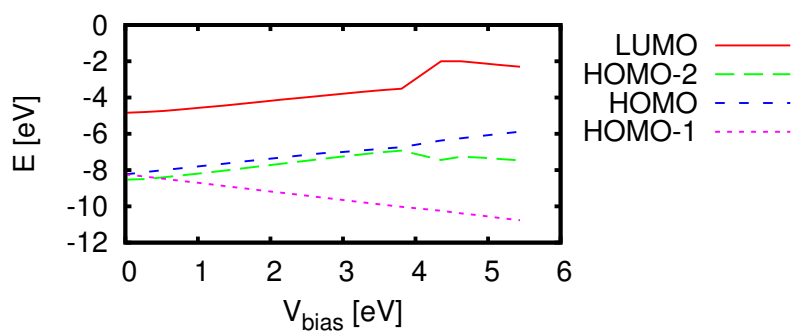


Figure 8.22: Orbital energies of Bipyridine under applied voltage. The two degenerate orbitals on Gold split up into left and right orbital. The energy of the orbitals partly localized on the molecule increases due to the increased charge on the molecule. For large voltages the charge on the molecule becomes smaller and the molecular orbitals shift to lower energies.

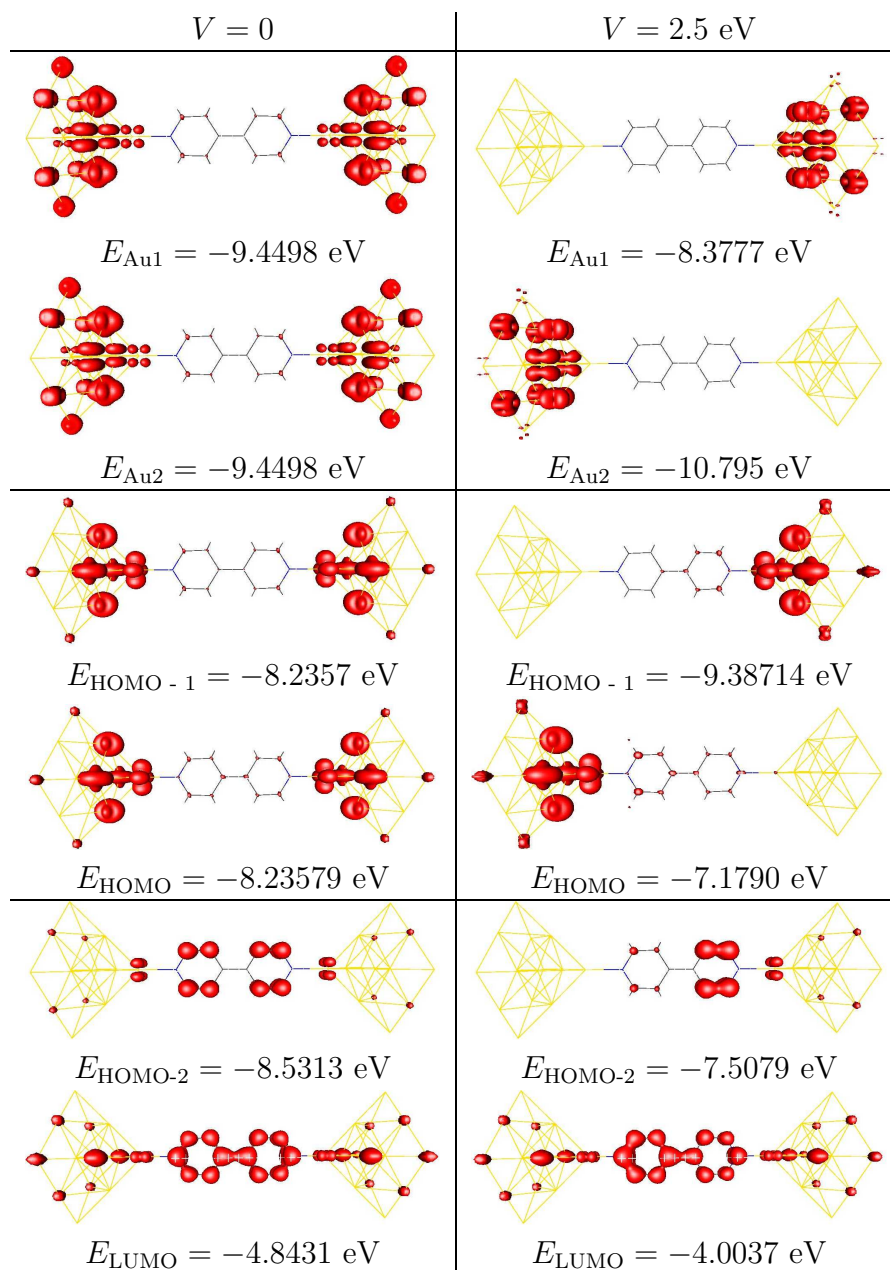


Figure 8.23: Orbitals of Bipyridine for zero bias voltage (left) and 2.5 eV (right). Top: orbitals localized on Gold. The former degenerate orbitals split up into left/right localized orbitals and the energy difference equals the applied bias. Center: the HOMO and HOMO-1 orbitals. Only very few weight is left on the molecule, thus the splitting is comparable to the Gold orbitals. Bottom: HOMO-2 and LUMO. The LUMO does not have a degenerate partner and shows a second order Stark effect with induced polarization. The HOMO-2 shows a linear Stark effect (its symmetry partner is not shown).

with the leads (Fig. 8.23). In vacuum these orbitals correspond to the free electron pair of the Nitrogen. In the coupled molecule they form the bond, forming hybrid orbitals with only few weight on the molecule. Importantly, these two orbitals are not shifted up in energy due to  $Q_M$  because the shifting depends on the weight of the orbital on the molecule (see Fig. 8.23).

The LUMO does not have a degenerate partner and should thus show a quadratic Stark effect under  $V_{\text{bias}}$ . However, this cannot be seen in Fig. 8.22. The most important shift of this orbital is due to  $Q_M$ . Since we know, that the energy of the LUMO will increase by  $U$ , when a single electron is added and the energy increase is linear, the energy should evolve like this:

$$E^{\text{LUMO}}(V_{\text{bias}}) = E^{\text{LUMO}}(0) + U \cdot Q_M(V_{\text{bias}}) + c \cdot (V_{\text{bias}})^2 \quad (8.1)$$

Here,  $c$  is a measure of the strength of the second order Stark effect and directly related to the polarizability of the orbital. We know the evolution of  $Q_M(V_{\text{bias}})$ , thus we can fit the prediction of the energy of the LUMO to the extracted  $E^{\text{LUMO}}$  (Fig. 8.22). From this fit<sup>9</sup> we gain  $U = 2.90$  eV (which is similar to the model prediction  $U = 2.5$  eV) and  $c = -0.0025$  1/eV. The induced dipole moment is negative, meaning that the energy will be reduced by increasing bias, as expected from Fig. 8.17. Note, that  $c$  differs by a factor of three compared to the vacuum calculation. This deviation can be addressed to the electric field, induced by a tetragonal pyramid, being not constant. Thus the two bias voltages are not equal.

**Bias induced charge reconfiguration:** The left side has the higher chemical potential,  $\mu_L$ , the right side the lower one,  $\mu_R$ , leading to an electric field between the leads. This polarizes the molecule. The polarization increases the electron density on the right side of the molecule, e.g. on the left Nitrogen (N) the electron density is reduced, while on the right N it is increased. The polarization of the Bipyridine molecule can be seen in the total electron density. To visualize the reconfiguration we calculate the electron line density,  $\rho_V$ , again and plot its deviation from zero bias in Fig. 8.24. The splitting is not left-right antisymmetric, because the overall charge on the molecule increases (Fig. 8.21), thus superimpose a simple picture of linear polarizability.

---

<sup>9</sup>For the fit only  $0 < V_{\text{bias}} < 3.5$  was considered

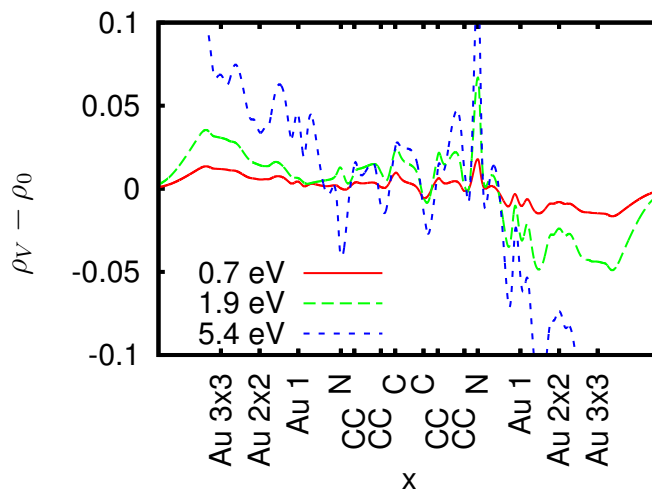


Figure 8.24: Difference in electron line density  $\rho$  for applied  $V_{\text{bias}}$ , integrated along y-z-plane.

**Transmission under applied bias:** To see the effect of the orbital shift on the electron transport, we have to analyze the transmission function for different applied voltages (see Fig. 8.25). The peak positions in the transmission function follow the orbital energies (see Fig. 8.22). The peak width of the LUMO stays almost constant because the induced polarization is weak. The wide peak between -9 and -8 eV is reduced in width because e.g. the HOMO-2 turns “dark” due to localization on one half of the ring (c.f. Chapter 7). Note, that in this transmission plot additional orbitals with a width of less than  $10^{-3}$  eV can be observed (only fully resolved in our zero bias transmission function). They originate from nearly localized molecular orbitals with only very weak hybridization.

**Robustness of the results for a different functional:** The results shown here are strongly influenced by the fact that the position of the LUMO is very close to  $E_F$  for zero bias voltage. To check the sensitivity of the results of our analysis to the approximations (i.e. functionals), we did an additional calculation with another functional, B3-LYP [67, 68]. While in the BP-86 functional the HOMO-LUMO-gap is underestimated by  $U$ , exact exchange is partly restored in B3-LYP, increasing the gap. Thus the position of the LUMO will shift to higher energies, and we can check the robustness.

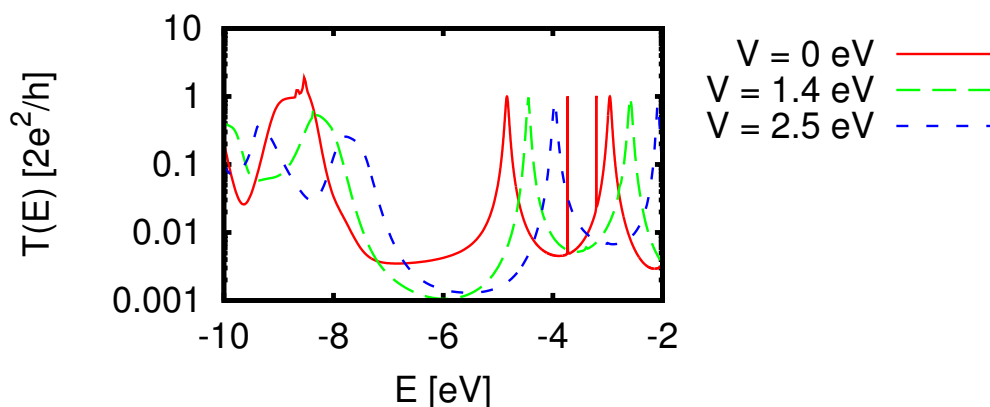


Figure 8.25: Transmission of Bipyridine under applied voltage. The peaks move, as the energy of the orbitals, to higher energies. The transmission of the HOMO-2 ( $\sim -8$  eV) decreases with increasing  $V_{\text{bias}}$  due to polarization. Additionally one can observe very sharp resonances ( $\Gamma < 10^{-3}$  eV), originating from molecular orbitals that show only a weak hybridization (in our calculation only resolved for zero bias, but they do exist in the other transmission functions as well).

The Fermi energy in this calculation was not fixed to  $-5$  eV but  $-4.62$  eV because of the different functional<sup>10</sup>. The choice of the functional is motivated, since B3-LYP is known to increase the energy of the LUMO. Experience shows, that usually the LUMO lies between the BP-86 and the B3-LYP result. Thus we can assume that our calculation is qualitatively valid, if the LUMO is even for B3-LYP much closer to  $E_F$  than the HOMO.

Figure 8.26 shows the transmission for BP-86 [64, 65] and B3-LYP relative to the Fermi energy. Both transmissions are calculated from fixed chemical potential calculations with the same parameters<sup>11</sup>. As expected for B3-LYP

<sup>10</sup> $E_F$  is usually determined by calculating a large Gold cluster. Different functionals lead in general to different values. For BP-86 large clusters can be done, leading to  $E_F \approx -5$  eV. But since B3-LYP is a hybrid functional with a HF part included, the calculational effort is dramatically increased, making large cluster calculations unfeasible. For estimation of  $E_F$  of the B3-LYP calculation we used the Bipyridine molecule with 14 Gold atoms attached and the same coupling parameters as for the BP-86 calculation.  $E_F$  was chosen such that the extended molecule remains charge neutral.

<sup>11</sup> $\eta = 0.1$  H,  $s = 0.063$  H, last layer of 9 Gold atoms coupled in the SC calculation, 13 atoms coupled for the transmission.

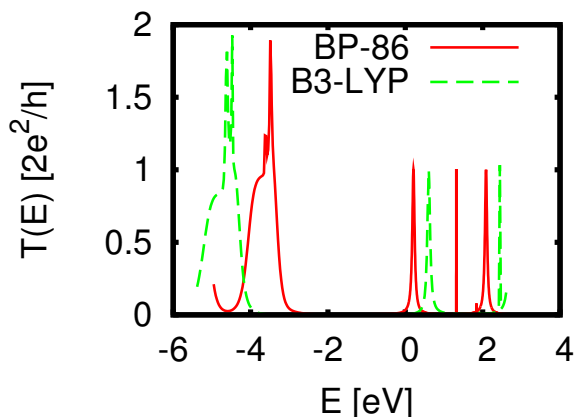


Figure 8.26: Transmission of Bipyridine for different functionals. Plotted is the relative energy with respect to  $E_F$  of the calculation, because  $E_F$  depends on the functional being used (BP-86:  $E_F = -5$  eV, B3-LYP:  $E_F = -4.62$  eV). In the B3-LYP functional the HOMO-LUMO-gap is about 1.5 eV larger than for the BP-86 result.

the HOMO-LUMO-gap is 1.5 eV larger and the LUMO is about 0.5 eV higher above  $E_F$ . But the LUMO is still much closer to the Fermi energy than the HOMO, which suggests that our previous findings remain valid (at least on a qualitative level).

Let us now analyze the energy of the LUMO for increasing excess charge on the molecule. The energy over the excess electrons  $E^{\text{LUMO}}(Q_M)$  will be a straight line with a slope  $U$ . On the other hand, in the hybrid functional B3-LYP with an exact exchange part this slope will be reduced due to partial compensation of the self-interaction. This is shown in Fig. 8.27, where both functionals show a straight line for  $E^{\text{LUMO}}(Q_M)$ .<sup>12</sup>

**$I(V)$ -curve:** From the transmission we can now construct the  $I(V)$ -curve and compare to the  $I(V)$ -curve we would obtain from non-SC calculations, which ignore the dependency of  $T(E)$  on  $V_{\text{bias}}$  (see Fig. 8.29). In the non-SC curve there are two steps, one at 0.5 eV, originating from the LUMO and one at 4 eV, originating from the LUMO+3.

The  $I(V)$ -curve for the SC-calculations (both, BP-86 and B3-LYP) show

<sup>12</sup>This only works because the LUMO shows only a weak induced polarization, less than 0.03 eV as explained before.

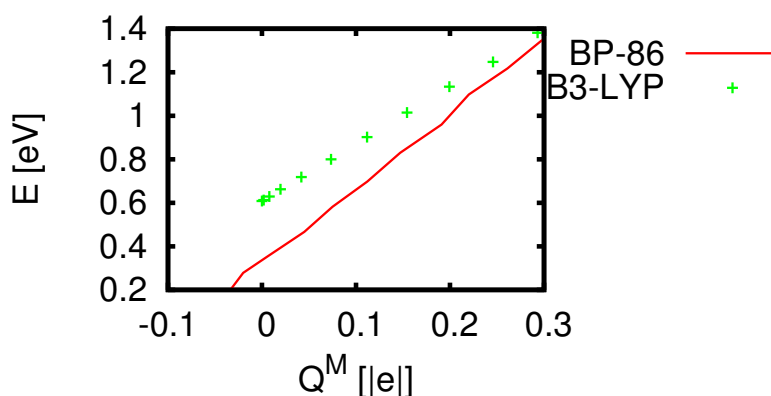


Figure 8.27: Relative position of the LUMO compared to the average chemical potential of the leads over  $Q^M$  for bias voltages between 0 eV and 2.7 eV. The LUMO has a higher relative energy for B3-LYP[67, 68], as expected.

a completely different shape. Since the energy of the LUMO slowly shifts up, the former step is smeared by  $U$  as the Coulomb blockade peak before (see Fig. 8.28 for a schematic picture). This smearing is again completely artificial. At higher voltages (3.5 eV for BP-86 and 4 eV for B3-LYP) a sharp step can be found. This corresponds to the crossing of the HOMO-3 and the lower chemical potential<sup>13</sup>

## 8.6 Structure relaxation under applied voltage

For the calculations of Bipyridine under applied bias voltage we used a fixed geometry. Now let us check if that is a valid assumption by relaxing the molecule under applied bias. If the change in the structure was large, the results from above could be qualitatively changed, but fortunately as we will see, the effect is very small.

The relaxation of the structure was done using *rdgrad* and *relax* from TURBOMOLE (see Appendix for more details). The program *rdgrad* calculates the gradient of the energy under variation of the atomic coordinates,

<sup>13</sup>HOMO, HOMO-1, and HOMO-2 turn “dark” because of showing a linear Stark effect. The LUMO+3 shifts to higher energies due to Coulomb repulsion.

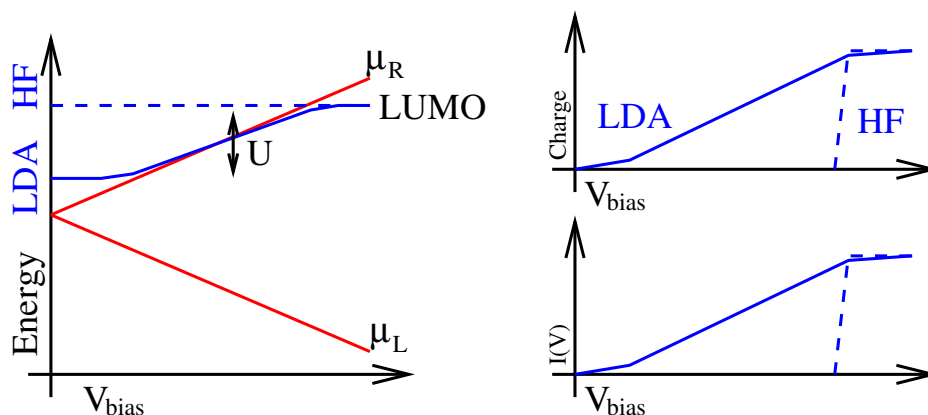


Figure 8.28: Schematic picture of the artificial level shift under  $V_{\text{bias}}$ . Left: energy flow of the LUMO under  $V_{\text{bias}}$ . When crossing the chemical potential the LUMO is being occupied and the energy shifted by  $U$ . Right top:  $Q_M$  over  $V_{\text{bias}}$ . Right bottom: A sharp step in the current is absent, since the LUMO is only slowly occupied. For comparison the exact exchange results are plotted as dashed lines.

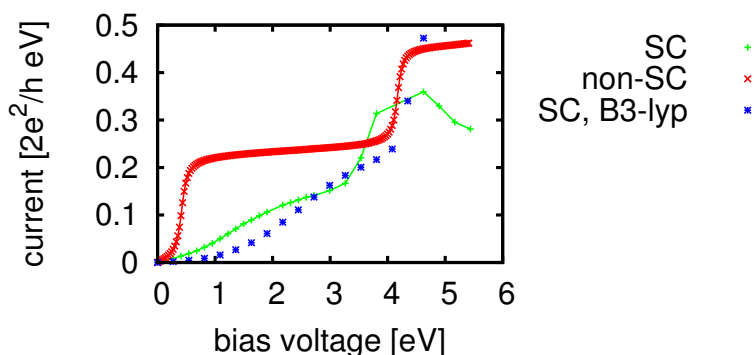


Figure 8.29:  $I(V)$ -curve for Bipyridine. The red (x) curve shows the non-SC prediction (integrated zero bias transmission), the green (+) one the BP-86[64, 65] result with applied bias, and the blue (\*) one the prediction for B3-LYP functional[67, 68] with applied bias. There is a dramatic change in the step position and the step width between non-SC and SC. The different functionals do only have a minor effect.

while *relax* shifts the coordinates according to the gradient. The coordinates of Gold were fixed. We know from previous calculations that relaxations in the leads only have a minor effect and mainly increase calculational effort. The coupling parameters were exactly the same as for the previous calculation of the applied voltage.

For the calculation of the gradient not only the density matrix is needed, but also the derivative with respect to atomic coordinates. Since a numerical calculation is not sufficient, *rdgrad* calculates this derivative from the density matrix, the overlap matrix, and the Hamiltonian. Unfortunately, the algorithm for this evaluation assumes that the molecule is in vacuum ( $\Sigma = 0$ ). There is no straight forward way of adopting the algorithm to the situation of a molecule coupled to reservoirs ( $\Sigma \neq 0$ ).

Thus we have to use an approximation for the relaxation of atomic coordinates. In Chap. 5.2 we showed that the coupling has only a minor effect on the charge density on the molecule. This allows us to still calculate the derivative of the density matrix analytically from the Hamiltonian of the extended molecule without the self-energy, because we only allow for a change of the atomic positions on the molecule itself. Only the density matrix itself will be exchanged by the one introduced in Chap. 3.3.

We performed 50 iterations of coordinate relaxation and compared the structure before and after (after 50 iterations the change of coordinates was in the order of  $10^{-2}$  au, which is sufficient for our purpose). Unfortunately the calculational effort is a lot larger than for molecules in vacuum, each iteration needs about 2 days on a single processor.

Tab. 8.2 shows the resulting change of coordinates. The bond lengths change by 5%. The molecule is polarized in such a way that the electron density is smaller on the left side and larger on the right side. That increases the bond distance of the right side in comparison to the left side. (The Gold atoms were fixed, meaning the length of the molecule could not change in this calculation.)

The transmission of the molecule is almost constant under the relaxation of the structure (see Fig. 8.30). The Au-N bond on the right side increases by only 1%, thus not affecting the transmission, while the other bond decreases by 3%. The changes in the pyridine rings are below 3%, which does not disturb the  $\Pi$ -electrons, thus not affecting the transmission.

vacuum	equilibrium	$V_{\text{bias}} = 2.5 \text{ eV}$
<b>N-Au left</b> 4.24 au	4.36 au	4.22 au
<b>N-Au right</b> 4.24	4.35	4.40
<b>C-C center</b> 2.82	2.80	2.81
<b>N-C left</b> 2.53	2.55	2.58
<b>N-C right</b> 2.53	2.55	2.62
<b>N-N</b> 13.6	13.4	13.7

Table 8.2: Distances for Bipyridine under applied voltage. Shown are different bond lengths for zero and 2.5 eV bias voltage. Only the N-Au bond changes under applied bias voltage. The other distances are almost constant. The bond distance N-Au on the right side increases because of the higher charge density due to polarization. The length of the Bipyridine is fixed because the position of the Gold atoms is fixed.

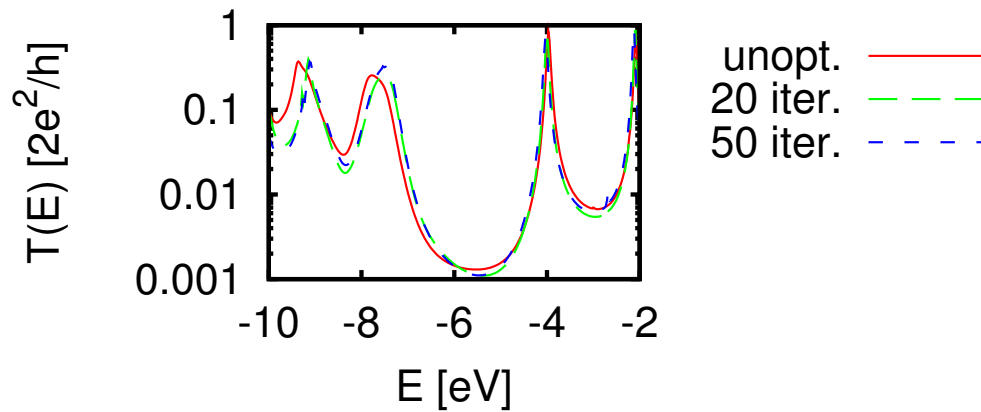


Figure 8.30: Transmission of Bipyridine for three different structures: un-optimized, after 20 iterations and after 50 iterations. The difference is very small close to the Fermi energy. The calculations were done under an applied bias voltage of 2.6 eV

## Chapter 9

# Metal organic complexes: molecular magnetism

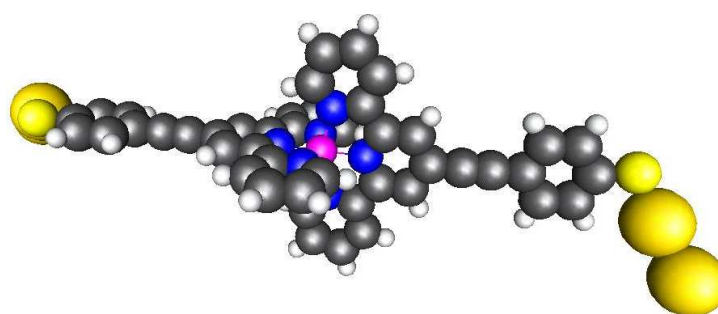


Figure 9.1:  $\text{Ru}^{2+}$  bis-terpyridyl complex. Gray is Carbon, white Hydrogen, blue Nitrogen, yellow Sulfur, orange Gold and magenta is the Ruthenium atom.

The focus of our interest shifts now towards metal-ion complexes, where metal ions are placed into an organic cage. The complexes represent a whole new class of highly technologically interesting materials due to their novel spin and electronic structures [83]. One interesting application to metal organic complexes (MOC's) is building frameworks, so called MOF's. They are three dimensional structures, where six spacer molecules couple to a central metal atoms, forming porous materials. A proposed application is as hydrogen storage[84].

Other possible applications are computer memory units. A transition between two spin states, Low- and High-Spin, is possible for special geometries.

The difference between the spin states can be seen in the different color of the material, the size of the molecule, and transport properties[85].

We will present only a single type of MOC, where a single transition-metal atom is trapped between 6 Nitrogen atoms, a complex of novel properties regarding magnetism and electronic transport [4]. Three of those Nitrogen atoms belong to one organic molecule, a terpyridyl ligand built from three pyridine rings. Two of the terpyridyl molecules couple to a single transition-metal atom. Fig. 9.1 shows the full structure, including the coupling to Gold (required by transport calculations). In this structure, we have two “on-axis”-Nitrogen and 4 “off-axis”.

**Low-Spin vs. High-Spin:** To understand why the molecules are scientifically interesting, one has to analyze the Nitrogen-metal bond in detail. Nitrogen couples with its free electron pair to the metal atom. The transition metal couples via its 5  $D$ -orbitals. In those structures, where 6 partners are available, the  $D$ -orbitals split up into 3 orbitals pointing between the partners,  $t_{2g}$ , and 2 orbitals directly along the direction of the partners,  $e_g$ . Due to greater distance to the N electrons,  $t_{2g}$  will experience lower Coulomb repulsion than  $e_g$ , leading to a split-up in energy,  $\Delta_{\text{oct}}$  (see Fig. 9.2). Some of the more obvious consequences of this phenomenon are different bond length between N and the metal resulting from only occupying  $t_{2g}$  (short, non-bonding) vs. also occupying  $e_g$  (long, anti-bonding). This shifting depends strongly on the corresponding ligand, e.g. forced bond length's.

Orbital	Function	symmetry
$d_1$	$xy$	$t_{2g}$
$d_2$	$xz$	
$d_3$	$yz$	
$d_4$	$(y^2 - z^2)/2$	$e_g$
$d_5$	$(2x^2 - y^2 - z^2)/\sqrt{12}$	

Table 9.1: D-orbitals

In realistic molecules, the octahedral symmetry is in general broken. The loss of the symmetry will break the degeneracy of  $t_{2g}$  and  $e_g$ . Let us now consider a special situation, where the symmetry is not fully broken (a symmetry that we will encounter later). The bond lengths to the four atoms in the Y-Z-plane are increased. The  $e_g$ -orbital in this plane will now be reduced

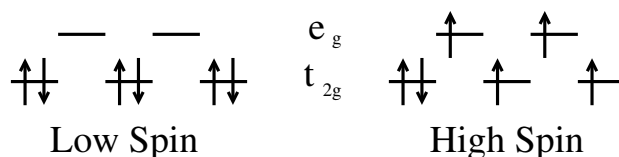


Figure 9.2: Schematic structure of the d-orbitals of transition metals coupled to 6 N-atoms. Left is the low spin structure, where all 6 spins are paired. Right is the high spin, where only two spins are paired.

in energy, because the repulsion from the ligands is weaker. On the other hand, the  $t_{2g}$ -orbital in this plane will feel less binding to the ligands and thus the energy is increased. The other two  $t_{2g}$ -orbital energies increase as well, but the effect is smaller because only half of the partners have an increased distance.

Importantly, any symmetry breaking will reduce the distance between  $t_{2g}$  and  $e_g$ . This very fact can be used to reduce the ligand field. The symmetry splitting can be made as big as  $\Delta_{\text{oct}}$ , leading to vanishing of the gap between  $e_g$  and  $t_{2g}$ .

If there is a large gap (compared e.g. to temperature) between  $t_{2g}$  and  $e_g$  due to a large ligand field strength (like a ligand that wants to sit close to the atom), the first 6  $D$ -electrons will fill the lower lying  $t_{2g}$  states. For metals like  $\text{Ru}^{2+}$ , where one has exactly 6  $D$ -electrons, this leads to a spinless ground state, called Low-Spin (LS). However, if asymmetry or a weak ligand field (if the ligand does not want to sit close to the atom) lead to comparable energies between  $t_{2g}$  and  $e_g$ , the ground state electron configuration may be different. According to Hund's rule, the most preferable configuration is a ground state with spin 2 for 6  $D$ -electrons (meaning 4 unpaired electrons), called High-Spin (HS) state. Because of the occupation of 2 anti-bonding states, the bond length between N and the transition metal will increase by approximately 10%.

Depending on the ligand field strength, the total energy difference between LS and HS can be very small (smaller than room temperature). In such a case, one can have a transition between both states mediated by pressure, temperature or light[86].

**Motivation of the study of transport through MOC's:** Apart from our interest in the origins of novel and tunable spin-crossover, the MOC's are

in our focus because the crossover is fairly well controllable and reproducible[85]. In the LS-state, there is a gap between the unoccupied and the occupied orbitals, leading to a stable and robust configuration. On the other hand, a HS-configuration does not have a gap between unoccupied and occupied, in other words the spin of the metal atom is controllable with a gate. The switchable spin can be used to e.g. switch a Kondo effect on the metal atom by changing the local spin.

The Kondo effect has already been reported in the type of molecules we are interested in Ref. [4], but the transition metal atom of their choice, Cobalt, has seven D-electrons. In this configuration, there will always be a localized spin on the Cobalt atom.

The spin of the metal atom cannot only be changed with a gate, but also with temperature, pressure, or light. In our studies, the switch between LS and HS is realized by pulling on the molecule. This will increase the asymmetry of the molecule and thus reduce the gap between  $t_{2g}$  and  $e_g$ . Increasing the bond length between N and the metal atom by about 10%, the molecule will in general switch from LS to HS.

In the following, we will investigate three different transition metal atoms: Ruthenium (Ru), Iron (Fe), and Cobalt (Co). Ru results can be compared directly to the experiment[47]. Fe has the same electronic configuration like Ru, but the atom is smaller, reducing the ligand field strength. On the other hand, Co is interesting because of the localized spin coming from the unpaired 7th electron.

## 9.1 Ruthenium as central atom: a stable spin zero molecule as test

Let us proceed with Ruthenium as central transition-metal atom. For Ru there is only the low spin state found in experiment (all  $D$ -electrons are paired). This makes the structure of the molecule quite clear from the experimental point of view. The spin and charge states are also known. A direct comparison of our result with the experiment is possible.

The structure of the molecule in equilibrium will be investigated and compared to the experimental findings. Further, we will try to change the spin state of the molecule by applying a gate voltage. For this, one needs to construct an artificial unstable HS-state by applying tensile stress on the

Atom	basis	ecp
Au	def-SV(P) [80]	def-ecp
Ru	def-TZVP	def-ecp
C, N, H, S	TZVPP [81]	–

Table 9.2: Basis sets used for Ru<sup>2+</sup> bis-terpyridyl complex

atoms	distance [pm]
N <sub>x</sub> –Ru	199.37
N <sub>-x</sub> –Ru	199.37
N <sub>y</sub> –Ru	208.92
N <sub>-y</sub> –Ru	208.87
N <sub>z</sub> –Ru	208.87
N <sub>-z</sub> –Ru	208.86

Table 9.3: Bond distances Ru-N

molecule. The impact on the transmission through the molecule for the different spin states will be addressed as well.

**Equilibrium structure of the molecule:** To obtain the structure of the molecule we relaxed the molecule in vacuum with two gold atoms on each side (see Fig. 9.1)<sup>1</sup>. The charge of the molecule was set to 2+ as in experiment[47]. The distances of the N to Ru (see Tab. 9.3) and the charge and spin state of the Ru were compared to the experimental data, and the experimental results fully reproduced. The charge state was extracted from the charge density by integrating the charge in spheres around the ruthenium atom (see Fig. 9.3). As one can observe from this data, the 6 surrounding Nitrogen are placed on a (distorted) octahedron.

The splitting between  $t_{2g}$  and  $e_g$  can be seen in Fig. 9.4, where the energies of the different orbitals are shown. The gap  $\Delta_{\text{oct}}$  is about 3 eV, while the splitting due to asymmetry is about 0.5 eV, leading to a stable LS configuration for Ru<sup>2+</sup>. Determining the value of  $\Delta_{\text{oct}}$  in experiments is quite challenging, but is between 2.5 and 3 eV[87], thus theory is in perfect agreement.

---

<sup>1</sup>For the calculation we used the following parameters: Tab. 9.2 shows the basis sets used for all calculations. The used functional is BP-86.

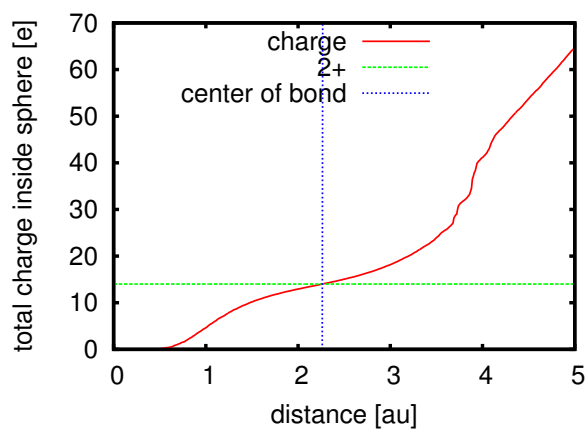


Figure 9.3: Charge density integrated in spheres centered around the central Ru atom. The center of the Ru-N-bond is defined as the point where the change in the charge density is minimal. The charge state of the Ru is 2+ (14 electrons excluding the effective core potential).

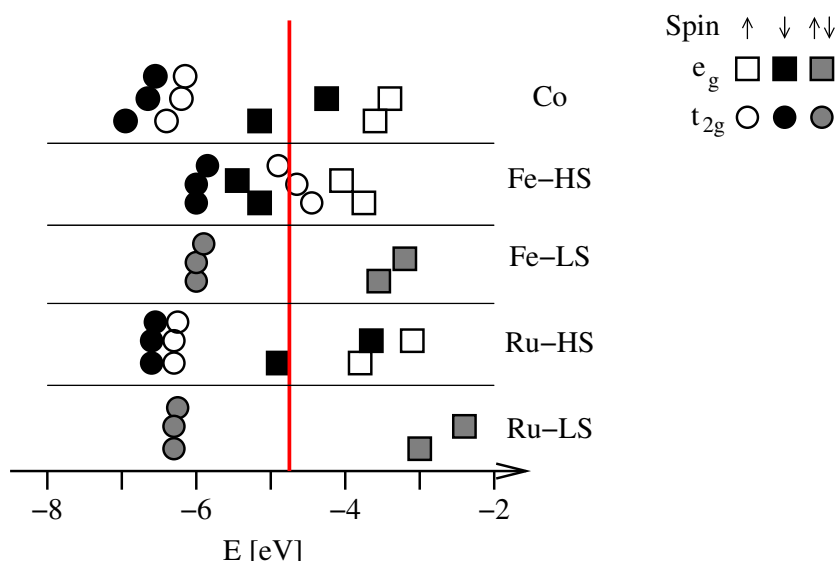


Figure 9.4: Energies of the D-orbitals of various transition metals. Presented are Ru, Fe, and Co. Ru and Fe (in LS-state) are spin degenerate, while Co and HS-states are spin split. This illustrates the different  $\Delta_{\text{oct}}$  for different transition metal atoms.

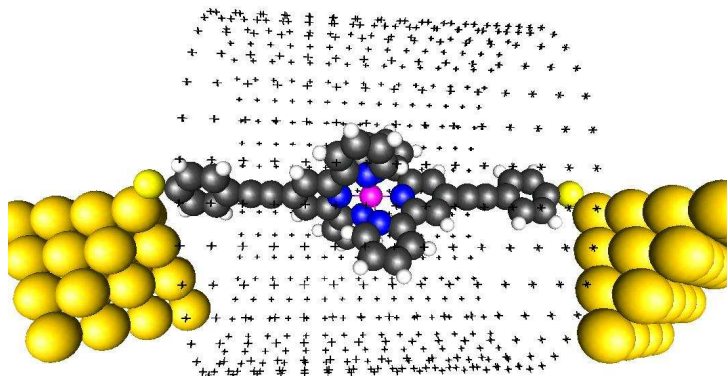


Figure 9.5:  $\text{Ru}^{2+}$  bis-terpyridyl complex coupled to leads (30 gold atoms). Also shown is the cylindrical gate for charging of the molecule.

**HS-structure:** A high spin configuration would have a longer bond distance (Pauli principle: the anti-bonding state has to be occupied)[85]. But since the Ruthenium is quite large (a 4D transition-metal), the deformation of the complex would cost a lot of energy ( $> 0.07$  eV), more than the gain in exchange coming from the formation of the local spin. This makes the low spin configuration the only stable state.

To be able to calculate a HS-configuration, one has to apply tensile stress to the molecule, meaning stretching the bonds by hand. We increased the on-axis distance from 199 pm to 222 pm and the off-axis distance from 209 pm to 238 pm and relaxed the new structure while keeping N-Ru bond length fixed. The calculation resulted in a local spin on the Ru atom, as one would expect.

But a close look at the orbital positions shows that the gap between  $t_{2g}$  and  $e_g$  did not entirely vanish, it is fairly reduced from about 3 eV to a spin split state with 1.5 eV for majority spin and 2 eV for minority spin. One  $e_g$  orbital of only one spin channel moved below the Fermi energy. This clearly points out, that the spin state of the molecule is still LS, but now an additional electron is attracted by the Ru atom.

This is not the configuration we were looking for, but it is still very promising. Applying a gate voltage to the stretched molecule can change the local spin, because the HOMO-LUMO gap is greatly diminished.

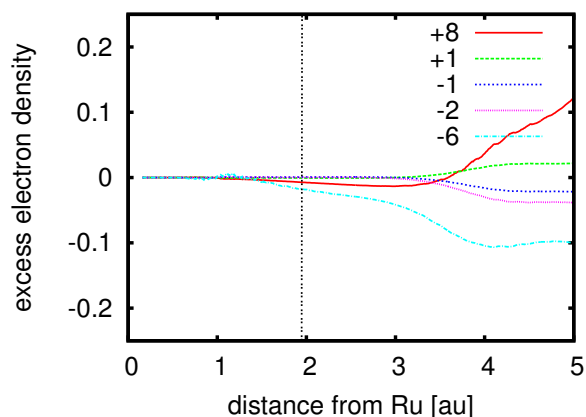


Figure 9.6: Excess electron density on Ru-complex (LS) for different gate charges. The excess electrons do not change the charge of the Ruthenium, only the surrounding terpyridyl is charged (the distance Ru-N is 4 au, the center of the bond is marked as a vertical line).

**Gating the molecule:** In order to judge about the stability of the charge state of the Ru-atom, a charging of the molecule was performed by means of applied gate voltage. Fig. 9.5 shows the used structure for the calculations, including the gate. Fig. 9.6 shows the excess electron density integrated in spheres around the Ru-atom. Between the Ru and the N (the distance is about 4 au), there is almost no excess electron density, showing that the charge state is very stable, indeed.

The same procedure was applied to the HS-structure, see Fig. 9.7. Here one can see that charge and spin state of the molecule change, as expected. The total energy of the HS structure is always about 0.07 eV higher than the LS structure, meaning the gate cannot induce a transition between the two states.

**Transport calculations:** The transport calculations were performed with the structure from Fig. 9.5 as well as the gating. A frequent problem for this kind of fairly large molecules is, that the leads cannot be large enough to reach the thermodynamical limit, where  $E_F$  of the extended molecule is approaching the Fermi energy of bulk Gold. So one has to analyze the effect of different lead sizes on the level positions and the Fermi energy in order to see which properties are robust and well described under changing the lead

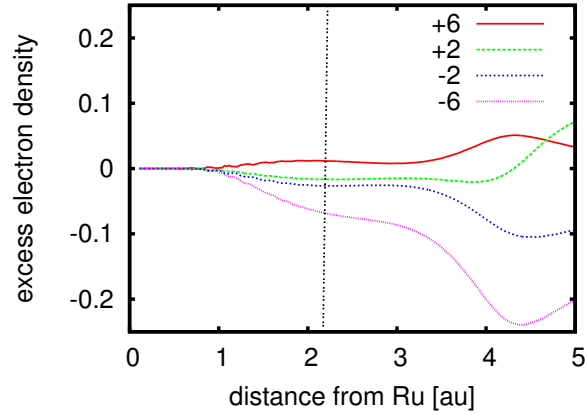


Figure 9.7: Excess electron density on Ru-complex (HS) for different gate charges. The excess electrons do not change the charge of the Ruthenium, only the surrounding terpyridyl (the distance Ru-N is 4.5 au, the center of the bond is marked as a vertical line).

Gold atoms	HOMO [eV]	LUMO [eV]
14	-4.332	-4.332
18	-4.631	-4.476
30	-4.586	-4.516
39	-4.623	-4.619

Table 9.4:  $E_F$  of Ru complex for different lead size. Shown are the energies of the HOMO and the LUMO,  $E_F$  is in between.

size and which are not.

The 2 gold atoms on each side were replaced by gold pyramids of 14, 18, 30 or 39 atoms on each side (see Fig. 9.5). Tab. 9.4 shows the HOMO and LUMO of the full *extended* molecule (not the HOMO and LUMO of molecular orbitals).  $E_F$  lies in between this HOMO and LUMO. In Fig. 9.8 the flow of orbital energies is presented. The relative position of the molecular LUMO compared to the Fermi energy of the finite system seems to converge fairly fast. While  $E_F$  is still 0.5 eV higher than the bulk value, the relative energy of the LUMO changes only by 0.1 eV. Only hybridization changes somewhat, showing that the energies of the molecular orbitals relative to  $E_F$  can be predicted well.  $E_F$  cannot be predicted well due to the number of electrons on the molecule (more than 300) is comparable to the number of electron in

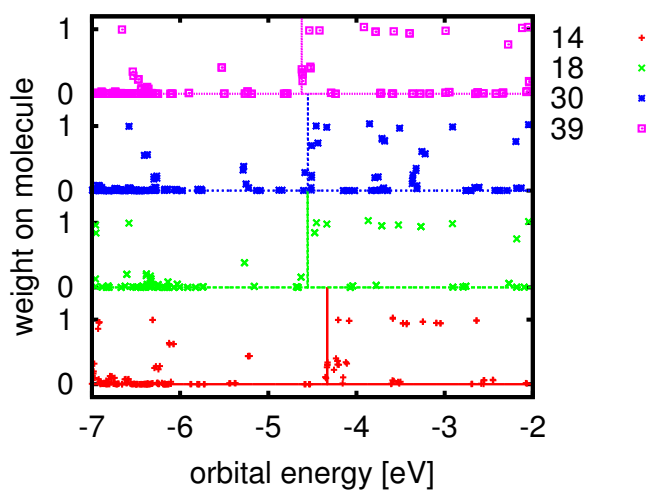


Figure 9.8: Flow of orbital energies for Ru complex. Shown is the relative weight of each orbital on the molecule for different lead size. The dots on the zero lines are almost fully localized on the leads, while dots close to one are almost localized on the molecule. Also shown is  $E_F$ . The position of the LUMO relative to  $E_F$  is almost constant, showing that the peak position relative to  $E_F$  is converging fast. On the other hand,  $E_F$  converges very slowly to the bulk value of gold ( $\approx -5$  eV).

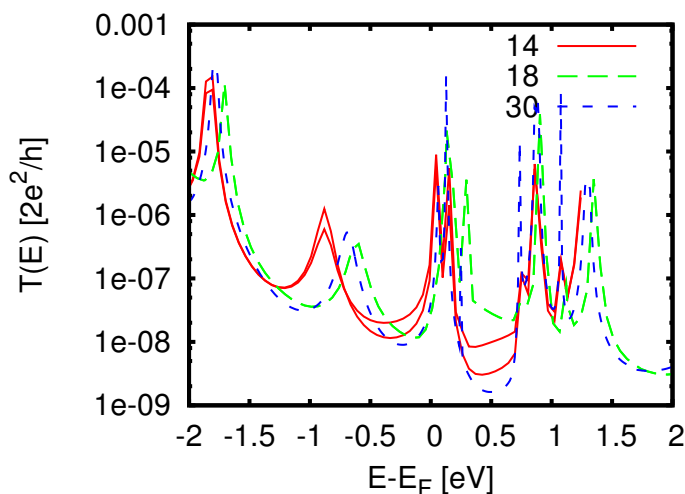


Figure 9.9: Transmission through the Ru complex for different lead size, plotted relative to  $E_F$ . The 14 atom transmission shows a weak spin splitting (two red lines). The peak position of the LUMO changes less than 0.1 eV.

the leads (about 500). The limit  $N_{\text{Au}} \gg N_{\text{M}}$  is not yet within reach.

Calculation of the transmission turned out to be much more involved than for smaller molecules. The standard convergence criteria from TURBOMOLE (energy convergence of  $10^{-6}$  and no density convergence) are much too weak, and only for energy convergence of  $10^{-7}$  as well as density convergence of  $10^{-8}$  the results of 14, 18 and 30 gold atoms were comparable with each other<sup>2</sup>. The transmission is shown in Fig. 9.9 for different lead sizes (relative to  $E_F$ ).

To show the convergence of the transmission for different coupling strength  $\eta$  the transmission was calculated for different  $\eta$  between 0.272 eV and 27.2 eV (see Fig. 9.10). For  $\eta$  between 1.36 eV and 13.6 eV the transmission is almost identical, while for the other values of  $\eta$  only the peak position is correct, but the height or the width are incorrect. We are at the plateau of  $\eta$  where the transmission is largely independent of the parameters, but the convergence is not great due to the small number of Gold atoms in the lead.

We do not have a real HS-state for Ru as central atom, but rather a spin split ground state, where only one spin channel is occupied at  $E_F$ . Impor-

<sup>2</sup>The last two layers of gold in the pyramids were coupled using absorbing boundaries and an  $\eta$  of 2.72 eV.

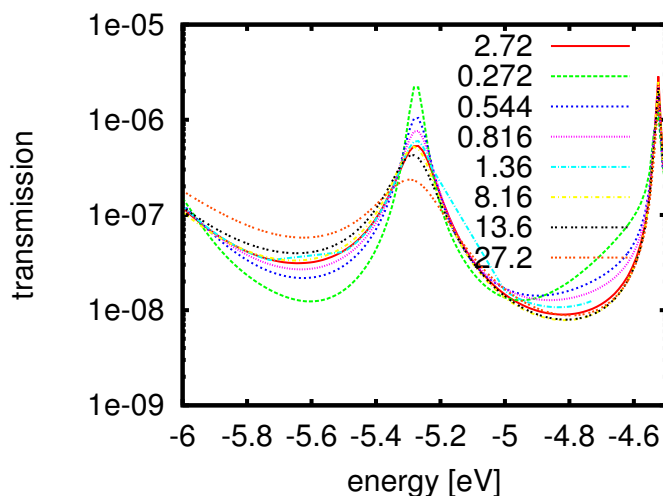


Figure 9.10: Transmission through the Ru complex for different  $\eta$ , showing that around  $\eta = 2.72$  eV the transmission does not change within small changes of  $\eta$ . Due to the smallness of the leads (30 Gold atoms here),  $\eta$  can only be changed within about one order of magnitude.

tantly, this shifts the  $e_g$ -peak of transmission function for the occupied spin directly at  $E_F$ , while the unoccupied orbital is still higher in energy, meaning that the transmission for  $V_{\text{bias}} < 0.1$  eV will differ (the voltage has to be smaller than the gap between  $E_F$  and the unoccupied  $e_g$  orbitals).

Conclusively, by pulling the molecule it turns into a spin filter, where the conductance for one spin is much higher than for the other spin. For this effect to take place, one has to stabilize the spin, meaning fix the direction. If the direction of the spin is not fixed, it may lead to a switchable Kondo effect.

## 9.2 Iron as central atom: Spin filter?

$\text{Fe}^{2+}$  (3d series) and  $\text{Ru}^{2+}$  (4d series) are isoelectronic transition metal ions, but Fe is much smaller due to having a shell less than Ru (see Tab. 9.5), making interaction with the rather rigid ligand field weaker and thus allowing for both high- and low-spin states. For the bis-terpyridyl complex without any modification still only the low spin configuration is stable. But with some modifications the high spin can be made stable. The energy difference

atoms	distance LS [pm]	distance HS [pm]
$N_x - \text{Fe}$	188.46	210.05
$N_{-x} - \text{Fe}$	188.57	210.15
$N_y - \text{Fe}$	198.70	220.57
$N_{-y} - \text{Fe}$	198.67	220.66
$N_z - \text{Fe}$	198.64	221.03
$N_{-z} - \text{Fe}$	198.69	221.12

Table 9.5: Bond distances Fe-N

between the two spin states is much smaller in comparison to Ru, so in this case switching to a real HS-state is possible by pulling.

For the calculation the same setup as for the Ru-complex was used, only Ru was exchanged by Fe. Again the molecule was relaxed with only two Gold atoms on each side, then the Gold atoms were replaced by 30 atom Gold pyramids<sup>3</sup>. The charge state of the complex is 2+ and the spin state of the central Fe atom is 0 as in the experiments[88]. The energy split  $\Delta_{\text{oct}}$  is reduced to about 2.5 eV (see Fig. 9.4 on page 112).

For the high spin state of the molecule ( $S^2 = 6$ ) the bond distances are known from experiment (from slightly different clusters with a strongly reduced ligand field [88]). The distances are a bit larger, as a direct consequence of the anti-bonding states being occupied. We changed the geometry to the high spin state (see Tab. 9.5) and let it relax. Relaxation lead back to the low spin solution, an apparent proof of the high spin state being unstable, which is in good agreement with the experiment. However, without relaxation and increased bond distances, the local spin of the  $\text{Fe}^{2+}$  is different compared to the LS structure, as can be seen in Fig. 9.4.  $\Delta_{\text{oct}}$  is reduced to less than 1 eV, below  $U$ . Here we really have a HS-state, where all orbitals of majority spin are occupied, while only one of the minority spin is filled. This clearly indicates how important the ligand field interaction is.

It can be understood easily, why the HS-state is not stable even for Iron between these ligands. The terpyridyl complex is very stiff. For the high spin state the bonds have to be even larger than the bonds for the Ru-molecule in LS (see Tab. 9.3). So the terpyridyl molecule has to be stretched too much, which is energetically rather unfavorable. Charging the molecule will not help here, either. The structure of the terpyridyl has to be modified. The

---

<sup>3</sup>The basis set information is given in Tab. 9.6.

Atom	basis	ecp
Au	def-SV(P) [80]	def-ecp
Fe	TZVPP [81]	–
C, N, H, S	TZVPP [81]	–

Table 9.6: Basis sets used for Fe<sup>2+</sup> bis-terpyridyl complex

analysis of this is work in progress.

### 9.3 Cobalt as central atom: Kondo physics

Experiments reported, that in molecules with Cobalt-II, the Kondo effect can be seen[4]. The difference between Co<sup>2+</sup> and Fe<sup>2+</sup> is that there is one additional electron in the *D*-orbital. In the low spin state, this additional electron has to occupy one of the anti-bonding states, because of all other orbitals being already filled. In such a case, we have a single spin localized on the metal atom. The direction of the spin is not fixed, opening the door for Kondo physics.

We did the structure relaxation of the same molecule as above, but with Fe exchanged by Co. There is no functional known yet which will reproduce the Kondo effect since this is an effect of strong correlation. Nonetheless, what one can still observe is the localized spin on the Co. If the spin is absent, then there is no Kondo effect.

From our calculation it can be observed that the orbitals look exactly like those of the Fe-complex, apart from having one additional electron on the Co. The ground state is a low spin system but with a single localized spin in an *e<sub>g</sub>* orbital. The electronic structure is comparable to the stretched Ru-structure (see Fig. 9.4), where we also observed a local spin. When comparing the bond distances Co-N (Tab. 9.7), one observes that the distances of one complex are comparable to the Fe-LS distances, while the off-axis distances of the other are close to the Fe-HS distances (c.f. 9.5). This indicates, that the additional electron is localized in the orbital  $d_5 = (-x^2 - y^2 + 2z^2)/\sqrt{12}$  (note, that the orbital now points in *z*-direction, not *x*). Relevance of these findings regarding experimental results has still to be established.

atoms	distance [pm]
$N_x - \text{Co}$	193.44
$N_{-x} - \text{Co}$	185.91
$N_y - \text{Co}$	199.06
$N_{-y} - \text{Co}$	199.21
$N_z - \text{Co}$	219.38
$N_{-z} - \text{Co}$	219.45

Table 9.7: Bond distances Co-N. The bonds  $x$ ,  $z$  and  $-z$  correspond to the terpyridyl molecule, which is affected by the additional electron (c.f. Tab. 9.5).



# Chapter 10

## Summary

In this thesis, we introduced a method for quantum chemistry calculations with coupling to one or more thermodynamic reservoirs. The method makes *ab initio* calculations of molecular systems coupled to macroscopic reservoirs efficient, since the results can be easily checked. Moreover, the analytical spectral integration that is feasible within our approach makes the computation reasonably fast, accurate, and relatively easy to implement. It is based on the observation that in a certain limiting case reservoirs can be described with an arbitrary accuracy by a model of absorbing boundary conditions (a procedure well established in quantum optics). Used with only one reservoir, gating of molecules or adsorption on surfaces can be described. When used with two or more reservoirs, non-equilibrium physics can be studied.

We implemented the method as a prototype version in the quantum chemistry package TURBOMOLE and then tested the algorithm carefully. We showed that our model coupling is applicable in all cases investigated and the results are essentially identical to earlier observations. We illustrated the effects of failure of the method, indicated by strong oscillations in the transmission function as well as the DoS that represent the cavity modes in the electrode pieces of the “extended molecule”. Importantly, we illustrated how it is possible to check whether our model coupling is applicable. This left us with an hierarchy of energies, where the level spacing of the orbitals in the “extended molecule”, where a small portion of the leads is included in the calculation, has to be much smaller than the level broadening of the molecular orbitals.

Using the developed method, we investigated different aspects of molecular electronics. One important topic is applying a gate voltage and analyzing

the effect on the electronic structure and the transmission function. The other is applying finite bias voltage and calculating the  $I(V)$ -curve in this non-equilibrium situation and investigating non-linear effects. Moreover, we studied the effect of the approximation in the exchange part of the LDA type functionals on these effects.

Gating of molecules is really important, one can learn a lot about properties of molecules, e.g. the energy of the LUMO. This information is of crucial importance when building devices that switch their properties under a gate voltage, because it determines the switching voltage.

With gating, we revealed dramatic discrepancies between the real physics and the results for LDA type (mean field) functionals. Instead of a step-wise increase of the electron number on the molecule (broadened only by hybridization), the calculations show a smearing of the order of the Coulomb interaction  $U$ . Since the energy gap between the steps in Coulomb blockade is  $U$ , this physics is completely hidden in this approximation. This approximation affects the transmission function as well, leading to an overestimation of the conductance while an orbital crosses the Fermi energy.

A simple but important effect of the finite bias on molecular orbitals is the “Stark effect”. Stark physics is well mirrored even for LDA type functionals. We showed that the linear and quadratic Stark effect driven by  $V_{\text{bias}}$  can be observed by analyzing the orbital energies. But, since applying a finite bias voltage may induce an excess charge on the molecule, the same problem as for gating molecules exists in this calculations as well. Depending on the molecule, this can lead to a dramatic change of the  $I(V)$ -curve, as we observed for the example of a Bipyridine molecule. In this molecule, the partially occupied LUMO shifts only very slowly in energy with  $V_{\text{bias}}$  due to self-interaction, which of course is completely artificial. This leads to a smearing of the step in the current by  $U$  again. However, for non-equilibrium calculations, not all physics is hidden. We observed, that under a finite bias voltage the linear Stark effect reduces the current. This is due to localization of the orbitals, like in a PN-junction. The electric field polarizes the orbitals, reducing the charge on one side of the molecule and thus diminishing conductance. Moreover, the linear Stark effect can shift localized orbitals out of resonance, leading to a “vanishing” of peaks in the transmission function and thus reducing the overall current (as compared to the non-selfconsistent calculation).

As an interesting application of the developed formalism, we investigated metal-organic complexes with nearly octahedral symmetry. We showed that

depending on the (transition) metal atom in the center, one can have a stable diamagnetic molecule (Ruthenium), a possible switching between two different spin states (Iron), or a localized spin (Cobalt). In case of Iron, switching between two different spin configurations (LS:  $S = 0$  and HS:  $S = 2$ ) by applying tensile stress is possible. This makes this molecule very interesting for a switchable Kondo effect, or a device for information storage.

**Outlook:** The method for calculating transport with model self-energies has been used in our group for many other molecules as well, which have not been reported in this thesis. It turned out to be fully reliable and efficient.

Since the coupling of molecules to reservoirs with our method turned out to be very successful, it is planned to fully include it into the package TURBOMOLE. This will allow (due to the expected speedup) for calculations of much larger molecules, as compared to the present implementation.

As we already mentioned, the coupling to thermodynamic reservoirs can also be used to model exchange between molecules and surrounding media. Quantum chemistry in non-trivial vacua is a very important field. One application is quantum chemistry in a electrochemical environment. The effect of the surrounding solution is not taken into account by now, except for a simplified treatment of screening. Applications in nano biology exist, as well. Our new way of introducing thermodynamic reservoirs into the quantum chemistry calculation is a small but perhaps very important step towards a better access to this intriguing class of problems. In the future, it would be important for such applications to come up with a more realistic model of screening and self-energies to better model the effect of solutions.

A further investigation on transport through metal-organic complexes would be very interesting. Small changes in the ligands change the ligand field and thus the electronic structure of the central metal atom. Studies of the impact of the effects on electronic transport are currently under way.



# Appendix A

## Program package TURBOMOLE

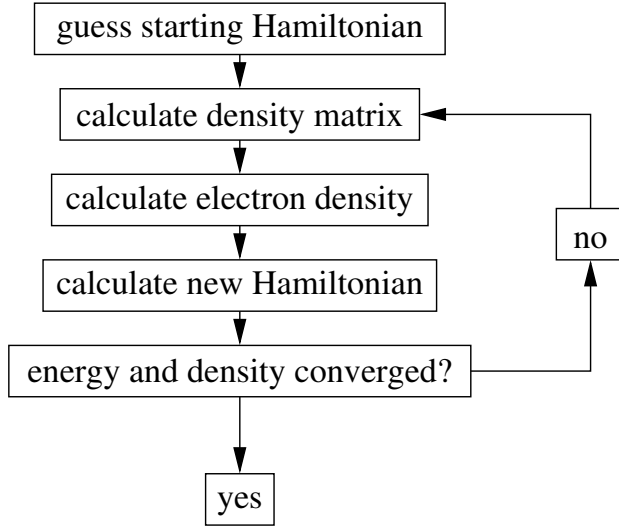
TURBOMOLE is a program package for DFT calculations[30, 89]. Here, we want to give a short explanation of how the Khon-Sham scheme is implemented.

The Khon-Sham states (eigenvectors of the Hamiltonian) are expressed in a non orthogonal basis set of Gaussian basis functions [80, 81]:

$$\langle \vec{x} | i \rangle = \sum_n P_n(\vec{x}) \exp(-\xi_n \vec{x}^2) \quad (\text{A.1})$$

where  $P_n(\vec{x})$  is a polynomial, defining the symmetry. S-type orbitals only have a constant and P-type orbitals a first order polynomial [].

TURBOMOLE starts the DFT calculation from a guess for the Hamiltonian. After that, the following self consistency loop is repeated until the energy and density of the molecule is converged.



To improve the convergence, additional parameters, like a finite temperature and a damping exist. The finite temperature smears the occupation of orbitals close to  $E_F$ , This helps for finding the real ground state of a system if the spin of the ground state is not known. To improve the convergence of the SC-loop, the Hamiltonian for the next loop will be a mixture of the old and new guess,  $H_N = \frac{1}{1+\alpha}(H_{N-1} + \alpha H$ , where  $\alpha$  is the specified damping.

Each iteration TURBOMOLE produces a new set of Khon-Sham states  $\Phi_\alpha^i$ . The Hamiltonian of the molecule can be built from them:

$$H = S^{1/2} |\Phi_\alpha \rangle \langle \Phi_\alpha| S^{1/2} \quad (\text{A.2})$$

Here the (Löwdin-)orthonormalization[90] is important, because the basis is non-orthogonal, the Khon-Sham states are the eigenvectors of this Hamiltonian. The density matrix is constructed out of this Khon-Sham eigenstates:

$$D = \sum_{\text{occ.}} S^{-1/2} |\Phi_\alpha \rangle \langle \Phi_\alpha| S^{-1/2} \quad (\text{A.3})$$

Important is, that only the occupied orbitals contribute to the density. The unoccupied orbitals do not have any effect for the DFT calculation. That's why in TURBOMOLE they are treated differently from the occupied orbitals. To prevent the (artificial) unoccupied orbitals from falling below  $E_F$ ,

a finite energy is added. Since this does not affect the ground state electron density, this procedure is allowed. But for calculating the full Hamiltonian for transport calculations, this artificial level shift has to be set to zero (in the transmission function the unoccupied orbitals contribute as well).

In our calculations we always used RI-DFT [91, 92]. It is much faster for our molecules, and the approximations are good.

### A.0.1 Relaxation of atomic structures

For the relaxation of molecular structures, TURBOMOLE can calculate the gradients of the energy with the program rdgrad []. The molecular coordinates are then shifted in direction of the gradient, then the DFT calculation is repeated. After some iterations this will converge to the configuration with minimal energy.

This takes a long time for large molecules, so we are not able to do this relaxation with large leads. Usually one can use a small lead to relax the structure, that is possible. But in this case the lead (or at least the part of the lead we want to couple to the infinite leads) has to be fixed. If not, they will form some stable cluster which is completely different from experiment, because the calculated molecule has only a finite size. For the fixed lead coordinates the convergence of the relaxation is very bad, but the coordinates of the molecule do not shift too much. That is because it is not the lowest energy configuration, there are still forces on the molecule. But they are coming from the coupling. The results in transmission usually do not depend on the small shifts of the molecule.

The gradients of the energy depend not only on the electron density, but also on the derivative of the density. The derivative is calculated analytically from the Kohn-Sham-orbitals.

### A.0.2 Including gates into TURBOMOLE

The atoms of the gate cannot be included in the calculation, because the system would be too large. Another idea would be to solve the Poisson equation with a different boundary condition (the electric field inside the metal is zero and on the surface orthogonal). On a metallic gate the parallel electric field is vanishing. A solution around the molecule completely screens the electric field, there is no field outside. But the calculation of the field is still complicated.

There is another very easy way of modeling gates: using point charges[72]. A point charge does not have electronic states. But there is an electric field. Since on a metallic gate all charges will accumulate on the surface, this is a good approximation. For a charged solution the point charges have to be cylindrical all around the molecule, because the molecule is surrounded by the solution.

The full system has to be charge neutral. If it is not, there will be an infinite sized electric field. But there is additional charge on the gate. The charge on the molecule has to be changed such that the system is neutral again.

Including gates with this method has one big advantage: there is almost no additional computation time. The additional potential from the point charges only has to be added to the Hamiltonian.

### A.0.3 Transport calculations with TURBOMOLE

To do transport calculations with TURBOMOLE one has to build the Hamiltonian out of the KS-states given by the DFT calculation. TURBOMOLE uses a non-orthogonal basis with Gaussian basis functions [80, 81]. But for the transport calculation the Hamiltonian  $H$  is needed in an orthogonal basis. It can be transformed using the overlap matrix built out of the overlap of different basis functions (Löwdin orthonormalization):

$$S_{ij} = \langle i|j \rangle \quad (\text{A.4})$$

$$H_{ij}^{\text{no}} = \sum_{\alpha} \Phi_i^{\alpha} \Phi_j^{\alpha} \quad (\text{A.5})$$

$$H = S^{1/2} H^{\text{no}} S^{1/2} \quad (\text{A.6})$$

The coupling to the left and right lead is given by  $\Sigma_L$  and  $\Sigma_R$ . From that we get:

$$\Gamma_{L/R} = \text{Im} \Sigma_{L/R} \quad (\text{A.7})$$

$$\Sigma = \Sigma_L + \Sigma_R \quad (\text{A.8})$$

Now we can construct the Green function  $G$  from this Hamiltonian with the coupling  $\Sigma$  to the leads.

$$G^{-1}(E) = E - H - \Sigma \quad (\text{A.9})$$

The self energy has to be given in the same orthogonal basis as the Hamiltonian  $H$ . For small systems the calculation of this self energy is very expensive. But we will show in chapter 4.3, that the coupling to the leads can be understood as absorbing boundaries. This makes the calculation much easier.

Now since we know all we need for the transmission, we simply plug everything together:

$$T(E) = \text{Tr} \Gamma_L G(E) \Gamma_R G^\dagger(E) \quad (\text{A.10})$$

Instead of using the orthonormal basis, one can as well calculate the transmission function in the non-orthogonal basis. In this case the transmission is calculated via:

$$T(E) = \text{Tr} \Gamma_L^{\text{no}} G^{\text{no}}(E) \Gamma_R^{\text{no}} G^{\text{no}\dagger}(E) \quad (\text{A.11})$$

Since the basis, in which the self-energy is expressed, has to be identical to the basis of the extended molecule, one can see, that the self-energy is not fully independent of the molecule. Only for large extended molecule, where the overlap of basis functions between the (calculated) leads and the molecule is close to zero, the self-energy can be fully independent of the molecule (note, that the size of the largest basis functions of Gold is about 10 au).

A model self-energy, as introduced in Chap. 4, will be sensitive to the overlap between Gold and the molecule, too. A finite broadening in the leads will lead to a direct broadening of molecular orbitals, if the broadened basis functions of Gold extend onto the molecule. The distance between the broadening region and the molecule has to be larger than the size of the orbitals of Gold.



# Appendix B

## Explicit calculation of the coupled density matrix

In Chapter 3.3 the algorithm for calculating the density matrix with open boundaries was developed. But since TURBOMOLE does not have a orthogonal basis, a Löwdin-orthonormalization is needed. The following scheme sketches the calculation of the density matrix including this orthonormalization:

Input:

- $\epsilon_p, c_{\nu p}$ : eigenvalues and expansion coefficients of molecular orbitals  $|p\rangle$  in basis  $|\nu\rangle$
- $\eta_{L/R}, \delta\epsilon_{L/R}$ : coupling parameters to left/right reservoir
- $\mu_{L/R}$ : chemical potential of left/right reservoir

Calculation steps:

1. Calculate  $S_{\nu\tau}, S_{\nu\tau}^{1/2}$  and orthogonalize molecular orbitals:  $\tilde{c}_{\tau p} = S_{\tau\nu}^{1/2} c_{\nu p}$
2. Construct  $H_{\tau\nu} = \epsilon_p \tilde{c}_{\tau p} \tilde{c}_{\nu p} + \Sigma_{\tau\nu}$   

$$\Sigma_{\tau\nu} = \begin{cases} \delta_{\nu\tau} (\delta\epsilon_{L/R} + i\eta_{L/R}) & \text{at coupling atoms} \\ 0 & \text{else} \end{cases}$$
3. Get eigenvalues  $Z_p$  and eigenvectors  $b_{\kappa p}$  of  $H_{\tau\nu}$ .
4. Calculate  

$$\tilde{n}_{\kappa\lambda}^{eq} = b_{\kappa p} \left[ 1 + \frac{1}{2\pi} [\ln(\mu_L - Z_p^*) - \ln(\mu_L - Z_p)] \right] b_{p\lambda}$$
5. Form  $b_{p\nu}^{-1}$ ,

calculate  $\tilde{N}_{pq} = b_{p\nu}^{-1} \Gamma_{\nu\tau}^R b_{\tau q}^{-1}$ ,

$$\Gamma_{\tau\nu}^R = \begin{cases} \delta_{\tau\nu} \eta_R & \text{at coupling atoms} \\ 0 & \text{else} \end{cases}$$

then

$$\tilde{M}_{pq} = \frac{\tilde{N}_{pq}}{Z_p - Z_q^*} \left[ \ln(\mu_R - Z_q^*) - \ln(\mu_R - Z_p) - \ln(\mu_L - Z_q^*) + \ln(\mu_L - Z_p) \right]$$

and finally  $\delta\tilde{n}_{\kappa\lambda} = \frac{1}{\pi} b_{\kappa p} \tilde{M}_{pq} b_{q\lambda}$ .

6. Transform back:  $n_{\nu\tau} = S_{\nu\kappa}^{-1/2} [\tilde{n}_{\kappa\lambda}^{eq} + \delta\tilde{n}_{\kappa\lambda}] S_{\lambda\tau}^{-1/2}$

# Appendix C

## Analytical calculation of the transmission of a tight-binding chain with a triple barrier

The Hamiltonian of this problem is:

$$H_{i,j} = t_i (\delta_{i,j+1} + \delta_{i+1,j}) \quad (\text{C.1})$$

with hopping amplitudes  $t_i$  given by

$$\begin{aligned} t_M &= V_L && \text{left barrier} \\ t_N &= V_C && \text{center barrier} \\ t_O &= V_R && \text{right barrier} \\ t_i &= 1 && \text{everywhere else} \end{aligned}$$

and barriers located at positions  $M, N, O$ . The scattering states in the four different sections of the wire can be written as

$$\begin{aligned} \Psi_j &= e^{ikj} + re^{-ikj} && \text{left lead} \\ \Psi_j &= ae^{ikj} + be^{-ikj} && \text{left to center barrier} \\ \Psi_j &= ce^{ikj} + de^{-ikj} && \text{center to right barrier} \\ \Psi_j &= te^{ikj} && \text{right lead} \end{aligned}$$

with energy  $E(k) = -2 \cos k$

Let us now write down the consequences of the Schrödinger equation left and right of each barrier:

$$\begin{aligned}
E\Psi_M &= \Psi_{M-1} + V_L\Psi_{M+1} \\
E(e^{Mik} + re^{-Mik}) &= e^{(M-1)ik} + re^{(1-M)ik} + V_L(ae^{(M+1)ik} + be^{-(M+1)ik}) \\
E\Psi_{M+1} &= V_L\Psi_M + \Psi_{M+2} \\
E(ae^{(M+1)ik} + be^{-(M+1)ik}) &= V_L(e^{Mik} + re^{-Mik}) + ae^{(M+2)ik} + be^{-(M+2)ik} \\
E\Psi_N &= \Psi_{N-1} + V_C\Psi_{N+1} \\
E(ae^{Nik} + be^{-Nik}) &= ae^{(N-1)ik} + be^{(1-N)ik} + V_C(ce^{(N+1)ik} + de^{-(N+1)ik}) \\
E\Psi_{N+1} &= V_C\Psi_N + \Psi_{N+2} \\
E(ce^{(N+1)ik} + de^{-(N+1)ik}) &= V_C(ae^{Nik} + be^{-Nik}) + ce^{(N+2)ik} + de^{-(N+2)ik} \\
E\Psi_O &= \Psi_{O-1} + V_R\Psi_{O+1} \\
E(ce^{Oik} + de^{-Oik}) &= ce^{(O-1)ik} + de^{(1-O)ik} + V_Rte^{(O+1)ik} \\
E\Psi_{O+1} &= V_R\Psi_O + \Psi_{O+2} \\
Ete^{(O+1)ik} &= V_R(ce^{Oik} + de^{-Oik}) + te^{(O+2)ik}
\end{aligned}$$

or in matrix notation:

$$\begin{aligned}
\begin{pmatrix} e^{(M+1)ik} & e^{-(M+1)ik} \\ V_L e^{Mik} & V_L e^{-Mik} \end{pmatrix} \begin{pmatrix} 1 \\ r \end{pmatrix} &= \begin{pmatrix} V_L e^{(M+1)ik} & V_L e^{-(M+1)ik} \\ e^{Mik} & e^{-Mik} \end{pmatrix} \begin{pmatrix} a \\ b \end{pmatrix} \\
\begin{pmatrix} e^{(N+1)ik} & e^{-(N+1)ik} \\ V_C e^{Nik} & V_C e^{-Nik} \end{pmatrix} \begin{pmatrix} a \\ b \end{pmatrix} &= \begin{pmatrix} V_C e^{(N+1)ik} & V_C e^{-(N+1)ik} \\ e^{Nik} & e^{-Nik} \end{pmatrix} \begin{pmatrix} c \\ d \end{pmatrix} \\
\begin{pmatrix} e^{(O+1)ik} & e^{-(O+1)ik} \\ V_R e^{Oik} & V_R e^{-Oik} \end{pmatrix} \begin{pmatrix} c \\ d \end{pmatrix} &= te^{(O+1)ik} \begin{pmatrix} V_R \\ E - e^{ik} \end{pmatrix}.
\end{aligned}$$

Since our interest is in the transmission  $T = |t|^2$ , we only extract an equation for the transmission coefficient,  $t$ :

$$\begin{aligned}
&\left[ (V_L^2 e^{ik} - e^{-ik})(V_C^2 e^{ik} - e^{-ik}) \right. \\
&\quad \left. - (V_L^2 e^{-(2M+1)ik} - e^{-(2M+1)ik})(V_C^2 e^{(2N+1)ik} - e^{(2N+1)ik}) \right] (V_R^2 e^{ik} - e^{-ik}) \\
&- \left[ (V_L^2 e^{ik} - e^{-ik})(V_C^2 e^{-(2N+1)ik} - e^{-(2N+1)ik}) \right. \\
&\quad \left. - (V_L^2 e^{-(2M+1)ik} - e^{-(2M+1)ik})(V_C^2 e^{-ik} - e^{ik}) \right] (V_R^2 e^{(2O+1)ik} - e^{(2O+1)ik}) \\
&= \frac{8}{t} V_L V_C V_R \sin^3 k. \tag{C.2}
\end{aligned}$$

After specializing to the case of a strong, symmetric barrier, where  $V_L=V_C=V_R=V \ll 1$  and  $M=0$ ,  $N=2$ ,  $O=4$ , we conclude

$$T(k) = \left( 2V^3 \frac{\sin^3(ka)}{|\sin^2(3ka) - V^2 \sin^2(2ka) + 2V^2 e^{ika} \sin(3ka) \sin(2ka) + o(V^4)|} \right)^2 \quad (\text{C.3})$$



# Acknowledgment

Many people helped me writing this thesis, thanks to them all:

- Ferdinand Evers, for supervising me,
- Peter Wölffe, for being second reviewer,
- Florian Weigend and Oliver Rubner, for introducing me into TURBO-MOLE and introducing me into quantum chemistry,
- Max Köntopp, Velimir Meded, and Alexej Bagrets for extended discussions,
- All members of both institutes, INT and TKM, for valuable discussions and a lot of fun,
- Axel Arnold, Velimir Meded, and Thomas Ludwig for correcting my thesis,
- and of course all my friends for having a nice time in Karlsruhe.

Ganz besonders will ich meiner Freundin, meinen Eltern, meinem Bruder und meinen Schwiegereltern danken, da sie immer für mich da waren.



# Bibliography

- [1] James M. Tour. Molecular electronics. synthesis and testing of components. *Acc. Chem. Res.*, 33:791–804, 2000.
- [2] M. Elbing, R. Ochs, M. Koentopp, M. Fischer, C. von Hänisch, F. Weigend, F. Evers, H. B. Weber, and M. Mayor. A single-molecule diode. *Proc. Natl. Acc. Sc. US*, 102(25):8815, 2005.
- [3] S. Kubatkin, A. Danilov, M. Hjort, J. Cornil, J.-L. Brédas, N. Stuhr-Hansen, P. Hedegård, and T. Bjørnholm. Single-electron transistor of a single organic molecule with access to several redox states. *Nature*, 425:698, 2003.
- [4] J. Park, A.N. Pasupathy, J.I. Goldsmith, C. Chang, Y. Yaish, J.R. Petta, M. Rinkoski, J.P. Sethna, H.D. Abruña, P.L. McEuen, and D.C. Ralph. Coulomb blockade and the kondo effect in single atom transistors. *Nature*, 417:722, June 2002.
- [5] S. Sapmaz, P. Jarillo-Herrero, Ya. M. Blanter, and H S J van der Zant. Coupling between electronic transport and longitudinal phonons in suspended nanotubes. *New J. Phys.*, 7:243, 2005.
- [6] Emanuel Lörtscher, Jacob W. Ciszek, James Tour, and Heike Riel. Reversible and controllable switching of a single-molecule junction. *Small*, 2(8-9):973–977, 2006.
- [7] R.O. Jones and O. Gunnarsson. The density functional formalism, its applications and prospects. *Rev. Mod. Phys.*, 61(3):689, 1989.
- [8] W. Kohn. Nobel lecture: Electronic structure of matter — wave functions and density functionals. *Rev. Mod. Phys.*, 71(5):1253, 1999.

- [9] J. A. Pople. Nobel lecture: Quantum chemical models. *Rev. Mod. Phys.*, 71(5):1267, 1999.
- [10] C.-O. Almbladh and U. von Barth. Exact results for the charge and spin densities, exchange–correlation potentials, and density–functional eigenvalues. *Phys. Rev. B*, 31(6):3231, 1985.
- [11] C. Fonseca Guerra, J. G. Snijders, G. te Velde, and E. J. Baerends. Towards an order-n dft method. *Theor. Chem. Acc.*, 99:391–403, 1998.
- [12] E. Runge and E.K.U. Gross. Density–functional theory for time–dependent systems. *Phys. Rev. Lett.*, 52:997, 1984.
- [13] R. van Leeuwen. Causality and symmetry in time-dependent density–functional theory. *Phys. Rev. Lett.*, 80:1280, 1998.
- [14] N.T. Maitra and K. Burke. Demonstration of initial state dependence in time–dependent density functional theory. *Phys. Rev. A*, 63:42501, 2001.
- [15] N.T. Maitra, K. Burke, and C. Woodward. Memory in time–dependent density functional theory. *Phys. Rev. Lett.*, 89:23002, 2002.
- [16] M. Di Ventura, S.T. Pantelides, and N.D. Lang. First-principles calculation of transport properties of a molecular device. *Phys. Rev. Lett.*, 84(5):979, 2000.
- [17] P.S. Damle, A.W. Gosh, and S. Datta. Unified description of molecular conduction: From molecules to metallic wires. *PRB*, 64:201403, 2001.
- [18] Y. Xue, S. Datta, and M.A. Ratner. First-principles based matrix–green’s function approach to molecular electronic devices: General formulation. *J. Chem. Phys.*, 115(4292), 2001.
- [19] J. Seminario, A.G. Zacarias, and P.A. Derosa. Analysis of a dinitro–based molecular device. *J. Chem. Phys.*, 116(4):1671, 2002.
- [20] J. Taylor and K. Brandbyge, M. and Stokbro. Conductance switching in molecular device: the role of sidegroups and intermolecular interactions. *cond-mat/0212191*, 2002.

- [21] K. Stokbro, J. Taylor, M. Brandbyge, J.-L. Mozos, and P. Ordejon. Theoretical study of the nonlinear conductance of dithiol benzene coupled to  $\text{Au}(111)$  surfaces via thiol and thiolate bonds. *Comp. Mat. Sci.*, 27:151, 2003.
- [22] K. Stokbro, J. Taylor, M. Brandbyge, J.-L. Mozos, and P. Ordejon. Theoretical study of the nonlinear conductance of di-thiol benzene coupled to  $\text{Au}(111)$  surfaces via thiol and thiolate bonds. 27(1-2):151, 2003.
- [23] J. Stokbro, K. Taylor and M. Brandbyge. Do aviram–ratner diodes rectify? *J. Am. Chem. Soc.*, 125:3674, 2003.
- [24] A. M. Bratkovsky and P. E. Kornilovitch. Effects of gating and contact geometry on current through conjugated molecules covalently bonded to electrodes. *Phys. Rev. B*, 67(11):115307, 2003.
- [25] Tomoya Ono and Kikuji Hirose. First-principles study of electron-conduction properties of helical gold nanowires. *Physical Review Letters*, 94(20):206806, 2005.
- [26] J.J. Palacios, A.J. P’erez-Jim’enez, E. Louis, E. SanFabi’an, and J.A. Verg’es. First-principles approach to electrical transport in atomic-scale nanostructures. *Phys. Rev. B*, 66:035322, 2002.
- [27] H.-W. Lee, H.-S. Sim, D.-H. Kim, and K.J. Chang. Towards unified understanding of conductance of stretched monoatomic contacts. *Phys. Rev. B*, 68:75424, 2003.
- [28] F. Evers, F. Weigend, and M. Koentopp. Conductance of molecular wires and transport calculations based on density-functional theory. *Phys. Rev. B*, 69:235411, 2004.
- [29] M. Brandbyge, J.-L. Mozos, P. Ordejon, J. Taylor, and K. Stokbro. Density-functional method for nonequilibrium electron transport. *PRB*, 65:165401, 2002.
- [30] R. Ahlrichs, M. Bär, M. Häser, H. Horn, and C. Kölmel. Electronic structure calculations on workstation computers: The program system turbomole. *Chem. Phys. Lett.*, 162:165, 1989.

- [31] C. Zhou, C.J. Muller, M.R. Deshpande, J.W. Sleight, and M.A. Reed. Microfabrication of a mechanically controllable break junction in silicon. *Applied Physics Letters*, 76(8):1160, August 1995.
- [32] N.J. Tao. Measurement and control of single molecule conductance. *J. Mat. Chem.*, 15:3260, 2005.
- [33] Bingqian Xu, Xiaoyin Xiao, and Nongjian J. Tao. Measurements of single-molecule resistance by repeated formation of molecular junctions. *Science*, 301:1221, 2003.
- [34] Yongqiang Xue and Mark A. Ratner. Microscopic study of electrical transport through individual molecules with metallic contacts. i. band lineup, voltage drop, and high-field transport. *Phys. Rev. B*, 68(11):115406, 2003.
- [35] Segey V. Faleev, Francois Leonard, Derek A. Stewart, and Mark van Schilfgaarde. *Ab initio* tb-lmto method for nonequilibrium electron transport in nano systems. *Phys. Rev. B*, 71:195422, 2005.
- [36] Gemma C. Solomon, Jeffrey R. Reimers, and Noel S. Hush. Single molecule conductivity: The role of junction-orbital degeneracy in the artificially high currents predicted by *ab initio* approaches. *J. Chem. Phys.*, 121:6615, 2004.
- [37] San-Huang Ke, Harold U. Baranger, and Weitao Yang. Contact atomic structure and electron transport through molecules. *J. Chem. Phys.*, 122:074704, 2005.
- [38] San-Huang Ke, Harold U. Baranger, and Weitao Yang. Models of electrodes and contacts in molecular electronics. *J. Chem. Phys.*, 123:114701, 2005.
- [39] K. S. Thygesen and K. W. Jacobsen. Molecular transport calculations with wannier functions. *Chem. Phys.*, 319:111–125, 2005.
- [40] Victor M. Garcia-Suarez, Tomasz Kostyrko, Steven Bailey, Colin Lambert, and Bogdan R. Bulka. Study of transport proerties of a molecular junction as a function of distance between the leads. *cond-mat/0610321v1*, 2006.

- [41] A. Grigoriev, J. Skoldberg, G. Wendin, and Z. Crljen. Critical roles of metal-molecule contacts in electron transport through molecular-wire junctions. *Physical Review B (Condensed Matter and Materials Physics)*, 74(4):045401, 2006.
- [42] Hisashi Kondo, Hiori Kino, Jun Nara, Taisuke Ozaki, and Takahisa Ohno. Contact-structure dependence of transport properties of a single organic molecule between two electrodes. *Physical Review B (Condensed Matter and Materials Physics)*, 73(23):235323, 2006.
- [43] J.P. Perdew, R.G. Parr, M. Levy, and J.L. Balduz. Density-functional theory for fractional particle number: Derivative discontinuities of the energy. *Phys. Rev. Lett.*, 49(23):1691, 1982.
- [44] J.P. Perdew and M. Levy. Physical content of the exact kohn-sham orbital energies: Band gaps and derivative discontinuities. *Phys. Rev. Lett.*, 51(20):1884, 1983.
- [45] M. Mayor and Th. Wandlowski. *Private communication*.
- [46] Shimin Hou, Jiaying Zhang, Rui Li, Jing Ning, Rushan Han, Ziyong Shen, Xingyu Zhao, and Quande Wu. First-principles calculation of the conductance of a single 4,4 bipyridine molecule. *Nanotechnology*, 16:239–244, 2005.
- [47] Mario Ruben. *Private communication*.
- [48] M. Gransbois, M. Beyer, M. Rief, H. Clausen-Schaumann, and H. E. Gaub. How strong is a covalent bond? *Science*, 283(5408):1727–30, 1999.
- [49] Sune R. Bahn and Karsten W. Jacobsen. Chain formation of metal atoms. *Phys. Rev. Lett.*, 87:26, 2001.
- [50] M. A. Reed, C. Zhou, M. R. Deshpande, C. J. muller, T. P. Burgin, L. Jones, and J. M. Tour. The electrical measurement of molecular junctions. *Annals of the New York Academy of Sciences*, 852:133–144, 1998.
- [51] J. Reichert, R. Ochs, D. Beckmann, H.B. Weber, M. Mayor, and H. von Löhneysen. Driving current through single organic molecules. *Physical Review Letters*, 88(17):176804, 2002.

- [52] C. Kergueris, J.-P. Bourgoin, S. Palacin, D. Esteve, C. Urbina, M. Magoga, and C. Joachim. Electron transport through a metal-molecule-metal junction. *Physical Review B*, 59:12505, May 1999.
- [53] H.B. Weber, J Reichert, F. Weigend, R. Ochs, D. Beckmann, M. Mayor, R. Ahlrichs, and H. von Löhneysen. Electronic transport through single conjugated molecules. *Chemical Physics*, 281:113–125, October 2002.
- [54] Gonzalez. Electrical conductance of molecular junctions by a robust statistical analysis. *cond-mat/0610303v1*, 2006.
- [55] X. D. Cui, A. Primak, X. Zarate, J. Tomfohr, O. F. Sankey, A. L. Moore, D. Gust, G. Harris, and S. M. Lindsay. Reproducible measurement of single-molecule conductivity. *Science*, 294(5542):571–574, 2001.
- [56] H. Park, A. Lim, A. Alivisatos, J. Park, and P. McEuen. Fabrication of metallic electrodes with nanometer separation by electromigration. *Applied Physics Letters*, 75(2):301, 1999.
- [57] M. Lambert, M. Goffman, J. Bourgoin, and P. Hesto. Fabrication and characterisation of sub-3 nm gaps for single-cluster and single-molecule experiments. *Nanotechnology*, 14:772, 2003.
- [58] Ajit K. Mahapatro, Subhasis Ghosh, and David B. Janes. Nanometer scale electrode separation (nanogap) using electromigration at room temperature. *Transactions on Nanotechnology*, 5(3):232, 2006.
- [59] M. Saifullah, T. Ondarcuhu, D. Koltsov, C. Joachim, and M. Welland. A reliable scheme for fabricating sub 5 nm co planar junctions for single molecule electronics. *Nanotechnology*, 659:2002.
- [60] S. Khondaker and Z. Yao. Fabrication of nanometer-spaced electrodes using gold nanoparticles. *Applied Physics Letters*, 81(24):4613, 2002.
- [61] K. I. Bolotin, F. Kuemmeth, A. N. Pasupathy, and D. C. Ralph. Metal-nanoparticle single-electron transistors fabricated using electromigration. *cond-mat/0310594*, 20032003.
- [62] P Hohenberg and W. Kohn. Inhomogeneous electron gas. *Phys. Rev.*, 136(3B):864, 1964.

- [63] W. Kohn and L.J. Sham. Self-consistent equations including exchange and correlation effects. *Phys. Rev.*, 140(4A):1133, 1965.
- [64] A.D. Becke. Density-functional exchange-energy approximation with correct asymptotic behavior. *Phys. Rev. A*, 38:3098, 1988.
- [65] J.P. Perdew. Density-functional approximation for the correlation energy of the inhomogeneous electron gas. *Phys. Rev. B*, 33:8822, 1986.
- [66] J.P. Perdew, M. Ernzerhof, and K. Burke. Rationale for mixing exact exchange with density functional approximations. *J. Chem. Phys.*, 105:9982, 1996.
- [67] A.D. Becke. Density-functional thermochemistry. iii. the role of exact exchange. *J. Chem. Phys.*, 98(7):1372, 1993.
- [68] A.D. Becke. Development of the colle-salvetti correlation-energy formula into a functional of the electron density. *Phys. Rev. B*, 37:785, 1988.
- [69] F. Evers, F. Weigend, and M. Koentopp. Coherent transport through a molecular wire: DFT calculation. *Physica E*, 18:255, 2003.
- [70] Leo P. Kadanoff and Gordon Baym. *Quantum Statistical Mechanics*. Addison-Wesley Publishing Comp. Inc., 1962.
- [71] K. Stokbro, J. Taylor, M. Brandbyge, and P. Ordejon. Transiesta: A spice for molecular electronics. *Ann. N. Y. Acad. Sci.*, 1006(212-226), 2003.
- [72] M. Koentopp. Theory of electronic transport through molecular nanostructures. *Wiss. Berichte FZK*, FZKA(7121):1-181, 2005.
- [73] R. Landauer. Titel missing. *IBM J. Res. Dev.*, 1:233, 1957.
- [74] R. Landauer. Electrical resistance of disordered one-dimensional lattices. *Philosophical Magazine*, 21:863, 1970.
- [75] S. Datta. *Electronic Transport in Mesoscopic Systems*. Cambridge University Press, 1995.
- [76] M. Di Ventura, S. T. Pantelides, and N. D. Lang. The benzene molecule as a molecular resonant-tunneling transistor. *Applied Physics Letters*, 76:3448-3450, 2000.

- [77] K. Stokbro. unpublished; data reproduced in Ref. [40], 2004.
- [78] I. Gutman and N. Trinajstić. Graph theory and molecular orbitals. xv. the hückel rule. *Journal of Chemical Physics*, 64:4921–4925, 1976.
- [79] Florian Weigend and Marco Häser. Ri-mp2: first derivatives and global consistency. *Theor. Chim. Acc.*, 97:331, 1997.
- [80] A. Schäfer, H. Horn, and R. Ahlrichs. . *J. Chem. Phys.*, 97:2571, 1992.
- [81] A. Schäfer, C. Huber, and R. Ahlrichs. Fully optimized contracted gaussian basis sets of triple zeta valence quality for atoms li-kr. *J. Chem. Phys.*, 100(8):5829, 1994.
- [82] Zong-Liang Li, Bin Zou, and Chuan-Kui Wang. Electronic transport properties of molecular bipyridine junctions: Effects of isomer and contact structures. *Physical Review B*, 73, 2006.
- [83] Thomas E. Janini, Jennifer L. Fattore, and Debra L. Mohler. Rapid assembly of rigid rods by metal complexation of bis(terpyridyl) ligands. *Journal of Organometallic Chemistry*, 578:260–263, 1999.
- [84] Max Fichtner and Mario Ruben. *Work in progress*.
- [85] Philipp Gütlich, Yann Garcia, and Harold A. Goodwin. Spin crossover phenomena in fe(ii) complexes. *Chemical Society Reviews*, 2000.
- [86] Yann Garcia, Petra J. van Koningsbruggen, René Lapouyade, Léopold Fournès, Louis Rabardel, Oliver Kahn, Vadim Ksenofontov, Geror Levchenko, and Philipp Gütlich. Influences of temperature, pressure, and lattice solvents on the spin transition regime of a polymeric compound. *Chem. Mater.*, 10:2426–2433, 1998.
- [87] Philipp Gütlich. *Private communication*, 2006.
- [88] Edwin C. Constable and Andreas D. Zuberbühler. Control of iron(ii) spin states in terpyridine complexes through ligand substitution. *Chem. Eur. J.*, 2:498, 1999.
- [89] TURBOMOLE V5-8. *University of Karlsruhe*, 2005.

- [90] P.-O. Löwdin. Quantum theory of many-particle systems. ii. study of the ordinary hartree-fock approximation. *Phys. Rev.*, 97:1490, 1955.
- [91] K. Eichkorn, O. Treutler, H. Oehm, M. Haeser, and R. Ahlrichs. Auxiliary basis sets to approximate coulomb potentials. *Chem. Phys. Lett.*, 242:652, 1995.
- [92] K. Eichkorn, F. Weigend, O. Treutler, and R. Ahlrichs. Auxiliary basis sets for main row atoms and transition metals and their use to approximate coulomb potentials. *Theor. Chem. Acc.*, 97:119, 1997.